Norwegian University of Life Sciences
Faculty of Veterinary Medicine and Biosciences
Department of Chemistry, Biotechnology and
Food Science

Master Thesis 2014
60 credits

Energetic Binders for Solid Rocket Propellants

Trond Heldal Hagen

Contents

Preface

Trond Heldal Hagen, master thesis in chemistry

FFI / NMBU

Regards, gratitude

A great appreciation is rightfully directed to the Norwegian Defense Research Establishment, for possessing an engaging environment and competence in nearly all possible fields. A special thanks to Erik Unneberg for outstanding mentoring throughout the process, Tomas Lunde Jensen for practical laboratory- and instrumental assistance, and Tor Erik Kristensen for guidance through various organic chemical aspects of rocket propellant research. Yngve Stenstrøm, NMBU, has been available and helpful by mail. Along the road of research, I got firsthand experience to a large variety of analysis methods in applied chemistry and material science. I was introduced to the industrial approach of research at Nammo, privileged to carry out quality control analysis at their facility in Raufoss. A specified gratitude is directed to Moja Løvlie Skalsbakken for laboratory assistance at Nammo.

1. Introduction

1.1 The purpose

Currently, the most popular solid propellant used both in space missions and for military purposes is a composition of essentially AP as an oxidizer, aluminum as fuel, and a polybutadiene based binder. Such a composition is non-detonable, exhibits good mechanical properties through a wide temperature span, and gives a lot of power (high specific impulse). On the other hand the AP/Al based propellants form a lot of smoke from the combustion products. Being of particular concern are hydrochloric acid aerosols and aluminum oxide. A visible tail of acid and oxides is neither favored in military tactical missiles, nor for the environment. Confronting these challenges, solid propellant research has turned away from the conventional components in order to search for promising propellant mixtures in the respects of low amount of smoke, long shelf life, temperature-insensitivity and high ballistic performance.

This master thesis is directed towards the search for optimal binder combinations of rocket fuel components, as a part of a rocket propellant research program at FFI (the Norwegian Defense Research Establishment).

1.2 Rocketry

History

The Chinese are believed to be the inventors of rockets. The first rockets were more like today's firework and were used in both combat and on festive occasions. These rockets were propelled by black powder (consistent of sulfur, charcoal and potassium nitrate) and balanced with a rod mounted at the rear end.

Figure 1. Drawing of a Chinese with his «arrow of flying fire» (NASA).

The first reported use of rockets in warfare was in 1232, during a war between the Mongols and the Chinese. The Chinese introduced their «arrows of flying fire» in the battle of Kai-Keng, with strategic success (NASA.gov 7. January 2014). Europe acquired the knowledge of rockets possibly through an ambassador sent by the Pope, William of Rubruck. He returned to England in 1257, and shortly after that, his friend, the friar and scholar Roger Bacon (1214 - 1294) began experimenting with gunpowder and rockets.

Konstantin E. Tsiolkovsky (1857 – 1935) introduced the modern age of rocketry as he developed the theory of jet propulsion in 1896, followed by the Tsiolkovsky rocket equation in 1897. This equation proposes the relationships between specific impulse, velocity, and change of mass due to loss of propellant. Tsiolkovsky stated that the single limitation of the range and velocity of a rocket is the exhaust velocity (NASA.gov 7. January 2014). Tsiolkovsky was highly interested in space exploration, and spent a significant amount of his life solving problems regarding space exploration (NASA.gov 7.

Figure 2. Picture of Robert H. Goddard with his liquid propellant rocket. (Wikipedia)

January 2014). He was supposedly inspired by science-fiction writer Jules Verne.

In America, the physicist and inventor Robert H. Goddard (1882 – 1945) experimented with the concept of rocketry, and successfully launched a liquid propellant rocket in 1926. It was fueled by liquid oxygen and gasoline. Goddard is called the father of modern rocketry (NASA.gov 7. January 2014).

The first *composite* solid propellant was invented by John Whiteside Parsons and co. in the 1940s. It contained 75 % potassium perchlorate and 25 % asphalt, and it was implemented on fighter planes as take-off assistance (JATO – *Jet Assisted Take-Off*). The seemingly primitive rocket booster actually revolutionized rocket technology, being also the first case-bonded propellant. The asphalt-bonded propellant could be melted and re-casted, thereby labeling it a *thermoplastic elastomer* (TPE) (Wikipedia 2014). TPEs are believed to play a role in future rocketry as the possibility of re-usage would be beneficial in many aspects.

Propulsion

Newton's 3rd law states that for every action there is a reaction in the opposite direction, with equal force. Rocket propulsion rests upon this principle. As the produced gases are ejected at the rear end of a rocket motor, the ejected matter gives thrust to the rocket body in the opposite direction. Thrust is the force vector (F), measured in newton($kg \cdot m/s^2$). The pressure is directed outwards in all directions inside the propulsion chamber, but escapes through the nozzle to give thrust.

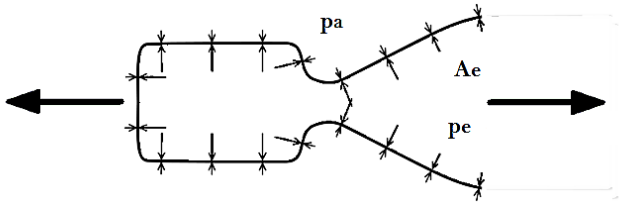

Figure 3. Propulsion is created from propellant escaping the nozzle. (Sutton and Biblarz 2001)

The thrust of a rocket is dependent on *momentary thrust* and *pressure thrust*. When the pressure at the end of the nozzle is equal to the external pressure, then thrust is dependent on the mass flow ($\dot{m}$) and velocity of ejected matter (v_e). If the pressure at the nozzle exit (p_e) is higher than the external pressure (p_a), then the pressure difference multiplied with the nozzle opening areal (A_e), represents a contribution to the propulsive forces. This means that a rocket operating at higher altitudes (or even in space) delivers more thrust than one at sea level. p_e is preferred to be of equal or slightly higher magnitude than p_a (Sutton and Biblarz 2001).

$$F = \dot{m}v_e + (p_e - p_a)A_e$$

Total Impulse (I_t) s is a more convenient way to describe propulsive performance than thrust, whereas the product of force and time gives an understanding of total consumed energy, in contrast to the momentary unit of force. The thrust of a rocket propellant varies during combustion (figure 5), therefore is I_t expressed as

the thrust force integral over burning time (t_b). A simplified approximation is often done, where the thrust is held constant:

$$I_t = \int_0^{t_b} F dt \; = \bar{F} t_b$$

$$I_t = F \times t$$

Total impulse does only communicate the available energy. The energy would preferably be large relative to its propellant mass. Specific impulse (I_{sp}) is defined as the total impulse per weight unit of propellant. Specific impulse is frequently expressed in seconds:

$$I_{sp} = \frac{\int_0^{t_b} F dt}{g_0 \int_0^{t_b} \dot{m} dt} = \frac{F \int_0^{t_b} dt}{\dot{m} \int_0^{t_b} dt} = \frac{F t_b}{m} = \frac{I_t}{m}$$

The change in velocity (Δu) is dependent on specific impulse (I_{sp}) and the initial, total rocket mass (M_0) over non-combustible mass (M_0 - M_p, where M_p is the mass of propellant). This equation is known as *the rocket equation* (Sutton and Biblarz 2001):

$$\Delta u = \; I_{sp} \cdot \ln\left(\frac{M_0}{M_0 - M_p}\right)$$

Solid propellant motors

When an airborne vessel needs high propulsive performance over a limited time span and the ability to operate virtually everywhere, a solid propellant motor would be the first among choices. In its most simple configuration, a solid propellant has no moving parts, thus advertising robustness and reliability. The propellants are designed to have a long shelf life (to endure a long period of storage, typically decades), and a minimum of maintenance. These qualities are highly favorable for military missiles, since they are often bought in large quantities and stored until necessary.

Solid propellant motors consist of a solid propellant capsuled by a casing. The propellant accounts for a major fraction of the total motor mass, typically 82 to 94 % (Sutton and Biblarz 2001). Some configurations vary within the concept of solid propellant motors. We assume a *case-bonded* solid propellant: The propulsive material is distributed around the sides of the chamber, leaving a cavity at the center along the longitudinal axis of the motor (FIG). The casing is capable of withstanding considerable pressure. It is constructed from either metal or reinforced composite materials. At the inner surface of the casing there is a layer of insulation to protect the casing from high temperatures during combustion. The single opening of the casing is a nozzle, responsible for converting as much energy from the ejected matter to propulsion as possible. The exhaust will continue expanding as it has left the narrowest cross-section, but the nozzle redirects the expanding gas, allowing it to contribute to the propulsion.

At the initial stage, an electronically activated igniter incinerates the propellant's inner surface, allowing it to combust steadily at a burning rate, which is dependent on temperature, the propellant's configuration and the internal pressure of the casing. From here on, the combustion supplies its own heat and pressure needed to maintain sustainable burning. The reaction will proceed until all propellant is consumed.

The exhaust consists of combustion products that leaves the rocket body in a solid, liquid, or gaseous state, often a combination of these (Sutton and Biblarz 2001). Solid propellant rockets are functional in the vacuum of space because they carry all of the elements needed for combustion within the vessel.

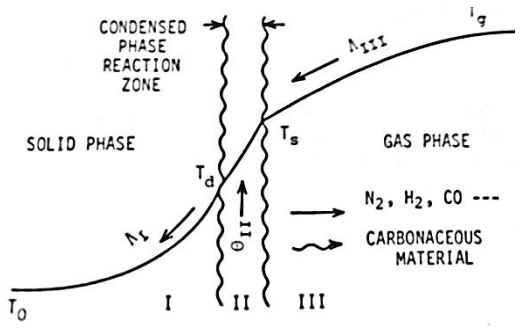

Figure 4. Illustration of a burning solid propellant surface. Phase I: solid. Phase II: condensed phase, initial reaction zone. The temperature increases drastically. Phase III: gas phase, further reaction to create gas and other end-products.

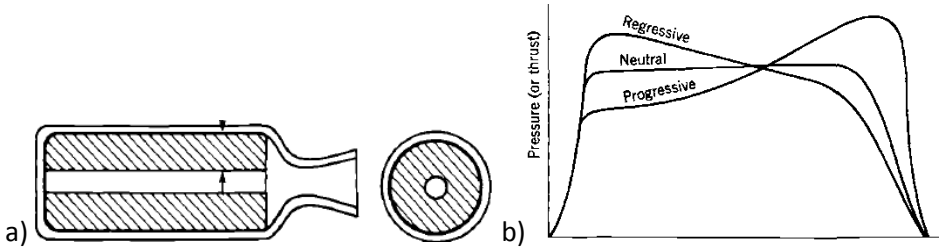

Figure 5. a) Ideal sketch of a chamber with nozzle and propellant (grey). The internal tubular area increases as the propellant burns away, giving it a progressive thrust. b) Thrust as a function of time for typical propellant configurations. Exported from (Sutton and Biblarz 2001)

Solid propellants are simple in construction, which also carries some limitations along the road. The thrust of a solid propellant rocket cannot be actively altered, but it can certainly be pre-defined. Burn rate is directly related to the burning surface. Considering an inner tubular cavity, as in FIG: As the rocket burns, the inner cavity increases and reveals a gradually increasing combustible surface. Consequently, more matter escapes through the nozzle, giving more thrust. If such a burn rate behavior is not preferred, one can change the *propellant configuration.* A star-shaped cavity would obtain a constant burn surface, thus a neutral thrust. The propellant configuration can promote a progressive, regressive, neutral burn, or a combination of these (FIG curve). A progressive thrust behavior would perhaps be beneficial for tactical missiles where the target is certain and a maximum kinetic energy at impact is preferred.

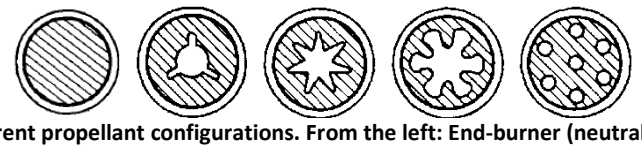

Figure 6. Cross-sections of different propellant configurations. From the left: End-burner (neutral burn), slots and tube (neutral), star (neutral), wagon-wheel (neutral), Multiperforated (progressive-regressive). Objects are exported from (Sutton and Biblarz 2001).

When the propellant configuration is more complex than just a casing completely filled with propellant (end-burner, see FIG), the strength of the propellant is of crucial importance. Firstly, a cavity with a large surface and complex configuration is more prone to weakening than a completely massive propellant (and the

weakening would be more severe). Secondly, a weakened propellant could fracture at the surface. A propellant cavity containing small cracks has suddenly, unintentionally, increased its burn surface. When ignited, the fractured solid propellant will adversely increase in burn rate – thereby build up pressure, and most likely end in an explosion nearby the launch site. The propellant's internal strength needs to be assured, and this is where the propellant *binder* gets crucial.

1.3 Essential components

Binder

The binder represents the medium in which all propellant substances are evenly distributed. It simply keeps things together, while additionally contributing as fuel in the propellant matrix. The choice of binder is vital regarding mechanical traits and applicability of other propellant components. In spite of the fact that its content rarely exceeds 15 % in high energy compositions, the binder governs the class and type of propellant. The binder is very important for the overall mechanical properties (Haas, Eliahu et al. 1994). Elastomeric polymers are desired as binders, and of these only the tougher ones can be used (Shusser 2012). A viscoelastic binder will increase the resistance to internal stress and external shock, due to its ability to dissipate energy. Such a trait complies with the increasing demands of so-called *Insensitive Munitions* (IM).

Chain extenders are smaller prepolymers that are used for prolonging the polymer chains. If implemented to produce *block copolymers*, chain extenders bring urethane groups together to form polar, *hard block* regions. These regions share the same alternating pattern of urethane and monomer units, which promote the formation of crystalline areas through hydrogen bonding (a dominant fraction of hard block segments could give the elastomer thermoplastic features. Not discussed in further detail). Chain extenders could also be introduced to form a random block copolymer, and possibly form similar physical cross-linkages, as well as increase the free volume between polymer chains.

An ideal binder prepolymer should be a liquid at the initial stage of the curing process, and be suitable for mixing at desired temperatures (30 – 60 °C). It should provide additional energy to the overall exothermic reaction when the propellant is fired, but have a minimum of exothermic nature during cure, have a minimal cure-shrinkage, and lastly provide a low *glass transition temperature* (T_g). Polysulfide was the first polymeric binder to be used in composite propellants in 1942. Nitrocellulose was the first *energetic* polymer to be used as such (Ang 2012). The concept of the current state of the art binder technology derives from two main elements that react to produce the binder matrix: The prepolymer and the curing agent.

Prepolymer

The choice of prepolymer is made regarding what properties one would like to promote. Polyether and -ester prepolymers provide extra oxygen for the overall combustion reaction. They also introduce a more polar environment into the propellant matrix, which could be favorable in combination with energetic plasticizers.

Glycidyl azide prepolymer (GAP) is classified as a high nitrogen content polymer, a subclass of energetic materials where the potential energy output derives from the positive heat of formation (see TABLE for comparison with HTPB) (Sun Min 2008). GAP exhausts large amounts of hot gases when combusted. The high nitrogen content (nitrogen arranged in cumulated double bonds) is responsible for a higher polymer density, compared to that of a purely hydrocarbon polymer chain. From the table TABLE, it is shown that the polyether backbone of GAP delivers more oxygen to the burning of propellant than the widely used polybutadiene prepolymer (HTPB). The oxygen balance tells how much oxygen that is needed for the substance to produce the most stabile combustion products (e.g. CO_2 and H_2O). Having a surplus of oxygen implies producing completely oxidized products, thereby obtaining an optimal energy output. A parallel can be drawn to the incomplete combustion of coal, which will produce carbon monoxide instead of carbon dioxide when access of oxygen is limited.

Table 1: Comparative characteristics of GAP and HTPB. Data extracted from (Ang 2012).

Polymer	Density (kg/m^3)	T_g (°C)	Heat of formation (kJ/mol)	Oxygen balance (%)
GAP	1.34	-34	+957	-121[a)]
HTPB	0.9	-68	-582	-325[a)]

a) The negative oxygen balance addresses an insufficient amount of oxygen present in the prepolymer to achieve the most stabile combustion products. A positive oxygen balance is not expected for a prepolymer. GAP has an advantage as it contains more oxygen than HTPB.

GAP is a promising energetic polymer for solid propellant purposes due to its availability, good binder properties, and low detonation sensitivity. On the other hand, solid propellants based on GAP suffers from inferior mechanical properties, especially low-temperature traits (Sun Min 2008).

Advances in synthesis

Linear, hydroxyl terminated GAP was first synthesized at Rocketdyne in the USA, 1976. Initially, epicholohydrin (ECH) was chosen to be the precursor. A substitution of chlorine with azide was carried out, thereby creating glycidyl azide (GA). But the monomer obtained low reactivity towards polymerization, and therefore an alternative route was necessary. By cationic ring opening polymerization of ECH to form PECH before azide substitution, an adequate reactivity was acquired throughout the synthesis. The azide group is introduced trough an excess of sodium azide (NaN_3) (Ang 2012).

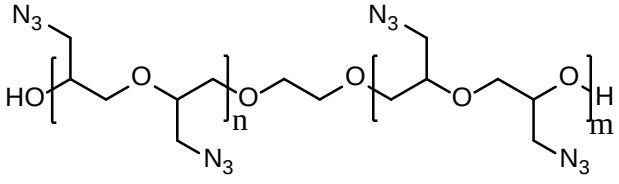

Figure 7. Glycidyl azide prepolymer (GAP) diol, with a molecular weight varying between producers.

Positioning of the hydroxyl group is important regarding to curing reactions with isocyanates. Primary hydroxyl groups give faster reactions than secondary. Also, a gassing problem that occurs with secondary

hydroxyl moieties is eliminated (Ang 2012). In 1993, Ampleman patented a synthesis route to produce linear GAP with higher functionality *and* primary hydroxyl moieties, by epoxidation of PECH. The epoxidation is highly region-specific, it occurs only at the polymer ends. Further ring opening of the epoxide terminated PECH allows for addition of selected primary alcohols of higher functionality, thereby increasing overall functionality of the practically linear polymer(Diaz, Brousseau et al. 2003).

Branched GAP introduces a functionality higher than two, a lower glass transition temperature, and a lower viscosity than linear GAP. The branched prepolymer is expected to utilize more rapid curing, improved mechanical properties and a less cumbersome processing (Ang 2012). Ahad patented a synthesis pathway for branched GAP in 1989; a single step degradation and azidation procedure of PECH (Bui, Ahad et al. 1996)

Table 2. Comparison of branched and linear GAP, data extracted from (Ang 2012). Note that the molecular weight of linear GAP analyzed by the author, is about two thirds of the reported values from Ang, displayed in this table.

Polymer	viscosity (Pas)	T_g (°C)	molecular weight (g/mol)	Functionality
Linear GAP	10	-50	3000	~2
Branched GAP	4,5	-60	4200	> 2

Curing agent

The curing agent is, by its name, held responsible for the solid propellant cast to be successfully cured, although it is dependent on the prepolymer to do so. A prepolymer is reacted with the curing agent to form the binder, which preferably becomes a moderately cross-linked elastomer (moderate in comparison with thermosets). The curing agent is a reactive and more or less selective reagent that reacts with specified moieties on the prepolymer. As an example, the resin containing epoxide in a two-component adhesive is labeled as the curing agent – as it is highly reactive, and considered responsible for the polymerization reaction in the first place.

Isocyanates

In the same sense as epoxides, isocyanates are reactive functional compounds often used for curing purposes. Reaction mechanisms of isocyanates will be further discussed in section 1.4. An isocyanate group is a cumulated moiety of nitrogen, carbon and oxygen. It possesses three resonance structures:

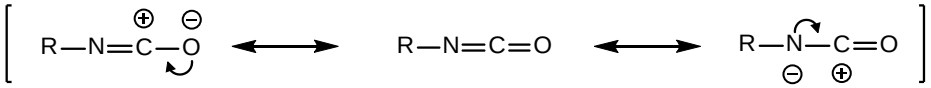

The first isocyanate synthesis was executed by wurtz in 1848, by esterification of isocyanic acid. Its use in industry was not yet known until O. Bayer and co. at I.G. Farbenindustrie discovered the step-growth polymerization of isocyanates with polyether and polyester diols, to synthesize polyurethane in 1937(Bayer 1969).

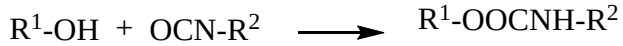

In 1996, only three isocyanate compounds made up for over 90 % of all the isocyanate production – polymeric *diphenylmehane diisocyanate* (p-MDI), MDI, and *toluene diisocyanate* (TDI) (Ulrich 1996). Isocyanates are toxic, and especially volatile isocyanates are recognized for being the most hazardous due to inhalation, which presents the greatest risk. Diisocyanates are claimed to be one of the main reasons for developing occupational asthma in the western world (Mehta, Mehta et al. 1990).

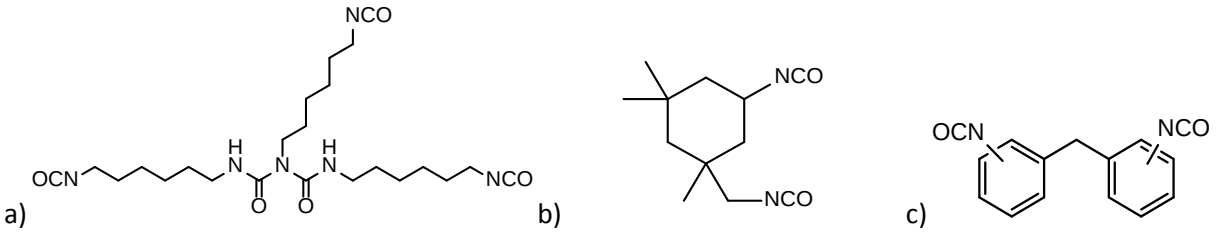

Figure 8. Commercially available isocyanates for curing purposes. a) the biuret Desmodur N100. b) Isophorone diisocyanate (Vestanat IPDI) c) (MDI), undefined placement of the isocyanate groups.

Desmodur N100 is a biuret of hexa-1,6-diisocyanate (HDI). The commercially available N100 is not limited to the illustrated biuret, but consists of numerous isomers. N100 has an average functionality at approximately 2.5, but is believed to comprise of HDI derivatives with functionality ranging from two to six. Vestanat IPDI is an aliphatic diisocyanate. The primary isocyanate of IPDI is more prone to react than the secondary, situated directly on the ring. MDI is an aromatic isocyanate. Compared to aliphatic compounds, aromatic substances introduce harder segments in an elastomer dominated by aliphatic polymer chains. The isocyanates on MDI are typically ortho – para oriented. It is di-functional in its pure form, but poly-MDIs have a higher functionality, because of one isocyanate per benzene ring.

Alkynes as isocyanate free curing agents

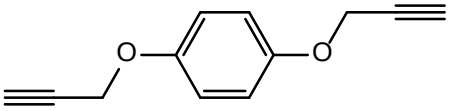

Figure 9. 1,4-bis(2-propynyloxy)benzene (BPOB)

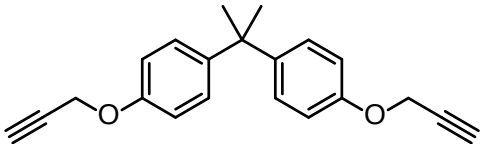

Figure 10. bisphenol A bis(propargyl ether) (BABE).

Alkynes can readily be reacted with azides to produce a triazole, which is frequently referred to as a «click reaction». This term implies a quick and uncomplicated reaction with few side-reactions and high yield. By first impression, an alkyne would give the impression of being the optimal curing agent in a solid propellant, and the cross-linkage of azide-containing energetic prepolymers by dialkynes has been suggested. Isocyanate curing of solid propellant binders suffers from side-reactions with e.g. water, but the cyclo-addition of alkynes and azides to yield triazoles are nearly free from side-reactions (Rostovtsev, Green et al. 2002)

Catalyst

The polymerization of the binder does not always proceed satisfactory, with respect to curing rate and the interference of other side-reactions. A curing catalyst may improve the process considerably. As for a urethane polymerization in a solid propellant binder system, the reaction rate and selectivity is of great importance for processing. An unsuccessful cure costs time and money, and may result in a hazardous highly energetic mixture that is difficult to handle.

Curing catalysts for polyurethane polymerization are typically metal compounds or tertiary amines. Tertiary amines either connect covalently to the carbon in the isocyanate group – thus activating it for a substitution mechanism, or it deprotonates the alcohol by acting as a Brønsted base (Dewhurst). Amines do, however, promote equally the reaction of water and alcohols with isocyanates. Tertiary amines are typically used as catalysts for urea reactions.

Metal ions are suggested to increase the electrophilic nature of the carbon in the isocyanate group by forming a complex with either its oxygen or nitrogen. Organotin catalysts as dibutyl tin dilaurate (DBTDL, FIG) are extremely effective catalysts, but stated by Blank et.al to be less selective regarding reaction pathways (Blank, He et al. 1999).

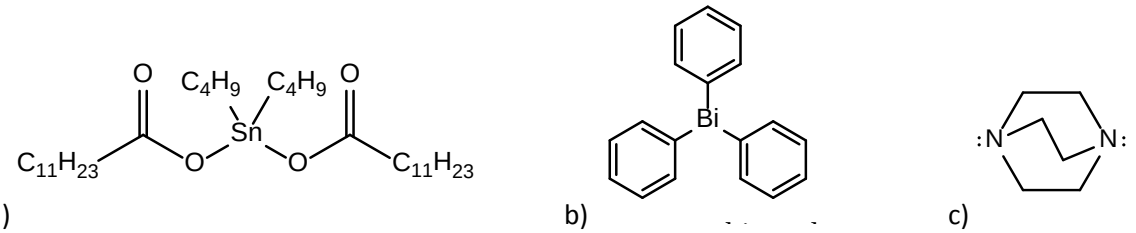

Figure 11. a) Dibutyl tin dilaurate (DBTDL), b) triphenyl bismuth (TPB), c) 1,4-diazabicyclo(2,2,2)octane.

Presently, the most favored catalyst for polyurethane synthesis of solid propellant binders is *triphenyl bismuth* (TPB, FIG), which is due to a favorable delay until the catalyst activates, and rapidly produced an adequate cure. TPB is compatible with both HTPB and high energetic systems, where other transition-metal ion based catalysts have shown to cause long-term degradation of propellant, thus making the propellant composition less stable (Shusser 2012).

A combination of TPB and DBTDL in a 10:1 ratio (respectively) was patented by Reed and Chan in 1983, to acquire minimal gassing and a favorable reaction rate (Reed and Chan 1983). Further work by Luo, Shan-guo et al. in 1997 presented erratic cures when curing co-polyether and N100 with DBTDL, and an adequate cure, with relatively little gassing when TPB was used. They further suggested that a complex of the two catalysts might occur, implying a new catalysis mechanism (Luo, Tan et al. 1997).

Plasticizer

As a homogenous unity with a solid propellant's binder system, the plasticizers are firstly responsible for an improvement in mechanical properties, making the propellant more flexible. They also assist processing, and can potentially function as burn rate modifiers(Ang 2012). And not to be forgotten for energetic plasticizers – they contribute to the combustion mechanics by an increase in overall enthalpy.

Generally, inert binder (i.e. HTPB) amounts to about 15% of a propellant, and the plasticizer content rarely exceeds 30 % of the binder (*pl/po* = 0.3). On the other hand, energetic binders (like GAP) constitute to about 30-40 % of the total mass in high energy propellants, and the nitrate ester plasticizer level could be as high as 80% of the binder. It has been stated that the pl/po ratio cannot be higher than 1 in a homopolymer GAP-system, due to the high free volume of GAP itself (Sun Min 2008).

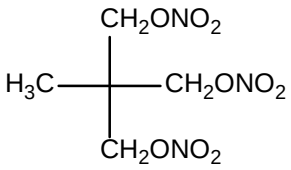

Figure 12. Trimethylol ethane trinitrate (TMETN)

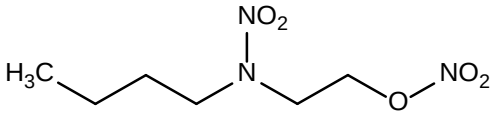

Figure 13. Butyl-N-(2-nitratoethylnitramine) (BuNENA).

The main concern of a plasticizer would be its long-term stability in a polymer. A parallel can be drawn to conventional plastic that is getting crisp and brittle when it ages – mainly due to the loss of plasticizer. A sweating propellant would, however, be more dangerous than eroding drain pipes. The overall sensitivity is adequate when merged into a polymer structure, but if the plasticizer perspires and accumulates along the walls of a solid propellant, the overall sensitivity would be drastically elevated. Many plasticizers are volatile, so handling aged propellants (or equally relevant – explosives) could be considered to be a hazardous task. *1,1,1-trimethylol ethane trinitrate* (TMETN) (FIG) is not as as nitroglycerine, but still withholds substantial energy. *Butyl-N-(2-nitratoethylnitramine)* (BuNENA) (FIG) is another energetic plasticizer that is even less volatile, again with the trade-off of being less energetic.

Oxidizer

Composite propellants are characterized by the large share of energetic filler particles, which are responsible for most of the energy. They are very strong oxidizing agents, being very potent in solitude, or together with an appropriate fuel source. *Ammonium perchlorate* (AP, FIG) is a relevant example. It is a widely used oxidizer, often accompanied with aluminum as fuel (readily oxidized) and hydrocarbons in conventional solid rocket propellants. *HMX* (octogen) has low fiction- and shock sensitivity, and is often used as the detonating component in polymer-bonded explosives (Wikipedia). Relative to AP, HMX burns with a clean fume. Being in a crystal conformation makes the oxidizers very dense, contributing to a lot of power for a relatively small solid propellant.

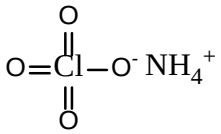

Figure 15. Ammonium Perchlorate (AP). Mp > 300 °C, ρ = 1.95 g/cm^3.

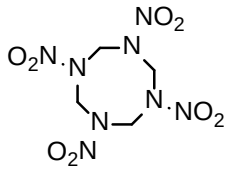

Figure 14. HMX. Mp = 280 °C, ρ = 1.9 g/cm^3.

Additives

There are numerous possible additives that compensate and tailor the final propellant properties. Of these may burn rate modifiers and bonding agents be the most important. Only the bonding agent additive is briefly discussed.

Bonding agent

Bonding agents serve as the cohesive linkage between binder and filler. Implementing a bonding agent could drastically improve mechanical properties since the filler surface often connects poorly with the binder alone. Landsem et.al (Landsem, Jensen et al. 2012) illustrated how a tailored bonding agent could affect cohesion in an HMX/GAP/BuNENA propellant matrix, by a considerable enhancement of tensile strength with only 0.001 % bonding agent introduced.

Table 3. The potential of improvement when introducing bonding agents to the propellant formulations based on HMX/GAP/BuNENA. Extracted from published results {Landsem, 2012 #226}.

Bonding agent	E modulus (MPa)	Stress at break (MPa)	Elongation at break (%)
None	2.5	0.33	51
0.02 wt %	4.3	0.58	37
0.20 wt %	5.3	0.71	21

1.4 Principles of polymer chemistry

Classification

Polymerization synthesis is generally divided into two reaction pathways: *chain-growth polymerization* (also called addition polymerization) and *step-growth polymerization* (also called condensation polymerization). Chain growth polymers consist of repeated units coupled *by free radical reactions* or *ionic addition*, adding one monomer at the time to a growing polymer chain. The reaction is initiated by a substance that destabilizes the electron balance in a monomer, creating a reactive site which will hand on the reactivity to the next monomer that is added to the polymer chain. A propagating polymerization can couple together more than one thousand monomers in less than a second (Min, Park et al. 2012). A generalized chain growth polymerization by free radicals may be:

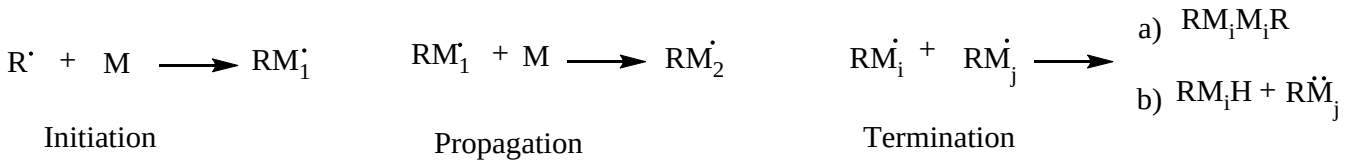

The polymerization is terminated when the active site on the chain regains electron balance. Termination occurs when a) two free radical chains react to create a covalent bond. The termination reaction is termed *combination*. The product is termed as «head-to-head» polymerized, because the remaining two chain ends origin from the initiation process – and feature the initiator reagent. b) *disproportionation* is the termination reaction where the radical electron jumps from one active site to another free radical, and trades back a proton. Also, termination of a growing chain can occur by the *chain transfer* reaction – which is not further discussed, but can proceed in numerous ways. The chain-growth mechanism does not eliminate any small molecules, as opposed to the step-growth mechanism, where two functional groups react together to combine the monomer units together. A typical approach would be the common Fischer esterification:

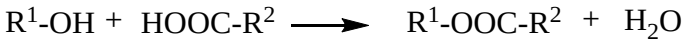

An alcohol and a carboxyl acid react to form an ester and water. In contrast to chain-growth mechanisms where monomers (in turn) couple with the polymer ends, step-growth polymerization is not dependent on the polymer ends to become active (ionized or free radicals). The functional groups react together, dependent of availability and potential for reactions to occur. Step-growth polymerization is characterized by the gradual growth of all the molecules simultaneously and proceeds until no functional groups are available in the growing chain's vicinity. A small molecule is typically, but not necessarily, eliminated. A relevant example is the reaction of alcohol and isocyanate to produce urethane (shown in next section).

The repeating unit must have a functionality of two or higher in order to create chains, and be more than di-functional to create a cross-linked network. A mono-functional molecule would terminate the polymerization at its site. A tri-functional molecule, on the other hand, would create an additional branch to the growing polymer.

Step-growth polymerization is dependent on equimolar amounts of functional groups to achieve an optimized polymerization reaction.

Urethane polymerization

The step-growth polymerization is sometimes termed «condensation polymerization» – a somewhat misleading term when referring to the formation of polyurethanes. In contrast to other condensation reactions, the reaction of isocyanate and hydroxyl groups to produce urethane does not eliminate any small molecule. Such a feature is arguably crucial for its applications in propellant binder synthesis.

The uses of polyurethanes are widespread and massive – from coatings, adhesives and foams, to elastomers. In 2010, more than 13 Megaton of polyurethane was produced worldwide, and by 2018 the annual production is predicted to reach 18 Megaton(plastemart 2011). The catalyzed mechanism is not fully understood, but suggested to include complexes with both the isocyanate and hydroxyl group.

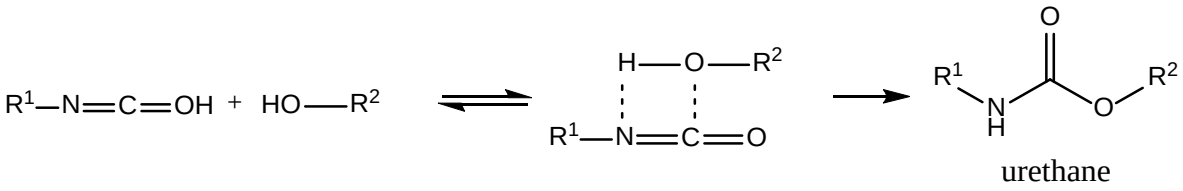

The reactivity of isocyanates is generally high. They can react readily with alcohols, water, amines and even other isocyanates. When water is introduced, carbon dioxide and a primary amine is firstly produced – then the excess isocyanates react further with amine to produce urea. In the presence of a base, isocyanate can react with itself to form isocyanurate.

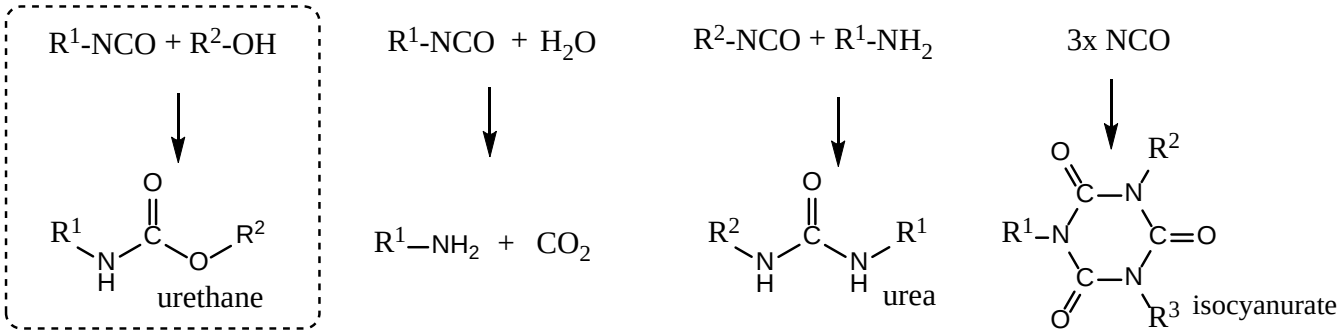

Water reacts with isocyanate to form carbamic acid, subsequently eliminating carbon dioxide to form a primary amine. The amine then reacts with isocyanate to produce urea, thus has one extra isocyanate been consumed (compared to the urethane reaction). As the reaction proceeds in a gradually cross-linking mold, the carbon dioxide creates air voids which are trapped inside the polymer. Degassing may remove some carbon dioxide, but will lose effect as the viscosity increases when a cross-linked polymer is gradually formed. Water contamination is a dreaded issue regarding polyurethane binder systems, because air voids will randomly increase the burning surface of a solid propellant, or introduce weak regions prone to ruptures.

Some catalysts favor the urethane reaction over urea reaction. As highlighted previously (in section 1.3), the choice of catalyst may govern how successful the end-product of a polyurethane based binder system. TPB has shown to suppress formation of urea (Reed and Chan 1983). In addition, isocyanates can react with their own end-products, like urethane to form allophanates, or urea to form a biuret:

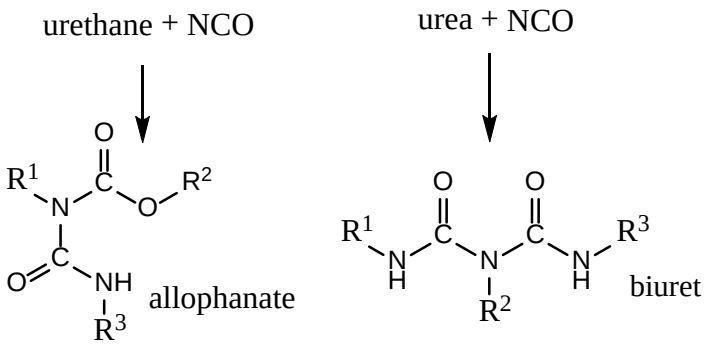

Isocyanate-free cross-linkage.

The reactivity of isocyanates is a two-faced trait. As an alternative to urethane polymerization, isocyanate free curing systems have emerged. Specifically regarding GAP, the azide moieties can be exploited to cross-link with alkynes through a *Huisgen cycloaddition* to form triazoles.

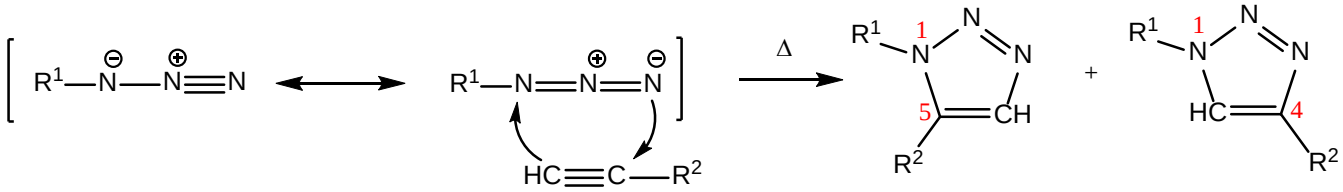

The reaction is predicted to yield two regioisomers – the 1,4- and 1,5-di-substituted regioisomers of triazole (FIG). Copper catalysts are known to accelerate and favor the 1,4-disubstituted 1,2,3-triazole (Rostovtsev, Green et al. 2002). The reaction of triazole cross-linkage is dependent on the extent of which electron withdrawing groups are present in the vicinity of the acetylene bond. According to Ang et al, such activated acetylene bonds react readily with azide polymers in a temperature range of 35-50 °C (Ang 2012).

Additionally, an electron donating backbone (saturated hydrocarbons) adjacent to the azide group is predicted to promote the Huisgen cycloaddtion reaction. Unlike conventional urethane synthesis, the isocyanate-free approach for curing GAP is not sensitive to humidity, nor is it very dependent on stoichiometric ratios of functional groups since GAP has an abundance of azide groups for alkynes to react with.

Polymer structure

Homopolymers

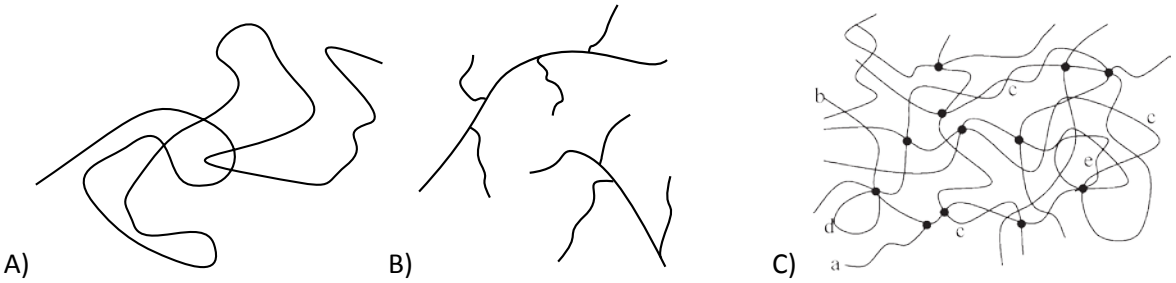

Figure 16. A) A linear polymer chain, liquid. B) Branched chains, liquid. C) An elastomeric polymer network, solid. The arrangements in the cross-linked network are annotated: a) dangling free chain, b) temporary entangled chain, c) trapped entanglement, d) elastically ineffective closed loop, e) elastically effective chain. illustration C exported from Sun Min (Sun Min 2008).

Linear polymer chains have a characteristically high melting point, due to the homogenous and easily interconnected chains. Upon freezing, linear polymers are stacked together, often forming crystalline regions. A branched polymer has a lower melting point because. The branches make the polymer more spatially demanding, and less willing to solidify. A cross-linked polymer however, is a solid for all temperatures below thermal degradation. The degree of cross-linkage is of crucial importance for the final behavior of the polymer. When cross-linkage is relatively moderate, the polymer is called an *elastomer.* The solid polymer has still preserved the polymer chain's inherent viscosity, and can ideally be stretched several times its original length.

Physical cross-linkage is the phenomenon of attraction between polymer chains through hydrogen bonds, which are reversible. When subjected to stress, some bonds in the elastomer will break. Broken covalent bonds are permanently damaged, while hydrogen bonds will still have the potential of creating new bonds with the vicinity. This recapitulation of cross-linkage is considered a favorable property for solid propellant binders, and urethane groups are recognized as promoters of physical cross-linkage, at which hydrogen bonding occurs between the polar moieties (as in FIG).

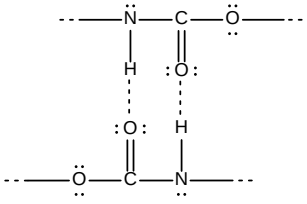

Figure 17. Hydrogen bonds between urethane groups

Thermoplasts are viscoelastic polymers that are not covalently cross-linked, but instead preserved as a solid by physical attraction between the polymer chains. The term «thermoplast» origins from the material's high dependency on temperature. At a sufficiently high temperature, the thermoplasts melt without degrading, allowing them to be re-molded.

Copolymers

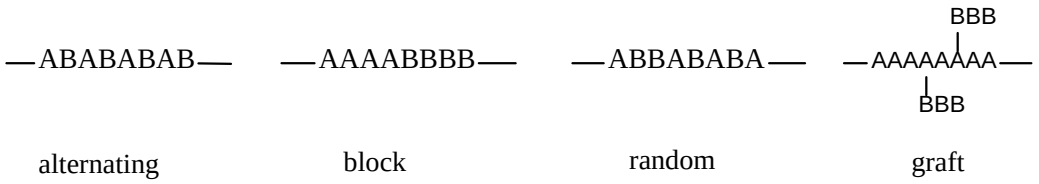

Figure 18. Symbolic illustration of different copolymer conformations.

Copolymers are polymers made up of different monomer units. FIG/SCHEME illustrates different copolymer structures in their simplest form (two monomers). *Alternating* copolymers have an absolute regularity in their structure, which makes them more prone to crystallize when cooled from the liquid state (McCrum, Buckley et al. 1997). *Random* copolymers have a coincidental distribution of monomers along the chain. The two building blocks have an equal affinity in coupling with themselves and with other available building blocks, creating a polymer with ideally no pattern. *Block copolymer*s are polymer chains with building block that are arranged in larger regions. Block copolymers can micro-phase separate, meaning that covalent bonded chains of normally immiscible blocks can arrange themselves to a pattern and create nanostructures. If the micro-phase separation is significant, then the block copolymer will exhibit split properties, similar to each of the repeating unit's properties (like glass transition temperature, see CROSS SECTION). A *graft copolymer* consists of a uniform chain, but with branches that have repeating units, different from the chain's repeating units. Note that each chain may consist of various types of subunits.

Analog to metal alloys, a polymer that consists of more than one element (repeating unit), may present qualities, better than polymers of the original repeating unit. The general outcome is that block and graft copolymers possess properties of both the homopolymers, where the alternating and random copolymers exhibit properties somewhere between the parent homopolymers.

Polymer characteristics

The glass transition temperature

All amorphous material exhibits a transition state where it alters physical properties. When surpassing this glass transition temperature region, the material's stiffness, heat capacity and thermal expansion coefficient changes significantly (Young and Lovell 1991). There are numerous ways of perceiving this transition region.

The molecular rotational movement associated with viscosity becomes retarded when cooling through T_g, and the material's structure changes from rubbery to glassy, a descripting which could be translated to a change in *free volume*. There is a steep increase in heat capacity upon heating, as a direct consequence of freely rotating molecules having higher heat capacity than glassy ones. But the T_g is *not* a phase transition temperature, at which the heat capacity is infinite at transition temperature. T_g is time dependent, meaning that heating- and cooling rate will influence a temperature lag on the observed T_g region (Sichina 2000). The glass transition region is also dependent on the degree of cross-linkage, prepolymer constituents, and the implementation of plasticizer.

Solid propellants require a binder system that stays elastomeric throughout all conditions. Practically, this requires a T_g sufficiently below working-, transportation-, and storage temperature. Surpassing the T_g one or

several times could induce internal stress and make a solid propellant prone to fracturing. Fractures will increase the burn surface, thus adversely increase the burn rate of the solid propellant.

The viscoelasticity of polymers

Polymers are considered to be viscoelastic materials, as they have elastic and viscous properties when a load is introduced. Newtonian fluids can dissipate energy, but not store it. An elastic solid can store energy, but not dissipate it. Applied energy that is stored and immediately released when the load is removed (like a spring), follows Hooke's law of linear elasticity: The longitude of strain is linear proportional to the magnitude of stress.

Figure 19. Left: elasticity explained by a spring, energy is stored. Right: dash pot, applied energy dissipates. In a viscoelastic polymer, both of the properties are represented.

Shear storage modulus (G') is a real quantification of the elastic energy (the recapitulating energy subsequent to a load), while the shear loss modulus (G'') is an imaginary quantification of dissipating energy (energy absorbed in the material, becoming diverging movement and heat), and represents the viscous nature of viscoelastic substances. The damping factor (tan δ) is a useful ratio when determining the *pot life* – the de-mold time of elastomer synthesis. The damping factor is given by:

$$\tan\delta = \frac{G''}{G'}$$

A rheometer could be used to monitor polymer curing, by measuring the viscosity and damping factor while the polymerization reaction happens. Consider the mixture of (reacting) prepolymer and curing agent at time = 0. The mix is viscous. As the curing agent links prepolymer chains into longer connections in a propagating fashion, the viscosity increases. The effect of cross-linking shows when most of all prepolymers and curing agents are utilized for chain-extension. The viscosity increases dramatically as cross-linking turns the fluid into an elastomer. A decrease in the damping factor is the direct consequence of increasing the storage modulus, and at tan δ equal to one, then G' is equal to G''. Time elapsed when tan δ equals one is often referred to as the pot life – a quantification of how fast a cross-linked polymerization reaction is. In practice, a pot life of typically ten hours is desired for production of a solid propellant as the process involves successive addition of components, mixing, pouring into a propellant-shaped mold and finally curing.

Time-Temperature Superposition principle

An ideal viscoelastic polymer, exposed to a dynamic load at a low enough frequency to allow all the polymer chains to comply and dissipate uniformly – will give a lower modulus than that of a higher frequency. At higher frequencies, the chains are not given the time to respond completely. This is the material's time-dependency. At a constant frequency, an increase in temperature will result in an increase in the material's free volume and chain mobility, thus leading to a lower elastic modulus. This is known as the temperature dependency. It was empirically shown that the material's behavior when altering temperature could be superposed to the behavior of altering time (frequency):

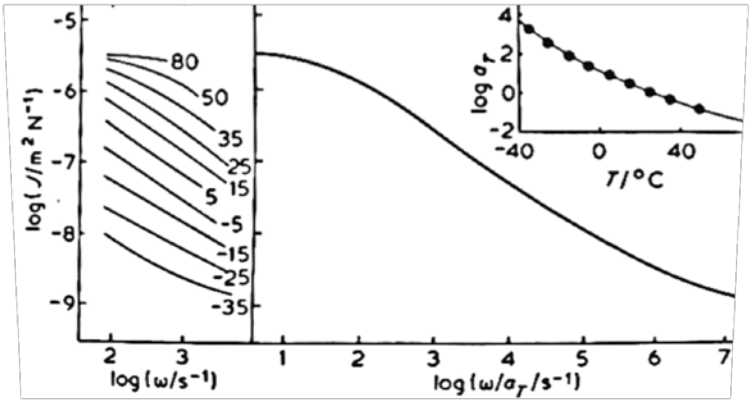

Figure 20. Left plot: Curves of a polymers shear compliance as a function of frequency, a total of 10 curves span the temperature region of -35 °C to +80 °C. Right: the finished master curve, estimating the polymers behavior in extrapolated frequencies (times). Small plot, top right: The WLF shift curve, explaining how the 10 curves will be shifted to best fit a master curve. Shift factor as afunction of temperature. One of the curves are fixed, the others are adjusted relative to the fixed one. Illustration exported from Energetic Polymers, by R. J. Young (Young and Lovell 1991)

A master curve consists of several superposed curves, of which a physical response (e.g. shear modulus, elastic modulus, or shear compliance) is described as a function of time or frequency. Both axes are logarithmic. The curves are shifted along the log frequency axis to overlap each other (FIG), relative The shift factor (a_T) defines the horizontal displacement of all the shifted curves along the log frequency axis (as a function temperature), and was explained empirically by the work of William, Landel and Ferry (Young and Lovell 1991) in their WLF equation:

$$\log a_T = \frac{-C_1(T - T_s)}{C_2 + (T - T_s)}$$

Where C_1 and C_2 are constants, T_s is the reference temperature from the fixed reference curve, and T is the curve temperature. When the WLF shift function (or another explanatory relation) is applicable, the behavior of a polymer can be predicted over a vast frequency (time) region. It should be mentioned that the curves also can be shifted vertically by a factor log T/T_s, in order to produce an optimal master curve. This is, however, of less importance. If a material obeys the time-temperature principle, then a master curve would provide a powerful tool for predicting the material's properties in time or temperature regions that are beyond measurable.

The approach

A short summary of promising solid propellant components will be listed to sweep the surface of traits a rocket scientist is concerned about: BuNENA is a high energy plasticizer with low sensitivity, compared to other nitrate ester plasticizers as NG and TMETN, a trait that eases production- and transportation regulations. HMX and RDX are high energy detonable nitramine crystals with relatively low sensitivity which burns steadily when utilized as oxidizing filler particles, introducing a lot of power and a minimum of smoke. An energetic binder would introduce more total energy, in addition to the conventional fuel contribution

(carbon backbone + oxidizer = combustion products). GAP is a high density prepolymer that introduces this additional energy. Furthermore, GAP is highly polar, and therefore compatible with the polar nitro based plasticizers.

A complete propellant formulation reported by Klaus Menke and Siegrfried Eisele {Eisele, 1990 #247} gave a maximum tensile strength of 0.65 MPa, 39.5 % elongation at break and an elastic modulus of 6.43 MPa for a GAP-based propellant. The mechanical properties were compared to an HTPB based formulation (See table 4). AP propellants are applicable to a variety of bonding agents. Enhanced mechanical properties could be a consequence of the implementation of such minor components.

Table 4. Reported mechanical properties for an HTPB based propellant, and a GAP based propellant.

Formulation by {Eisele, 1990 #247}	**«No. 27A»**	**«No. 103»**
Filler	AP (86 %)	AP (20 %) + HMX (45.5 %)
Binder system	HTPB/IPDI/DOA (12 %)	GAP/N100/TMETN (30 %)
Burn rate catalyst	2 %	4.5 %
Mechanical properties at 20 °C		
Elastic Modulus (MPa)	5.59	6.43
Peak stress (MPa)	0.64	0.65
Elongation (%)	19.5	39.5

Table 4 cannot be straightforwardly compared to the results obtained in this work, but gives an approximate understanding of how the mechanical properties are expected to be in a complete solid propellant formulation.

All the work behind this master thesis is directed towards improving composite solid propellant systems based on the energetic binder GAP. The main focus has been revealing and improving the mechanical and thermal properties of the propellant binder, since the binder is vital for the characteristics of these properties.

The work has been to prepare cross-linked polymers at laboratory scale, monitor their curing characteristic, as well as unveiling their mechanical and thermal qualities. T_g has been determined by DMA and DSC. Combustion characteristics have been investigated by TGA and DSC. The curing process has been monitored – quantitative measurements by rheology, and qualitatively by FTIR. Quantitative analysis of functional groups was conducted at Nammo, Raufoss. A large share of effort has been handed to the development of a versatile method for tensile testing of soft, energetic cross-linked polymer systems.

The cross-linked polymers that were prepared and characterized, contained prepolymer, curing agent, curing catalyst, and in selected binder systems, energetic plasticizer.

2. Experimental

2.1 Chemicals

Table 5. Summary of reagents and catalysts that has been used to create binder matrices.

Prepolymers	Lot # /type	CAS #	Producer
GAP diol	1. 06S12 2. 04S13	143178-24-9	Eurenco (groupe SNPE)
HTPB (R45M)	IRIS/DE/809296	N/A	Provided by Nammo
EP1900	1. SL 13091505 2. WH20091503	62628-35-7	Dow
TEG	BCBJ5792V	112-27-6	Sigma Aldrich
1,4-Butanediol	STBD2268V	110-63-4	Sigma Aldrich
PPG-PEG (D21/150)	-	N/A	Clariant
HTPE	898958 /PC-2	N/A	Provided by Nammo
HTCE	CAPA 7201A	N/A	Solvay
Curing agents			
Desmodur N100	1. LLO-621 2. LL2-675		
Baymidur K88 HV L		See table 9	Bayer
Baymidur K88		See table 9	Bayer
Desmodur VL 50		See table 9	Bayer
Vestanat IPDI	134168	4098-71-9	Evonic Degussa GmbH
Progargyl alcohol	STBB0293	107-19-7	Sigma Aldrich
BPOB	-	34596-36-6	Synthesized at FFI
Curing catalysts			
TPB	BSC-152-6-1001	603-33-8	-
DBTDL	5,6226-250	77-58-7	-
Plasticizers			
TMETN	-	3032-55-1	Provided by Nammo
BuNENA	-	82486-82-6	Provided by Nammo
Substances at the Nammo facilities, during quality analysis:			
Desmodur N100	ABL-4823	53200-31-0	Bayer
GAP diol	06S12	143178-24-9	Eurenco
EP1900	WH20091503	62628-35-7	Dow

Most chemicals are long-term stored in a refrigerator. HTCE and HTPE are stored in a freezer. The catalysts are stored separately in a closed cabinet.

A note to the reader: This thesis is sprinkled with trade names. Many prepolymers and curing agents are available as a crude mixture of statistically distributed isomers and homologs, of which the indiscrete blend of substances represents a quality in itself. It might be less convenient when newly discovered properties ought to be explained, but some depth is practiced on certain substances – with the means of enlightenment.

Aromatic isocyanates

As a supplement to the aliphatic isocyanate N100 and the di-functional aliphatic IPDI, three different MDI based isocyanate products has been ordered from Bayer Material Science. Being regarded as curing agents for retail and industrial scale, all three were unspecified isomers and homologs of MDI. The exact composition is unknown, but some information has been obtained. All of them are fluids at ambient temperature, which does not completely agree with 4,4-MDI being a solid at room temperature.

Table 6. Aromatic isocyanates and their respective components. Functionality has been aquired through regular curing reactions with GAP diol.

Trade name	functionality	Wt %	content	CAS #
Baymidur K88	> 2	75<100	Diphenylmethane diisocyanate, isomers and homologs	9016-87-9
		10<20	Diphenylmethane 4,4'-diisocyanate	101-68-8
		5<10	Diphenylmethane 2,4'-diisocyanate	5873-54-1
		1<5	Diphenylmethane 2,2'-diisocyanate	2536-05-2
Baymidur K88 HVL	> 2	≤100	Diphenylmethane diisocyanate, isomers and homologs	9016-87-9
Desmodur VL 50	≤ 2	50<75	Diphenylmethane 4,4'-diisocyanate	101-68-8
		25<50	Diphenylmethane 2,4'-diisocyanate	5873-54-1
		10<20	Diphenylmethane diisocyanate, isomers and homologs	9016-87-9
		1<5	Diphenylmethane 2,2'-diisocyanate	2536-05-2
		0.1<0.3	Isophtaloyl dichloride	99-63-8

They were all brown, low-viscous liquids, contained in aluminum flasks. Baymidur K88 is made up of diphenylmethane diisocyanate, in a somewhat intricate blend of different isomers (see table 9). Baymidur K88 was subjected to qualitative analysis at Nammo Raufoss.

Quality control

GAP diol, EP1900, N100 and K88 were subjected to quality control at Nammo, Raufoss. The analyses of relative OH- and NCO-levels were carried out with a Metrohm 751 GPD Titrino autotitrator, accompanied by a magnetic stirrer, 2 shifting units and a small printer. EP 1900 was subjected to water content quantification by *Karl Fischer oven titration,* where the water content of EP1900 was determined with a Metrohm Oven Sample processor, 851 KF Coulometer, and 801 Stirrer.

NCO-level determination

An isocyanate group reacts spontaneously with an amine to form urea. If a known amount of amines (abundant) is reacted with a known mass of isocyanate compound, then the amount of excess amino groups can be determined using strong acid, weak base titration.

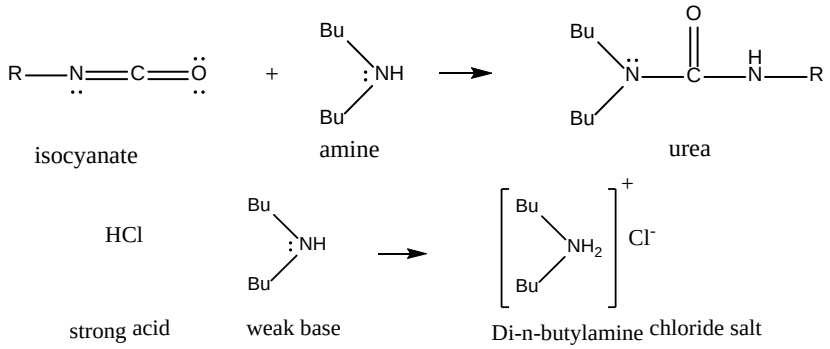

Solvents: Isopropanol, Toluene (dried with molecular sieve type 4A), di-n-butylamine solution (DBA), HCl, 1N. The analyte solution was placed upon a stirring unit, and both potentiometer and burette hose was sunk into the solution. The autotitrator was preprogrammed to coarsely add titrant before reaching the equivalence point (see FIG).

130 g of DBA was diluted with toluene in a 500mL measuring flask, and kept in a dark place for 24 hours. Two parallels of 5.0 ± 0.2 g N100 were weighed into 250 mL Erlenmeyer flasks (see APP for exact weights). Alongside the sample flask, two blind sample flasks were introduced from this point. Approximately 20mL toluene and exactly 25mL DBA-solution was added (with pipette and Peleus balloon). The samples were stirred with magnetic stirrer until the solutions appeared to be homogeneous, and rested for about 20 minutes. Prior to the titration, 100 mL isopropanol was added to each sample flask. The preparation of Baymidur K88 was performed in accordance with an approach identical to the preparations of N100, apart from weighed mass of analyte. According to the BAYER product data sheet (APP), K88 has a larger isocyanate group concentration than N100. Therefore approximately 3 g of K88 would avoid the necessity of altering the amount of titer solute and other solutions.

OH-level determination:

OH groups react with acetic anhydride in a 1:1 equimolar ratio, given the right circumstances. Acetic acid and an acylated derivate of the alcohol is the outcome, where the acetic acid can be quantified using a strong base titrant (SCHEME). The acetic anhydride is introduced to the analyte through an acylation reagent, consisting of 1 part acetic anhydride and 6 parts pyridine (blended in a measuring flask). The pyridine acts as a catalyst towards acylation.

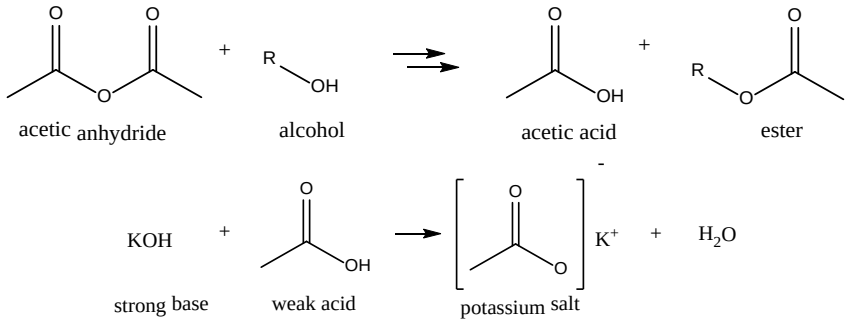

Solvents: Acetic anhydride, alcoholic potassium hydroxide (0.5 N KOH in methanol), isobutanol, toluene. The quantitative determination of hydroxyl groups in GAP diol and EP 1900 was processed by autotitrator, using a preprogrammed titration method tailored for the analysis.

GAP diol and EP 1900 were subjected to a general method: 2 g (for exact weights, see section 5.4) of prepolymer was weighed into three parallels of 100 mL Erlenmeyer flasks with ground glass heads and corresponding glass stoppers. From this step, three parallels of blind samples were subjected to an identical preparation method. Exact 5 mL of acylation reagent was added to each flask (a total of six) with glass pipette. The samples were placed into a 98 °C water bath for 2 hours. After 3 min cooling, 5 mL distilled water was added. 15 min later, 25 mL isobutanol and 15 mL toluene was added with glass pipettes. After thorough shaking, each sample was ready for potentiometric titrations using potassium hydroxide as titrant.

Water content

In general, the water content is commonly determined using *Loss on drying* (LOD), although drying may remove other volatile compounds as well as water (Bruttel and Schlink 2003). *Karl Fischer Titration* is an analysis method specific to water (Fischer 1935). The method is versatile and yield reproducible results, but non-soluble compounds need another approach. The *Karl Fischer Oven Method* is simply an extension of the original method: A sealed sample vial is heated, the vapor is extracted with a needle and carried towards a conventional titration cell (Porter, Margareth et al.).

2.2 Preparation and characterization

Safety precautions

Handling of viscous materials of highly energetic nature has been performed inside closed facilities built for this purpose. Lab coat or flame retardant work wear, protective shoes, gloves and glasses were of absolute necessity. Disposals were destructed at the facility. Safety data sheets of potentially unstable compounds were examined before handling.

Preparation of polymer samples

A constant fraction of curing catalyst (0.05% TPB), and as similar preparation steps and curing conditions as possible has been practiced. However, processing a GAP/N100 based cure has to personal experience demanded careful attention, as the polymerization reaction often accelerated at the stage of degassing. A lot of effort was contributed to the curing method at an early stage, and resulted in a mostly static procedure, except the degassing intensity, which had to be adjusted at site. Preheating the prepolymer at 60 °C was considered, because it would lower viscosity and thus aid the degassing process. However, preheated substances caused the weight to be less stable. If not mentioned otherwise, the preparation of the binder matrix proceeded as follows:

If retrieved from the refrigerator or freezer, the compounds have been acclimated in a ventilated environment at ambient temperature. Every ingredient has been weighed on a Mettler Toledo AB 104 laboratory weight. The substances were weighed in aluminum beakers. Firstly the curing catalyst, secondly the prepolymer, and lastly the curing agent. Then stirred thoroughly, but carefully, for 1-2 minutes – until the mixture became homogeneous – with a glass rod, degassed for 10 to 15 minutes at 60 °C, 5 to 20 mBar, and set to cure at 60 °C. Mixes prepared for the purpose of tensile testing were cast cured in 45mm x 109mm PTFE molds, with the bottom side covered with aluminum foil, a degassed a second time until the sample had a sufficiently void free structure. One day was normally sufficient for the cross-linkage to be complete. The heat- and vacuum chamber is a *Vacutherm* produced by Heraeus instruments, connected to an *Alcatel 1005* vane pump. For temperature- and humidity monitoring, a handheld *Rotronic Hygropalm* thermometer was used.

Several other published works have reported to consequently dry components before synthesis. Each effective day at the laboratory has been monitored by a handheld, potentiometric thermo- and hygrometer stationed by the weight and vacuum chambers. The conditions are appended (FIG APP), and one can observe the seasonal changes from October to April regarding humidity. The temperature is roughly unchanged throughout.

Cure monitoring

Rheology

The apparatus used for cure behavior monitoring was an Anton Paar Physica UDS 200 rheometer, and works as follows: A circular spindle with a known surface area is mounted on an air bearing vertical axis. The sample is positioned between the spindle (MP 30, 25mm, 0 ° cone) and a planar, thermally regulated surface, with a distance of 0.5 mm. Optionally, the spindle can fully rotate or oscillate at given amplitude and frequency.

Standard inputs are 1 % oscillation at 1 Hz. Either shear load or shear force is set, and the opposite parameter is measured over a function of time. This method is used to observe curing qualities of polymer substances. If not mentioned otherwise, the settings for Paar Physica UDS 200 is set to have 216 data point, with 5 minutes of measure duration, at a temperature of normally 60 °C.

FTIR

The instrument used was a Thermo Nicolet FTIR with a ZnSe-crystal plate application. The plate works as a beam reflector, sending a single infrared beam to several points on the surface of the plate. This accessory collects data over a relatively large area. Also, the horizontal plate makes it easy to apply and remove samples. In order to comply with Beer-Lambert law, the absorbance had to be below a value of 1.5. With that in mind the plate should not be completely covered by the test sample, which might overload the largest signal peaks. The software was Omnic, preset to the ARK. HATR smart accessory ZnSe plate. Number of scans was 32, with a resolution of 4. The beam source was a DTGS KBr with an aperture of 100 and sample gain of 8.

Mechanical testing

Tensile testing

Inert tow Tensile testing was carried out on a MTS (high rate test system), with a Flextest 40 digital controller, and Testworks 4 software. The dog bones were cut out in one piece with an ASTM D1708 sharp-edged stamp, provided by Qualitest. The cutting was assisted by a Blell DW 7082 hydraulic machine press. The sample specimens were fixed with two custom developed clamps specially intended for soft polymer samples. Tensile testing was conducted with a break Sensitivity of 75 %, a break threshold of 10 N, the data acquisition rate was 10.0 Hz, and the crosshead speed was 50 mm/min.

When a single stress/strain curve is selected as a representative to illustrate the performance of a binder matrix, the median curve in respect of modulus and strain, will often be the appropriate option. An objective selection process is exercised. All tensile test specimens (except T2-6,7,8) have been monitored and individually documented for re-traceability when observations were worth mentioning. The net dimensions of dog bone samples were each manually measured regarding thickness and width, with a caliper. The samples were approximately 21 mm long (between the two clamps), 5 mm wide, and preferably about 4 mm thick. The thickness was dependent on the volume of sample poured into the mold.

Tensile testing is conducted to examine stress- strain properties of the polymeric substances. Temperature is of great importance regarding the mechanical properties of a polymer matrix. Dog bone samples have been handled with the intention of maintaining internal sample temperature equal to room temperature. Tensile tests were conducted 14th of February, 4th of March, 17th of March and 9th of April. The appended temperature table (appended TABLE in section 5.1) should be representable, and ambient temperature when tensile tests were conducted is arguably set as 21°C.

Shore A hardness

The Shore A hardness was measured with a Bareiss BS61 durometer. The samples were indented with the durometer five times each, at spread regions – giving five parallels for each polymer sample. Where possible, the samples were measured both at the top and the bottom of the sample.

Thermal analysis

DMA

Polymer samples were subjected to *Dynamic Mechanical Analysis* (DMA) on a DMA 2980 from TA Instruments. Data has been processed with the «Universal Analysis 2000» and «TTS Data Analysis» softwares. The Poisson's ratio parameter was preset to 0.44. According to STANAG 4540 (STANAG), T_g should be defined by the 1 Hz peak loss modulus obtained from DMA. The curves have a delayed response due to the limited thermal conductivity in the sample subject. The effect of such a delay is previously reported to be negligible if the change in temperature does not exceed roughly 0.3 °C/min (Knut Magne Hansen 2003).

T_g acquisition was performed in a dual cantilever mode, except for the stiffest samples, which were run in 3-point bending mode. A frequency of 1 Hz was utilized, whereas the oscillating amplitude was 15 µm. Due to temperature lag in the samples upon heating and cooling, each experiment was conducted by both heating and cooling through the glass transition region (3 °C/min). T_g was determined by the average of the two temperatures (heating and cooling) that gave a maximum in the loss modulus.

For master curve acquisition seven frequencies (0.1, 0.3, 1, 3, 10, 30 and 100 Hz) were applied. The experiments were performed in dual cantilever mode with an oscillating amplitude of 20 µm. After 30 min at -60 °C, the temperature was increased in steps of 2 °C until it reached 40 °C, and a frequency sweep was carried out at each temperature. Before each frequency sweep, the sample was allowed to settle isothermally for 2 min. This temperature profile led to an average heating rate of 0.3 °C/min, low enough to extract T_g value from the 1 Hz curve.

TGA

Thermo-Gravimetric Analysis (TGA) was carried out on a Mettler Toledo TGA/SDTA861 instrument, with a TSO 801RO sample robot, and STARe evaluation software. The samples were placed in 70µL open alumina crucibles, and heated (10 °C(min) in nitrogen atmosphere, in the temperature range of 40 °C to 500 °C.

The Sample mass subjected to TGA should exceed 1 mg to avoid measurement inaccuracy, but not surpass 2-3 mg to obtain a reproducible weight loss (Knut Magne Hansen 2003). An optimal temperature increment has been investigated at FFI by Knut Magne Hansen (Knut Magne Hansen 2003), where 0.1 °C/min allowed unwanted side-reactions to interfere. 1 °C/min gave good results, but the overall duration was long. A practical approach that achieves proper results was shown to be 10 °C/min.

DSC

Differential Scanning Calorimetry (DSC) was exercised on a DSC Q1000 from TA Instruments, aided by the software Universal Analysis 2000. The samples were weighed and placed in aluminum pans with a shrink-fastened lid, and were subjected to temperatures from -80 °C to 400 °C at a heating rate of 10 °C/min in nitrogen atmosphere.

3. Results and discussion

Terms and relations

Every sample is tagged as **T1, T2 or T3**, followed by a chronologically increasing number (except T1). **T1** is related to the introductory research prior to tensile testing, typically 10 gram of sample. **T2** samples are principally of 30 gram PTFE molds, a suitable size in order to yield five parallels for tensile testing and still have enough material for other relevant analysis, e.g. DMA. **T3** samples are in total five promising binder systems, where plasticizer is introduced.

As a simplification, the use of curing catalyst is not specified in most of the composition tags. The reader can assume an addition of triphenyl bismuth (TPB), normally in 0.050 wt % for each sample. Exceptions will be declared. Processing of each sample required active involvement and adjustment to yield acceptable polymer matrices, specifically homogeneity, a minimum of air voids, and of course conditions for a steady curing reaction. The work towards a versatile curing method is explained in section 3.1. For further ease in interpreting the results, the parameters that are highly characteristic for these polymer samples have been assigned suitable abbreviations:

NCO:OH — explains the stoichiometric ratio of isocyanate per hydroxyl group. Alternative expressions are c/p (*curative/prepolymer)*, or *R ratio*. They are all identically calculated. NCO:OH is tightly related to cross-linkage, and used as such for comparison of polymers with the same curing agent (here, mostly Desmodur N100).

BPOB:GAP — is a c/p- oriented expression of curing agent concentration for isocyanate free polymerization (specifically BPOB. See APP calc.) It is intentionally comparable to isocyanate polymerization, and complies with the research topic of isocyanate free curing at FFI.

po2/po1 — is an abbreviation of *prepolymer2/prepolymer1*: Quantifies the presence of secondary prepolymer relative to primary prepolymer (always GAP diol), regarding molar amount of hydroxyl group (see APP calc).

pl/po — *plasticizer:prepolymer* is a measure of plasticizer content. One could also use weight fraction of plasticizer, but pl/po is easier to use in polymer preparation, and is just as explanatory when the binder system is based on the same prepolymer.

The presented values of shore A hardness, peak stress and elastic modulus are assigned the precision that their respective standard deviations allow them to have. Standard deviations are calculated with the loss of one degree of freedom.

3.1 Introductory research

Curing conditions

The choice of curing mold has shown to be of crucial importance when isocyanates are involved in the elastomeric polymer synthesis. Preliminary experiments gave unpredictable results – often a highly accelerated reaction while still under degassing (pressure < 100 mBar). White weighing ships of polystyrene (PS) disintegrated after two days when introduced to certain isocyanate liquids at 60 °C, namely: IPDI, K88 HVL, and VL 50. The isocyanates are believed to simply dissolve the polystyrene weighing ships. K88 HV L and VL 50 are aromatic substances that are believed to readily merge with the highly aromatic PS. K88 did, however, not visibly interact. A similar experiment with hard, transparent plastic vials (supposedly PS) resulted in the following observation: VL 50 disintegrated the vial, whereas the other did not. Plastic cups/vials are believed to contain additives as pigment compounds, antioxidants or plasticizers, which might cause side reactions, but any further conclusions on this were not drawn. Polyethylene (PE) is recognized as chemically inert, and early experience with PE-cups did not present any issues. As a safe choice, aluminum cups are preferred and used with success for most sample preparations and small scale molds.

a)  b) 

Figure 21. a) Aluminum cups for weighing of substances, molds for smaller preliminary cures, and occasionally curing of tensile tested products. b) The PTFE mold in which the liquid polymer solution is poured, and set to cure. The bottom is covered with aluminum foil, tighened to give a smooth surface. Normally 30 grams of sample is sufficient for tensile tests, DMA and Shore A hardness tests.

Curing molds of PTFE did also, to my surprise, cause a relatively intense gaseous escape under vacuum (somewhere between normal degassing and boiling, considering the highly viscous solution). A possible explanation could be a high specific surface area on the PTFE modules, at which gas could have a large affinity towards and accumulate. An inconclusive but pragmatic approach was made. The bottom of the molds was covered with aluminum, as shown in figure FIG. This gave clear, smooth cures practically free from bubbles.

The conclusive method of preparing an adequate polymer matrix can be found in section 2.2.

Quality control

NCO-level determination

The method required blind samples to calculate functional group consume (see section 2.2). The mean of two blind titrations were used in both calculations of K88 and N100, since the tests were executed with the very same solvents, method, and instrument at the same day.

$$NCO\ content\ (meq/g) = \frac{(B - S) \times N}{W}$$

Where *B* is average blind titrant consume (mL), *S* is analyte sample titrant consume (mL), *N* is titrant normality (eq/L), and *W* is weight of analyte (g). NCO content is often denoted % NCO, which demands only a small advance from the former calculation:

$$\%NCO = \frac{NCOcontent\ (meq/g)\ \times 42\,{}^{g}/_{mol} \times 100\%}{1000}$$

NCO content analysis of Baymidur K88 gave precise results which concurred with values presented by the manufacturer. Analysis of 2 different N100 samples gave almost equally precise results, and reveal.

Table 7. Results from two NCO-level titrations of Baymidur K88 and Desmodur N100.

Substance	Titration 1	Titration 2	Average	σ	product datasheet
Baymidur K88	31.20 %	31.91 %	31.6 %	0.5 %	31.5 ± 0.5 %
Desmodur N100	22.03 %	21.87 %	22.0 %	0.1 %	22 %

OH-level determination

$$OH\ content\ (meq/g) = \frac{(B - S) \times N}{W}$$

Presents the equation for OH content determination, where B is mean blind titrant consume (mL), S is analyte sample titrant consume (mL), N is Normality of titrant (eq/L), and W is measured mass of analyte (g). The titration of GAP diol gave OH values comparable with previous results at Nammo, regarding accuracy and precision. The titration results for EP1900 were less precise. Some more parallels may have been favorable in order to find a more accurate OH-level.

Table 8. The comparable results from Nammo is from three different lots, each a mean of three measurements.

Prepolymer	Titration parallels			Average	σ	Nammo results
	Titration 1	Titration 2	Titration 3			
GAP diol (meq/g)	0.800	0.823	0.817	0.81	0.01	0.75
EP1900 (meq/g)	0.345	0.171	0.280	0.27	0.09	-

Water content analysis

The water fraction of prepolymers is dependent of its exposure to air moisture, hence are measured values of water content expected to vary. An average of three parallels were chosen to represent the water content (in wt %).

Table 9. Water content in EP 1900, determined by Karl Fischer water determination. Three parallels, their average and standard deviation for the discrete set of samples.

Voranol EP 1900	Parallels			Average	σ	Dow® product catalogue
	1	2	3			
Water content (wt %)	0.0524	0.0399	0.0443	0.046	0.006	< 0.1

Isocyanates and water react to produce polyurea. Water is highly mobile, and once it is introduced to isocyanate, it is believed to react easily. The literature presents a slightly more favorable reaction towards water (than n-butanol reacting with isocyanato-benzene) when no catalyst is involved {Dewhurst, #206}. EP 1900 is a diol with an approximate molecular weight of 4140 g/mol. The water content, given in molar fraction of prepolymer, becomes:

$$water\ content, molar\ fraction\ of\ prepolymer = \frac{\frac{0.00046\ g}{18\ g/mol}water}{\frac{1g}{4140\ g/mol}prepolymer} \times 100 \approx 10\ \%\ ^{n}/_{n}$$

A weight fraction of 0.046 % water in the EP 1900 batch corresponds to about 10 % water molecules per EP1900 prepolymer. Recognizing EP1900 as a diol, the water molecules make up for 5 % of total hydroxyl groups. One water molecule consumes an extra isocyanate to produce urea:

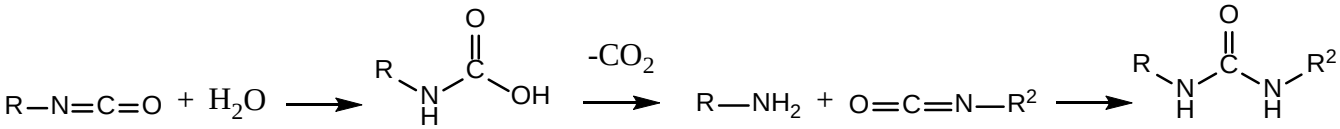

TGA

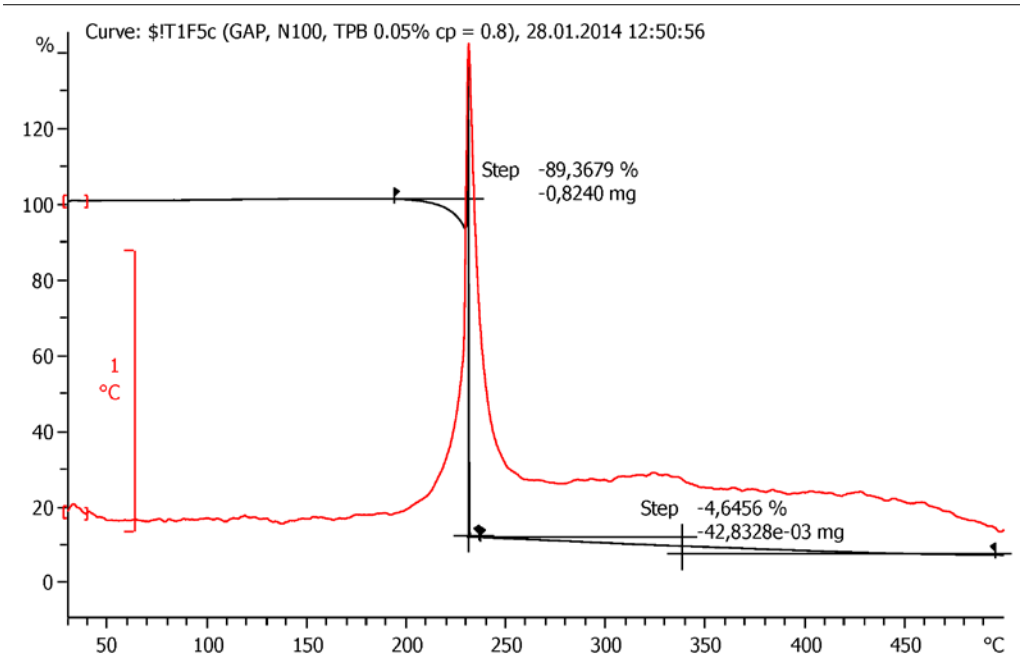

Figure 22. TGA curve of a GAP/N100/TPB matrix. The black curve is relative weight loss, the red curve is a calculated SDTA curve.

A representative thermo-gravimetric analysis of GAP/N100 (sample T1F5c) is illustrated in figure FIG. The scission of N_2 from the azide group is observed at 230 °C, where also 90 % of the total weight loss is located, specifically in the temperature interval of 200-235 °C. In an ideal composition with GAP where the scission of azide to form nitrogen gas occur separately with other reactions, the first weight loss would represent the scission of N-N_2 bonds, at which the weight fraction would relate to the mass fraction of N_2. More specific (scheme obtained from Haas et al. (Haas, Eliahu et al. 1994)):

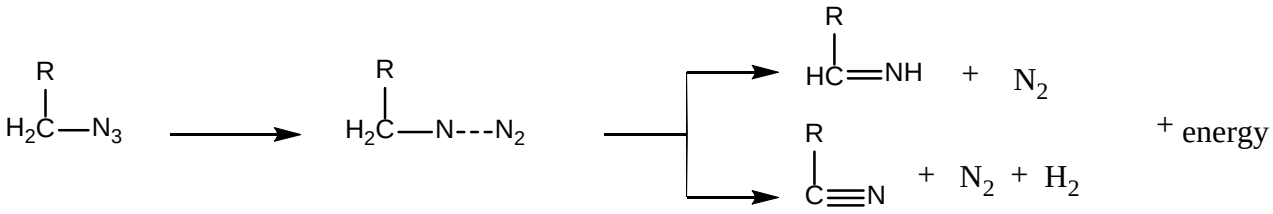

The release of N_2 would, for a GAP/N100 sample with an NCO:OH ratio of 0.8 (sample T1F5c in FIG) relate to about 25 % weight loss. A 90 % weight loss does not harmonize with the assumptions of basically just nitrogen gas to be produced in the pyrolysis. The heat production causes nearly everything to disintegrate at once. HCN, CO_2, CO, H_2O and other gases are released (depending on the chemical composition of the sample). From 235 °C to 500 °C, about 5 % of the mass has been lost, which implies 5 % carbonaceous residue in the crucible. A proper incineration with a blow torch was sufficient to remove the char remnants and reuse the crucibles.

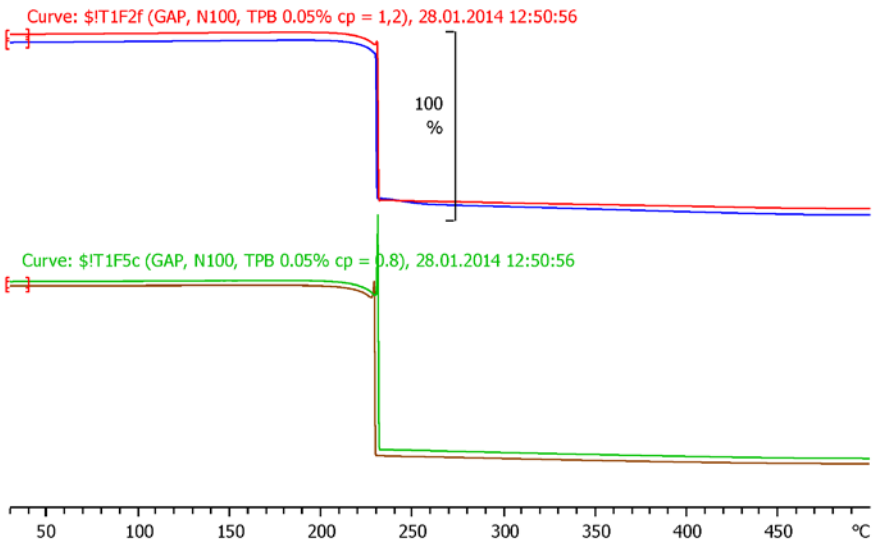

Figure 23. TGA. Comparison of two NCO:OH variations of GAP/N100. The Y-axis is floating in order to allow a curve offset.

FIG compares two parallels for each two NCO:OH variations of GAP/N100 (NCO:OH = 1.2 above, 0.8 underneath). One can observe an accelerating mass drop starting at 200 °C, ending in a sudden, devastating degeneration at 230 °C. GAP is more dominant at the two lowest curves. A small weight increase was observed, which comes from a small thrust upwards from the open 70 µL alumina crucible (green curve in FIG: At a cross-linkage ratio of 0.8, less curing agent is applied). The combustion of GAP/N100 is exothermic, which can be illustrated in differential scanning calorimetry, but also indirectly through *Single Differential Thermal Analysis* (SDTA, red curve on FIG). The STDA curve is a feature from Mettler Toledo, which calculates a theoretical heat flow:

$$SDTA = T_s - T_r$$

Where T_s is measured sample temperature and T_r is reference temperature calculated from the furnace temperature. It should be announced that SDTA cannot replace DSC. An example follows:

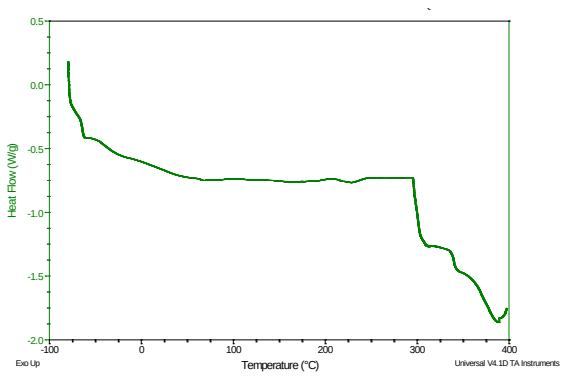

Figure 25. DSC curve of PPG-PEG/N100. Should be compared to the calculated SDTA curve from TGA to point out its contradiction to the measured heat flow from this DSC curve. Exothermal upwards.

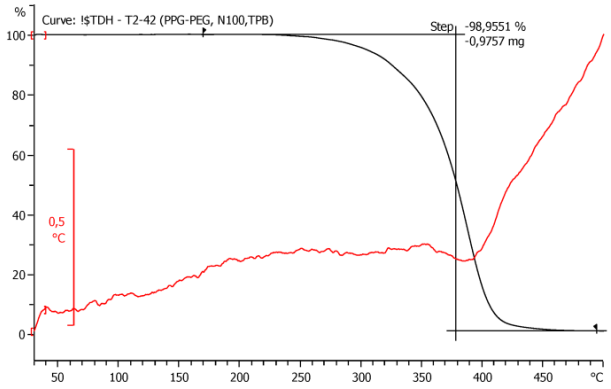

Figure 24. Thermo-gravimetric analysis of PPG-PEG/N100. The seemingly exothermic finale at 400 – 500 °C is highly ambiguous when compared to DSC. Exothermal upwards.

FIG and FIG are comparisons of the same sample (T2-42). Although they are not entitled with the same units, they are both a measure of endo-/exothermic behavior. In this case, they are fundamentally disagreeing. When the weight loss by determined by TGA is small, the SDTA is concluded to be unreliable. The use of heavy alumina crucibles could be responsible for unreliable SDTA calculations.

DSC

From previous work conducted by Haugmo at FFI {Haugmo, 2007 #225}, the temperature increment in a differential scanning calorimetry run should not be too low, thus veiling some signals. 10 °C/min gave clearer signals than 1 °C/min for DSC analysis of BuNENA, specifically.

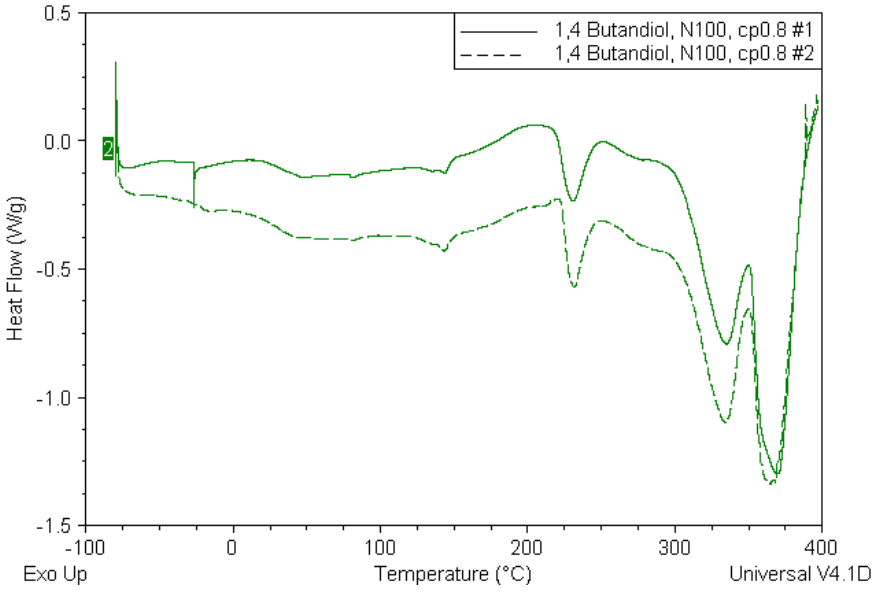

Figure 26. Differential Scanning Calorimetry of 1,4-butanediol/N100 (sample T1-1,4But0.8).

Some differences in heat flow are observed from most DSC parallels. Although the signal magnitude is different, the peak temperatures are equal. Proper contact between crucible and instrument is considered important in order to get accurate DSC measurements. Twofold DSC curves of HTPE, HTCE, HTPB and TEG are appended, and reveal varying precision. When conducting DSC analysis, two parallels is advised (as a time saver, in case of one corrupt curve).

Determination of T_g by DMA and DSC

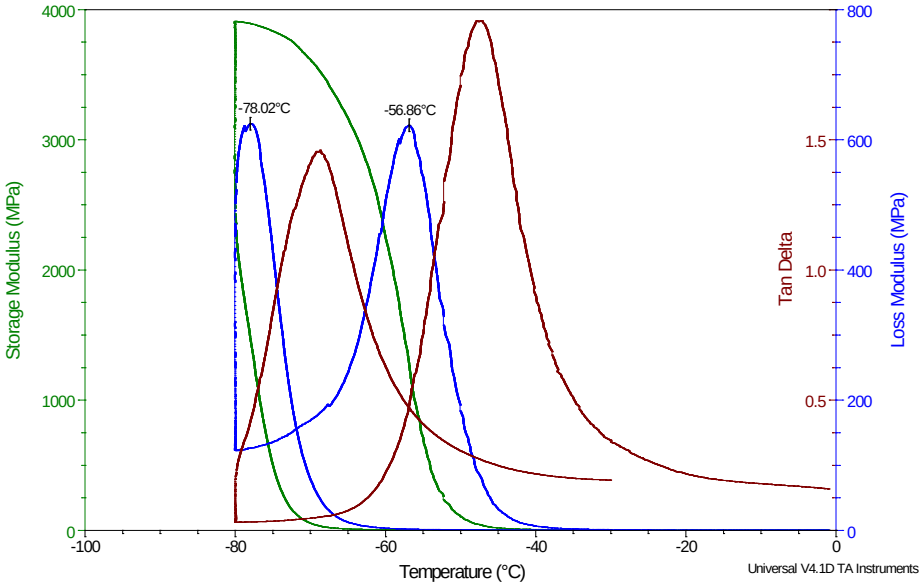

Figure 27. Dynamic mechanical analysis of T2-43. Glass transition temperature region is passed twice at 3°C/min, the average of both loss modulus peaks determine T_g.

$$T_{g\,(T2-43)} = \left(\frac{-78.02°C - 56.86°C}{2}\right) = -67.44°C$$

By DMA, the glass transition temperature of EP1900/N100 (T2-43) is -67 °C. The glass transition region can also be found by differential scanning calorimetry:

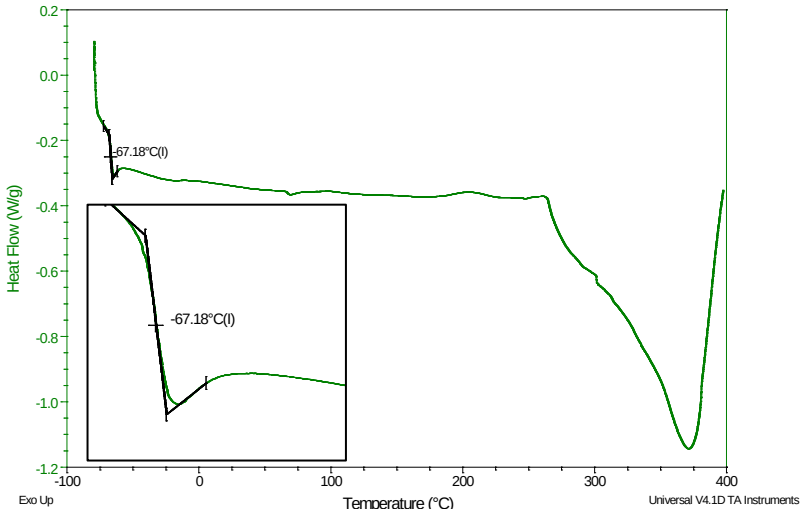

Figure 28. DSC curve of EP1900/N100 (T1F6a2). The suspected T_g-point is magnified. DMA analysis of T2-43 confirmed T_g.

Figure FIG is a DSC analysis of the same composition (sample T1F6a2, which is formally identical to T2-43), where an endothermic signal is observed below -60 °C. The mid-set point (the turning point for tangent line of the heat flow) is systematically chosen to the determine T_g: -67°C. To ensure that an endothermal signal is not a phase transition or vaporization of an extremely volatile compound, DSC should be compared to DMA,

which observes physical changes as a significant change in the storage modulus. When the glass transition region is predicted to appear within a region, DSC is a versatile and fast approach.

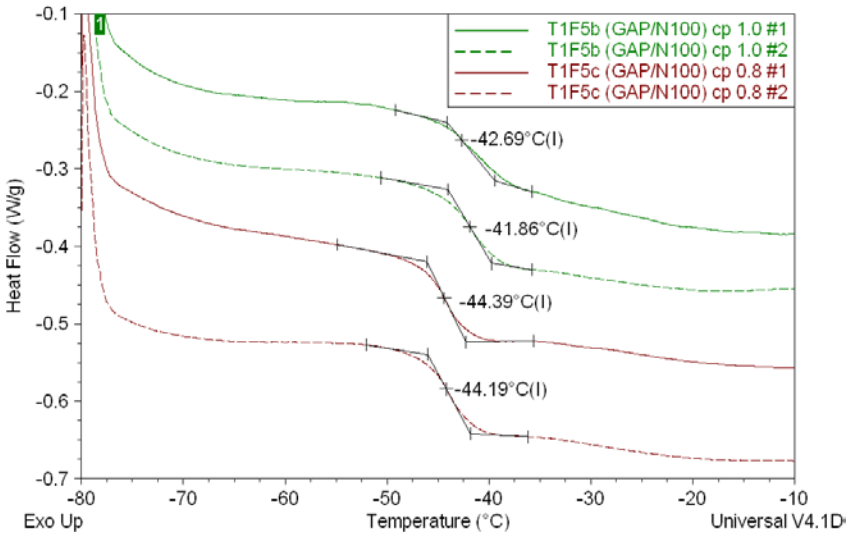

Figure 29. Two varieties of GAP/N100, having two parallels each.

FIG reveals that the NCO:OH ratio influences T_g, which concurs with the recognition of T_g being dependent on cross-linkage. The deviance is, however, not severe. When perceiving T_g as a region, all DSC runs address a roughly uniform T_g for GAP/N100. T_g is determined to be -43 °C for GAP/N100 at a NCO:OH ratio of 1. A more comprehensive research of the relationship between T_g and NCO:OH ratio is reported by Kasicki et al. (Kasicki 2001).

Rheology

The curing processes was frequently monitored by rheology, where one could observe the complex viscosity |η*| and storage modulus G' increase, while loss modulus G'' decreased, implying an increasingly cross-linked polymer matrix. Complex viscosity (red curve) displays that cross-linkage had already started when the sample was placed on the rheometer. Pot life (tan δ) can be visually recognized by the intersection of the storage modulus curve (green) and the loss modulus curve (blue). Significant amounts of rheometrical data was gathered, although, lastly, a limited necessity for curing characteristic interpretations was needed. All the successfully cured binder samples showed an essentially similar curve as the one illustrated in figure FIG, whereas the unsuccessful were recognized by not increasing in complex viscosity or storage modulus.

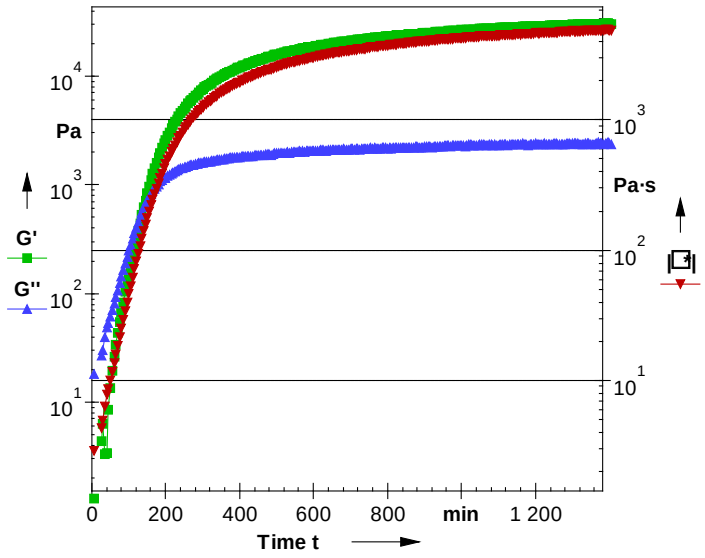

Figure 30. Typical curve obtained from rheometrical monitoring. GAP/IPDI/N100/TPB.

FTIR

A characterization of the reaction kinetics has not been the main concern of this work, as tensile testing required the vacant effort. Nevertheless, some recognition of the versatile tool FTIR has been made. FIG: Urethane polymerization is clearly addressed with FTIR curves at the initial stage, and after the curing of GAP/TEG/N100/TPB (sample T2-23). The blue curve is a spectrum of the initial stage of isocyanate depletion to form urethane. The red curve displays a spectrum recorded after the reaction was completed.

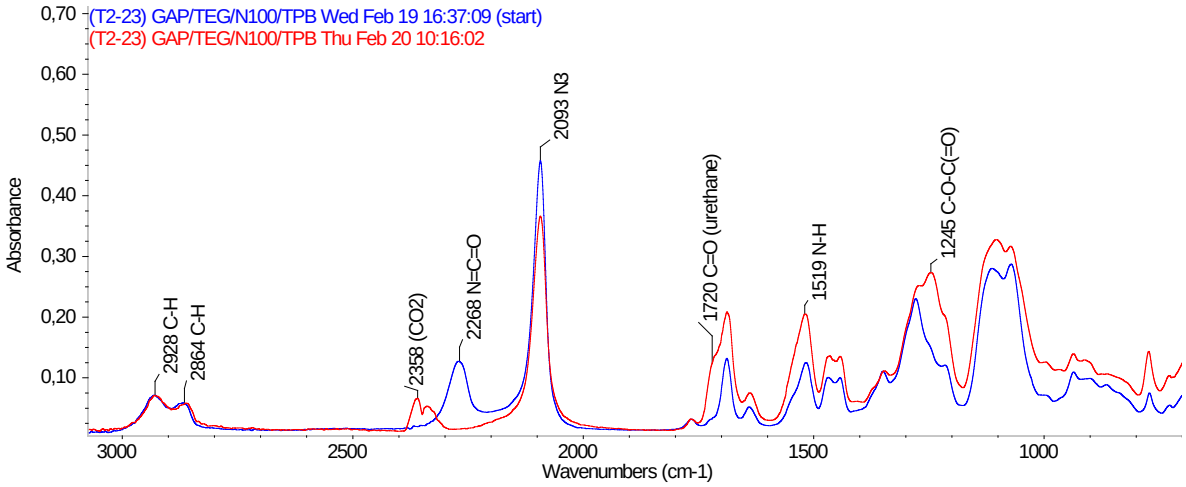

Figure 31. FTIR of T2-23, at the initial stage, and after urethane polymerization.

The two IR bands at 2928 cm^{-1} and 2864 cm^{-1} are assigned to asymmetrical and symmetrical C-H stretching, respectively. They are typically used as internal standard when quantifying peak heights or areas, because interference of these bonds is not expected. In FIG, they are roughly aligned to standardize the two curves. 2268 cm^{-1} is the characteristic isocyanate signal. The depletion of isocyanate is characterized by weakening of the isocyanate signal. In order to conclude that the consumption of isocyanate produces urethane, one can check if the intensities of typical urethane absorptions increase. Characteristics are the shoulder at 1720 cm^{-1}

which represents the carbonyl of urethane, the 1519 cm^{-1} bend which is the respective secondary amine of urethane, and 1245 cm^{-1}, that arguably represents ether with carbonyl vicinity. The largest band of 2093 cm^{-1} is the characteristic azide absorbance of GAP. Unwanted side reactions could possibly be revealed by IR. Urea possesses a characteristic carbonyl absorbance at 1695 cm^{-1}. However, the urea polymerization is difficult to observe due to the veiling urea resemblance of the biuret N100.

Tensile testing

Shusser states a preferably high tensile strength and elongation, but low modulus of elasticity for binder systems (Shusser 2012). Characteristics as those spoken of origin from low cross-linkage density, offering respectable tear resistance in a solid propellant, which is important to reduce the potential of internal stress and thereby risk of ruptures in a long perspective.

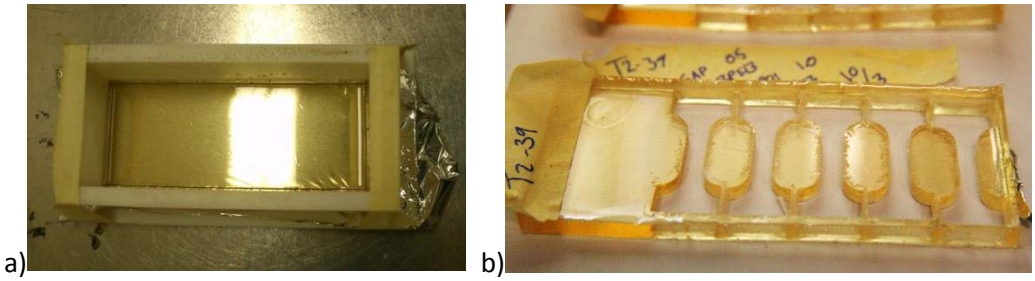

Figure 33. a) A finished cure of a binder sample, still in its PTFE mold. b) the left-overs after the specimens have been cut out.

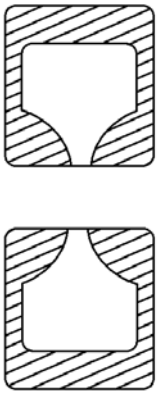

Figure 32. simplistic sketch of how the static jigs are formed.

Mechanical properties for an acceptable solid propellant are typically: ≥ 0.7 MPa in tensile strength, ≥ 50 % elongation and an elastic modulus of 3 MPa. Note that those are values for the whole propellant, including filler, plasticizers and additives.

Mechanical strength is an important and principally simple property that reveals the most important feature of the binder – namely how well it can hold on to the solid propellant composition. At a constant rate of 50 mm/min, the sample specimens comply differently.

Alternative methods

A conventional approach to tensile testing is the d*og bone* test. The sample is cut out in one piece from the sample material. Solid jigs fixate the largest ends of the dog bone (FIG). The forthcoming issue lies in the stretching. At elongation, there is a possibility that the massive ends contribute some to the elongation of the sample, creating an immeasurable interference. This may not be a problem for the stiffer, complete solid propellant compositions, but would be more relevant for tensile testing of soft binder matrices.

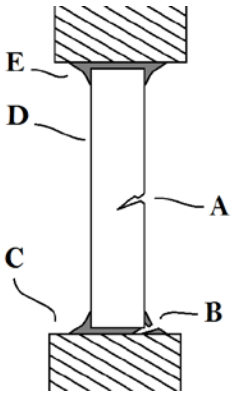

Figure 34. end-bonded set up of a tensile test sample. D is the sample, C is metal cubes on which the sample is mounted, by glue at point E. A marks cohesive breakage, B is adhesive breakage.

A material-efficient method is the end-bonded adhesion toward solid cubes. The cubes are glued to each end of a rectangular piece of the sample, giving two anchoring points. This method is prone to adhesive breaks (FIG adhesive-cohesive),

giving an accurate elastic modulus, but possibly a premature break. Tensile test results are preferred to have a *cohesive* break – the terminating break should occur because of the strength of the sample itself, not due to any weakness in the fixation.

A more comprehensive approach would be the conventional dog bone test with static jigs and two marked spot on the dog bone, monitored by a camera to read the displacement of the spots and thereby getting a more ralistic measurement of the elongation. For very soft elastomers, the load output would still be corrupted if the sample specimen would slip out of the jig.

Personally developed dynamic clamps

In the absence of any immediate solution to the problem, a set of personally designed dynamical jigs emerged (FIG). The concept was deliberately simple, and had characteristics directly smuggled from tensile testing of more rigid materials. Specifically the angle α (FIG a) was of crucial importance. A too narrow angle would give both exaggerated tightening and too much false strain by the gradually increasing load as the sample stretches. The angle was chosen to be 16.5 °. The «teeth» (the movable parts, FIG) were shortened in order to keep the fixed dog bone sample within the clamp body, so that the load did not focus on the screws that held the teeth in place – but instead utilized the force to tighten the sample.

Although mounting a dog bone sample to the clamps require some initial «fingerspitzgefühl» to deliver comparable results, the approach is fairly easy. The bottom clamp has two small springs that pulls the weight of the teeth upwards. This simplifies the mounting of a sample, as it is preferably fastened at the bottom first, allowing one hand to adjust the height, and the other to handle the top clamp teeth. The teeth surfaces are roughened to give more friction towards an elastic polymer, simply by indenting the aluminum teeth with a engraving pen with a small angle to create a barbed surface. The teeth are locked by one screw each, but sufficiently loose in order to allow them to move freely up- and downwards.

a) b) c) d)

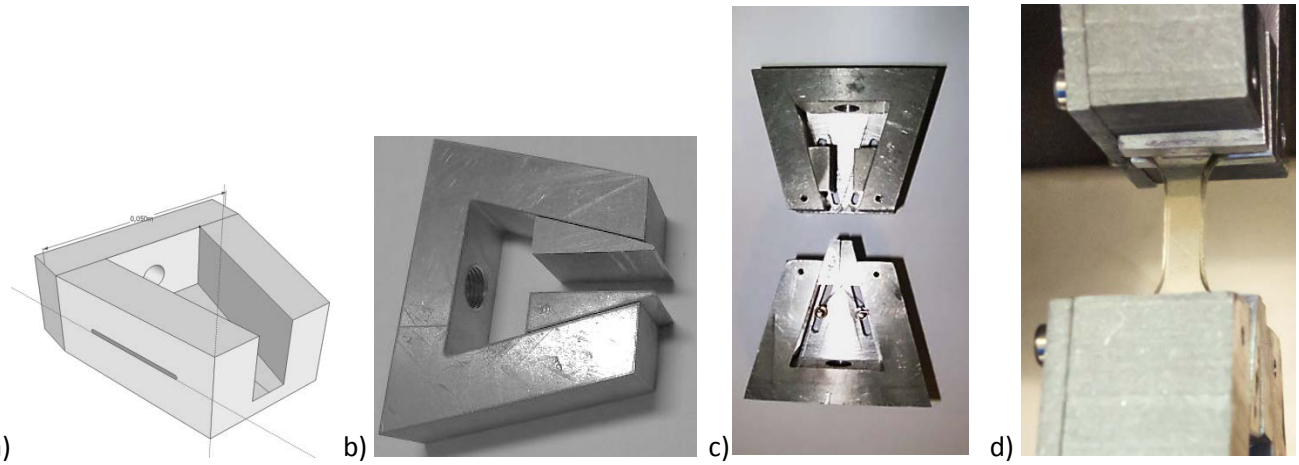

Figure 35. a) Basic ideal sketch of the construction, early stage. Constructed in Google Sketch Up 8.
b) One set of the components. All parts were cut out from the same aluminum piece, using a water jet cutter.
c) The finished pair of custom-engineered clamping tools. Fairly simple, but thoughtfully designed.
d) The clamps in action, at the initial stage of a tensile test.

a)  b)  c) 

Figure 36. Sample specimens subjected to tensile testing. a) EP1900/N100 (T2-6) b) GAP/N100 (T2-7) c) HTPB/IPDI (T2-8)

A material naturally gets slimmer when pulled. A dog bone sample utilizes its geometry to focus the strain to the narrowest region. Withholding the samples at their largest surface would arguably minimize any elongation caused by the dog bone material gradually delocalizing out of its grip. A contribution will, however, be caused by the tightening movements of the teeth. Such a factor is believed to be reliable, and can be found.

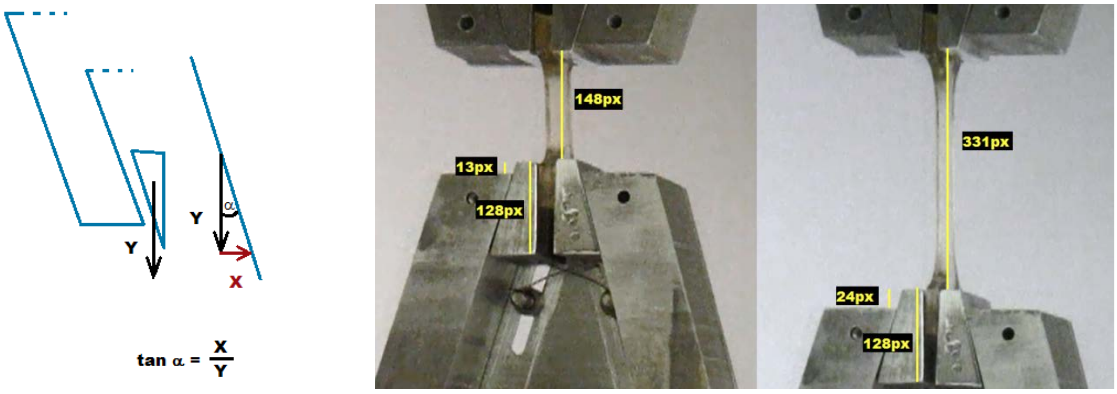

Figure 37. Elongation caused by dynamic clamping, a simple demonstration of start and close-to break of dog bone sample, pixel count with one of the clamp teeth as an internal size, for the assurance.

Simply obtained from pixel counting, an actual tensile test of a dog bone specimen could evaluate the method applicability:

$$total\ elongation = \frac{331px - 148px}{148px} \times 100\ \% = 124\ \%$$

The dog bone is stretched 124 % (2.2 times its original length)

$$\frac{elongation\ caused\ by\ tightening}{total\ elongation} = \frac{(24px - 13px)}{(24px - 13px + 331px - 148px)} = 0.57$$

At which 5.7 % of the total elongation (of 124 %) is explained by the gradually compression of the sample specimen. The effect of tightening can be compensated for, and the dynamic feature of the clamps could be considered beneficial as a significant aid of withholding the tensile specimen beyond breakage.

As for the method sensitivity, a plasticized binder (T3-1, see section 3.5) showed the smallest load at peak stress, due to its thin sample specimen, merely 1.8 mm. The software requires data of width, thickness and subjected length to translate the results into the material-specific unit of Pascal. The input load of about 130 g is nevertheless considered low.

3.2 Polyurethane binder systems

It is believed that nearly all synthetic polymers that create a flexible matrix, have been investigated for solid propellant binder applications – with varying success (Shusser 2012). The step-growth polymerization of urethane from alcohol and isocyanate exhausts no elimination of small molecules, thereby giving a uniform, dry and compact polymer matrix. Urethane elastomers are relatively strong, likely by the aid of physical cross-linkage. The reaction kinetics of urethane polymerization can readily be tailored to fulfill processing requirements with the aid of curing catalysts.

Curing system

Desmodur N100

GAP diol together with the aliphatic isocyanate biuret N100 is recognized as a simple route to ensure adequate mechanical properties to an energetic binder system. Arthur Provatas tested Desmodur N3400 (a blend of the isocyanurate trimer and uretidone dimer of hexamethylene diisocyanate) with polyglycidyl nitrate (PGN), and found N100 to be superior over N3400 regarding cross-linking and thus mechanical properties (Provatas 2001).

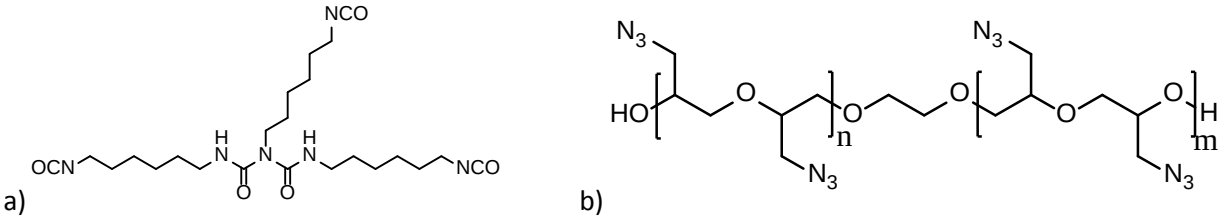

Figure 38. a) N100, b) GAP diol.

The plotted tensile curves of samples with three different NCO:OH ratios (FIG) gives an intuitive perception of the limitations within a simple GAP/N100 matrix. These results set the benchmark in performance of a cross-linked GAP matrix. Research regarding the curing agent N100 is well-reported, and the majority of the results presented in this thesis derive from GAP based binders, mostly cross-linked with the tri-functional N100.

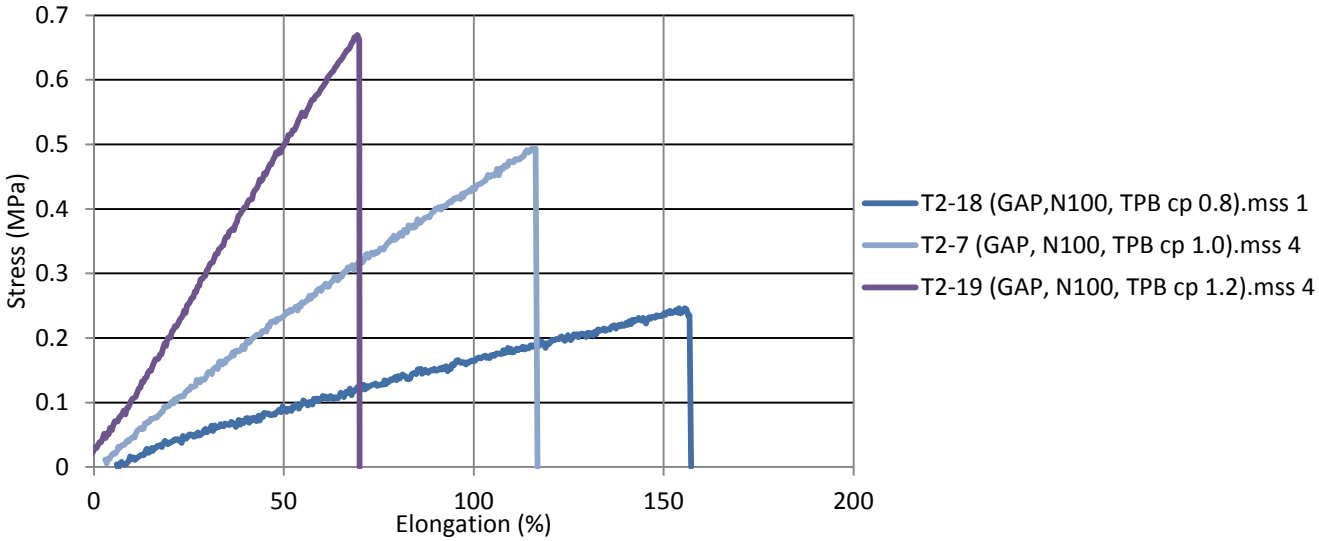

Figure 39. Tensile tests of GAP/N100, the median curves of five parallels each. Illustration show how cross-linkage influences mechanical properties.

As stated by Provatas, polyurethane binder systems possess mechanical properties, strongly dependent on the isocyanate-hydroxyl relationship (NCO:OH ratio) (Provatas 2001).

At an NCO:OH-level of unity, all the functional groups are theoretically consumed. At higher levels, there is an excess of isocyanates. If the excess isocyanates were to be unreacted, there would be no elevation in elastic modulus. There would probably be a decline in stiffness, but increase in elongation due to a plasticizing effect of the freely moving and displaced isocyanate-ended chains. But such is not seen. Instead, what we observe from tensile tests (FIG) is a significant increase in stiffness, increase in Peak stress, and consequently reduction in elongation at break for an NCO:OH ratio of 1.2. Compared to the sample with an equimolar ratio. The mechanical altering is explained by the reactivity of isocyanates. As briefly noted in section 1.4, isocyanates can react with urethanes to produce allophanates). An isocyanate connects to a nearby urethane moiety and thereby forms another cross-linkage, given that the viscosity does not immobilize the functional groups too much. The tensile curve of GAP/N100 with an NCO:OH ratio of 0.8 is softer, has a lower strength, although it delivers more elongation. An NCO:OH below unity means lower degree of cross-linkage and an excess of hydroxyl groups, thus ineffective, loose ends of polymer chains which will probably soften the sample. The low degree of cross-linkage implies longer chains between the cross-links, thus more compliable length when the tangled chains are subjected to elongation.

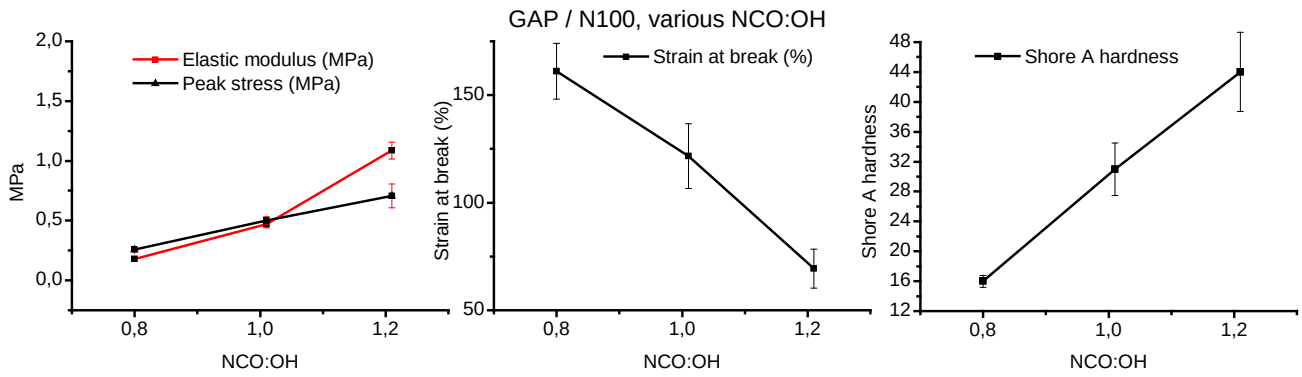

Figure 40. tensile tests and shore A hardness tests of GAP/N100 specimens. Respons as a function of NCO:OH ratio.

Peak stress seems to have a linear relationship with the NCO:OH level. And a correlation exists indeed:

$$Peak\ stress\ (MPa) = 1.09 \times NCO{:}\,OH(n/n) - 0.61 \qquad R^2 = 0.9989$$

The range is limited. On the other hand, a range between 0.8 and 1.2 is also quite applicable to the realistic freedom that is given for the modifications of a solid propellant. A more comprehensive study is reported by Mathew et.al (Mathew, Manu et al. 2008), where a plateau level in the peak stress slope due to the formation of allophanate cross-linkage, is more explicit at higher NCO:OH ratios.

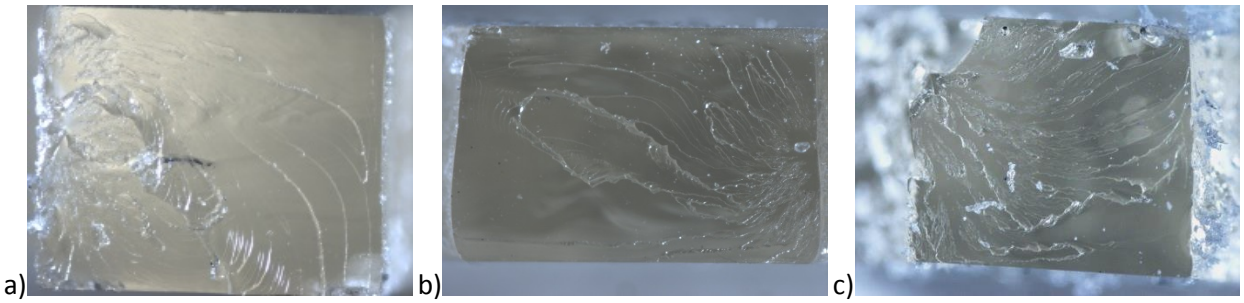

Figure 41. Images of the cross-sectional ruptures of specimens, shot through microscope. a) Sample T2-18, specimen 5 b) sample T2-7, specimen unspecified c) sample T2-19, specimen 2.

It was firsthand experienced that GAP/N100 was more reactive with an aliphatic curing agent than EP1900 and HTPB, by the comparison of time until reaction of sample T2-6 (EP1900/N100), T2-7 (GAP/N100) and T2-8 (HTPB/IPDI). A fraction of 0.05 % TPB was used in all three samples. The high reactivity of GAP can be deductively explained by its polar nature, believed to be more miscible with an isocyanate.

Aromatic isocyanates

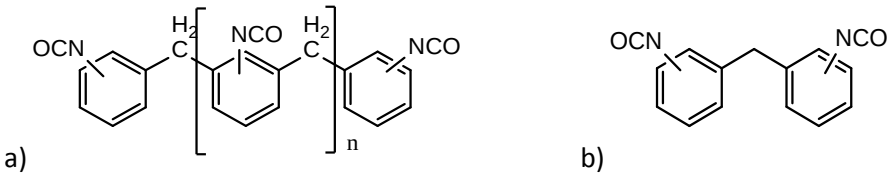

Figure 42. molecules that the aromatic curing agents constituted of. a) A homolog of MDI, suggested to have n = 0-4 repeating units. b) MDI, unspecified isomerism

Baymidur K88 HVL inherent slightly higher viscosity than K88. It consists only of crude MDI, which is a polymeric MDI (FIG.) The number of repeating units is speculated to range between 0 and 4. Desmodur VL 50 is sold as a hardener for coatings or adhesives. Failed attempts of achieving indicate an average functionality lower than 2. The mixture viscosity increased to a syrup-like consistency when cured with GAP, but never passed gelling point. VL50 seems to be of a more complex nature, as it consists of three specific MDI isomers, the crude MDI, and a stabilizer (see TABLE). It should be mentioned that a cross-linked polymer was produced when NCO:OH ratios were approximately 2. Cross-linkage through formation of allophanate groups are believed to cause cross-linkage.

Baymidur K88 HVL was the only MDI based polyurethane matrix to be subjected tensile analysis, due to its slightly better processability properties.

It was visually experienced that aromatic isocyanates are more reactive than aliphatic, which is recognized by the electron withdrawing nature of the benzene rings that promotes a nucleophile attack on the carbon in the isocyanate.

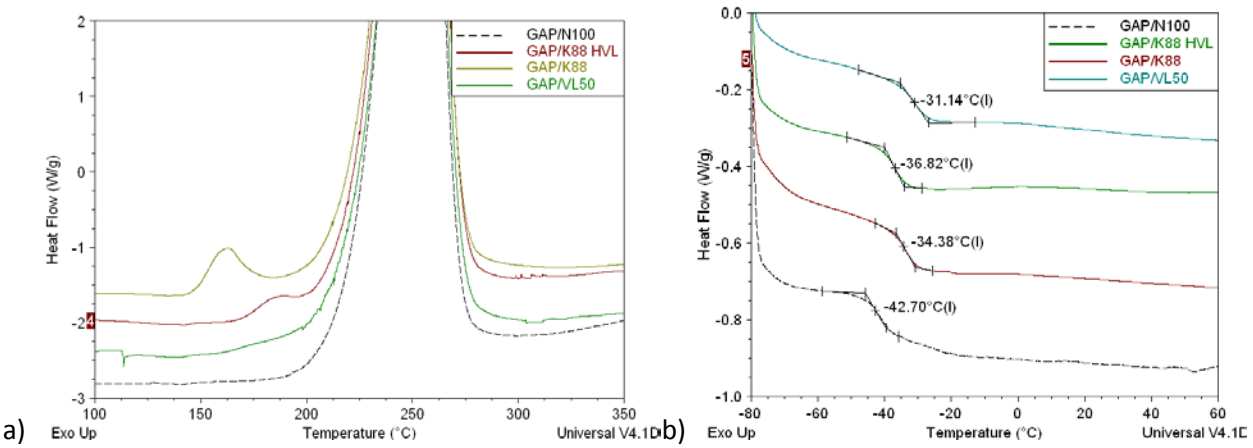

Figure 43. a) Tg of GAP cured with different aromatic isocyanates, compared to GAP/N100 (black dotted line), b) a focused view on DSC curves of GAP-cures with different aromatic curing agents, compared to a GAP/N100.

Through DSC curves, an unexplainable exothermal signal was present when the aromatic isocyanates K88 and K88 HVL were introduced (FIG). The peaks are located around 150-180 °C and is larger for K88. VL50 does, however, not exhibit any exothermal signal, which is strange since VL50 comprise of all the substances that is present in K88.

The aromatic isocyanates corrupted T_g, compared to N100. That was expected, since aromatic compounds introduce hard segments that promote crystalline behavior. Note that the FIG b) should be recognized merely as guidelines, because NCO:OH ratio varied some.

Table 10. Mecahnical properties of two formally identical samples containing GAP and the most promising aromatic curing agent, K88HVL.

Sample	Shore A hardness	Elastic modulus (MPa)	Peak stress (MPa)	Strain at break (%)	Comments
T2-12	17	0.22	0.26	132	2parallels

T2-21	23	0.30	0.27	138	3parallels

Table 10 shows hardness and mechanical properties of GAP cross-linked with the aromatic curing agent K88 HVL (tensile curves are appended, section 5.5). The curing of aromatic compounds was regarded to be secondary priority in means of preparation and characterization. Two formally identical samples address deviating performance. Corresponding tensile curves are appended in section 5.5, which gives a more comprehensive picture of mechanical performance.

N100/IPDI

Three samples of GAP, cured with N100 and IPDI, were prepared and subjected tensile testing. The di-functional IPDI works as a chain extender, while N100 cross-links the mixture to an elastomer.

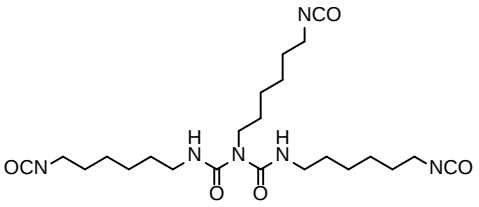

Desmodur N100

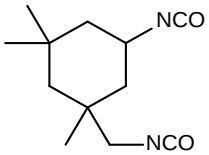

The molar amount of isocyanate groups are distributed almost equally between N100 and IPDI. Consequentially, an IPDI/N100 ratio of unity and an NCO:OH of unity (as in sample T2-29) would have a considerably less cross-linked nature than of a comparable polymer matrix without IPDI – because IPDI creates longer distance between the cross-links. The mechanical properties of the samples were generally high, relative to GAP/N100. The tensile test results displayed a tough, compliant matrix with a versatile range of mechanical traits when the degree of cross-linkage were adjusted. GAP/IPDI/N100 could seemingly be a promising binder system which could meet various requirements.

Table 11. Mechanical property results for GAP/IPDI/N100-samples. The parent tensile curves are appended in section 5.5.

Sample	NCO:OH	IPDI/N100	Shore A hardness	Elastic modulus (MPa)	Peak stress (MPa)	Strain at break (%)	Comments
T2-29	1.02	0.95	7	0.082	0.23	285	very soft, difficult to handle.
T2-30	1.21	0.99	25	0.315	0.52	192	4 parallels
T2-31	1.40	1	36	0.60	0.76	147	

An NCO:OH ratio of 1.4 relates to a high amount of excess isocyanate groups. Since the stiffness increased almost equally from 1.0 to 1.2 and 1.2 to 1.4, the excess isocyanate groups are believed to readily form allophanate cross-linked moieties.

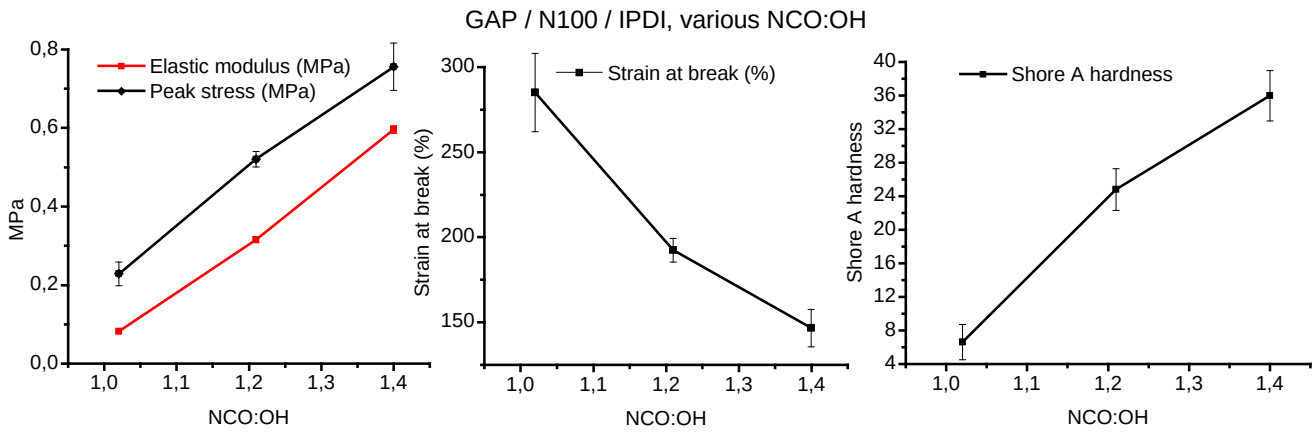

Figure 44. Mechanical properties of GAP/N100/IPDI-samples. The results of elastic modulus, peak stress, strain at break and shore A hardness are plotted as functions of NCO:OH-ratio.

Given a linear correlation of shore A hardness explained by NCO:OH ratios. Then the sample with lowest NCO:OH ratio would supposedly be a little higher than the trend predicts, due to a slightly lower IPDI/N100 ratio, thus containing some more cross-linking agents which would harden the sample. The exact opposite is shown. The minor difference in IPDI/N100 did not compensate for the variations in NCO:OH ratio.

Figure 45. Dog bone samples subjected tensile testing, GAP/IPDI/N100 samples with an NCO:OH ratio of a)1.0 (T2-29) b)1.2 (T2-30) c) 1.4 (T2-31).

Dog bone specimens of sample T2-29 were almost too soft for tensile testing, as they complied to every little load while handling. Shore A hardness results of 7 addresses the softness of sample T2-29.

Prepolymers

Table 12 gives a review of relevant prepolymers, each cross-linked with N100 to form a urethane polymer (except HTPB, which is cured with IPDI), in which isocyanate groups are added to an equimolar amount of hydroxyl groups. GAP is overall the main concern, although this section directs some emphasis to other prepolymers applicable in a binder system.

Table 12. Shore A hardness and T_g for comparable polyurethane binder systems, with emphasis on characteristic qualities of the prepolymer. T_g values are obtained from DSC.

Sample	Prepolymer	$\bar{M}$w (g/mol)	classification	Shore A hardness	T_g (°C)
T2-7	GAP	≤ 2000	Polyether with azide groups	33	-43
T2-8	HTPB[c)]	2600	polyolefin	36	-68[a)]
T2-42	PPG-PEG	2700	polyether	38	-65
T2-43	EP1900	4140	polyether	33	-67
T1F6d2	HTPE	4200	polyether	48	-80 [a)]
T1F6e2	HTCE	2000	Polyester and polyether	65	-70 [a)]
T1F6f2	TEG[b)]	150	oligo-ether	86	10
T1-1,4But1.0	1,4-butanediol[b)]	90	Aliphatic hydrocarbone	82	10

a) T_g values of HTPB ({Ang, 2012 #25}), HTPE {Knut Magne Hansen, 2003 #213} and HTCE {Unneberg, 2006 #230} are extracted from literature.

b) The molar mass values are approximations, except those of 1,4-butanediol and TEG are exact values, since they comprise solely of one monomer unit.

c) Cured with IPDI

The glass transition temperature has a certain cross-linkage dependency. A long-chained prepolymer like EP1900 is responsible for an increased distance between the cross-linkage regions caused by the biuret isocyanate. Consequently, a smaller mass portion of curing agent is needed to attain equimolar amounts of hydroxyl- and isocyanate groups. TEG and 1,4-butanediol are both small prepolymer units. That is reflected on T_g, which is around 10 °C for both. A generalized statement is that factors leading to increased stiffness in the molecular segments tend to elevate T_g.

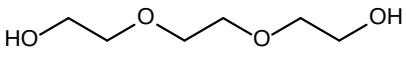

Figure 47. Triethylene glycol (TEG)

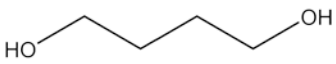

Figure 46. 1,4-butanediol

Mechanical properties of successfully cured binder matrices are sohwn in TABLE. For EP1900/N100, several samples have been mechanically tested. T2-16 corresponds to the most promising specimen, mechanically.

Table 13. Collective table of comparable polyurethane binder matrices cured with N100 set up against GAP/N100.

Sample	Composition	Shore A	Elastic modulus (MPa)	Peak stress (MPa)	Strain at break (%)
T2-7	GAP/N100	33	0.47	0.50	122
T2-8	HTPB/IPDI	36	0.44	0.91	348
T2-42	PPG-PEG/N100	38	1.1	0.33	40
T2-16	EP1900/N100 [a)]	21	0.20	0.48	295

a) T2-16 is cured with 100ppm DBTDL instead of TPB.

Table 13 shows a relatively high elastic modulus and shore A hardness for sample T2-42. On the other hand, the same sample also exhibits poor stress and strain at break, which communicates the fact that stiffness and hardness measurements describes the material's properties at an initial point – not at the yield point.

HTPB

Polyurethane cross-linked HTPB is presently the favored prepolymer for solid propellant motors. A cured sample of HTPB and IPDI was subjected to tensile tests, to illustrate the superior strain of the binder. First tested in a rocket motor in 1972, HTPB has since then become the state of the art in solid propellant formulations, having excellent mechanical properties, thermal properties, and improved IM behavior (Ang 2012). On the other hand, HTPB is inert. It does not contribute to the overall energy output at combustion, other than to provide carbons for the oxidizer to react with. Therefore would an energetic binder with adequate mechanical properties may be preferred.

HTPB has in fact functionality larger than 2, due to some reactive double bonds that were created under the addition polymerization of butadiene to form HTPB. Therefore, a cross-linked polymer is readily achieved when a curing agent with functionality of two is used. A suggestion of how the butadiene monomer units are arranged is illustrated below (FIG).

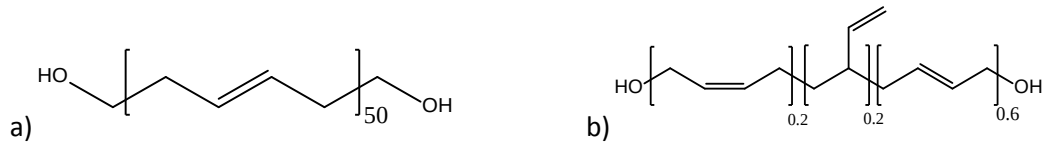

Figure 48. hydroxy-terminated polybutadiene. a) Generalized projection with emphasis on molecular mass. b) a distribution of arrangements internally in the HTPB chain.

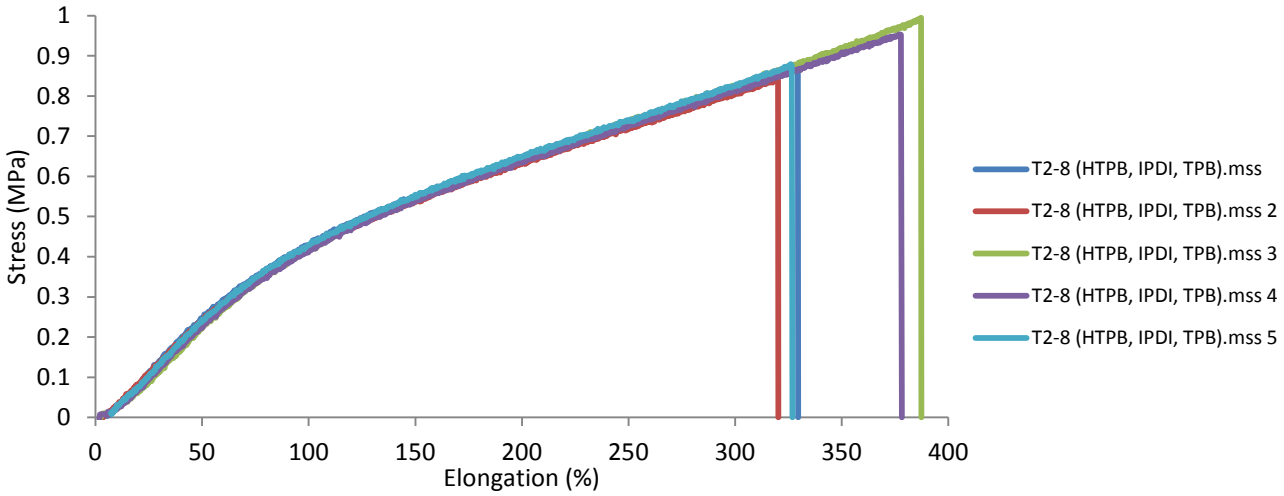

Figure 49. Tensile test results of HTPB/IPDI.

The tensile test of HTPB/IPDI (T2-8) gave an outstandingly high maximum elongation (figure 49). The median curve is stretched 348 %, whereas the extreme curve is 387 %, almost five times its original length. The elastic modulus is calculated from the near-by initial elongation slope where it obeys Hooke's law, which does not longer apply after the slope retardation at roughly 70 %. Average elastic modulus for T2-8 is 0.44 MPa. Compared to characteristic tensile tests of different polymers, HTPB/IPDI resembles a true rubber and arguably some relations to a semi-crystalline polymer, with a remarkably stiffer region at 0-70 %.

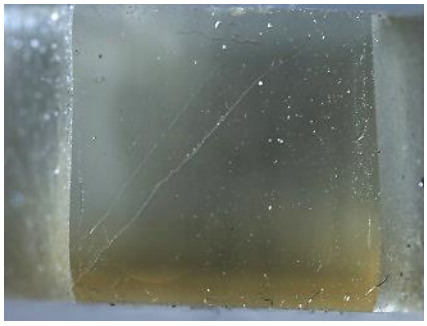

Figure 50. Photo of cohesive break, T2-8

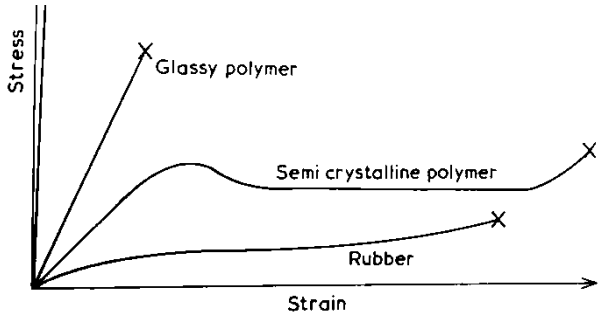

Figure 51. Stress-strain behavior of polymers. Extracted from {Young, 1991 #212}

A close-up photo through a microscope (figure 50) shows a clean, straight cohesive rupture. The break point was sudden and randomly located on each of the five parallels (figure 49), which implies a homogenous structure with no outlined weak regions of the dog bone specimen.

EP1900

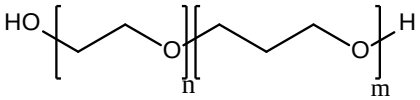

Figure 52. Voranol EP1900.

Voranol EP1900 is a block copolymer marketed as an ingredient for high performance elastomers and footwear (e.g. shoe soles).

Table 14. An outline of EP1900 cure samples, focusing on behavior and differences under varying curing conditions.

Sample	Cured by	Cure temp. (C°)	Curing characteristics	Visual inspection of product	Shore A hardness
T2-6	N100/TPB	60	tan δ = 1 at 9h	Tacky surface. Opaque	25
T2-16	N100/DBTDL [a)]	60	cross-linked, almost fully cured after 1h	Somewhat tacky. Opaque	21
T2-17	K88HVL	60	cross-linkage started after 4h	Tacky surface, clearer appearance	15
T2-24	N100/TPB	75	tan δ = 1 at 3h	Significantly more transparent	24
T2-43	N100/TPB [b)]	80	-	Almost completely transparent	33

a) Cured with 100ppm DBTDL.
b) New batch of EP1900.

During the tensile testing of EP1900/N100 (T2-6) it was observed that one side of the dog bone ruptured first, namely the side facing downwards in the mold. This could be explained by a settling of the curing agent, which has a somewhat larger density (1.03 g/mL for EP1900, 1.14 g/mL for N100). There would consequently be a NCO:OH ratio gradient through the matrix. The top side would have a lower degree of cross-linkage, thus a more strain compliant matrix than the bottom side.

EP1900/N100/TPB, cured at 75 °C (T2-24), revealed a clearer matrix. Curing temperature shortened the pot life, resulting in a more homogenous and stronger matrix (FIG comparison). More specific, the increased transparency could imply an elevation in activity of the catalyst – from being suspended (and less active) in the mixture, to dissolve nearly completely as the temperature was elevated. T2-43 is formally identical to T2-6 (except from containing a new batch of EP1900), but subjected to different processing.

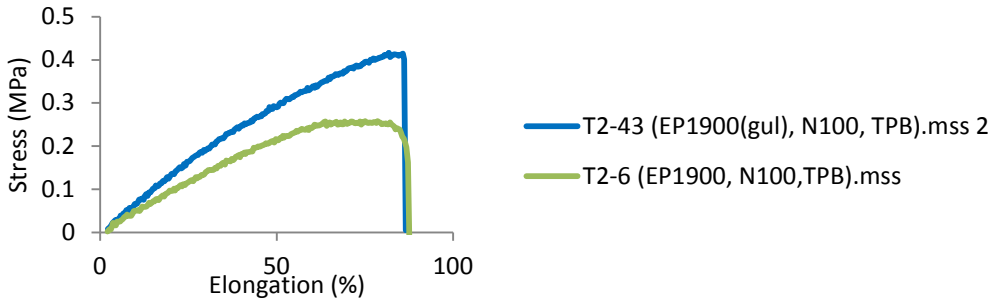

Figure 53. Median curves of two formally identical samples of EP1900/N100.

Water content is a potential problem regarding isocyanate curing (See section 1.4). EP1900 could possibly be guilty as a carrier of water into the cure, which could explain the mechanical differences between two samples that contained various batches of EP1900 (FIG). However as the undoubtebly change in temperature is emphasized, the uncertain variations in quality between batches is supressed.

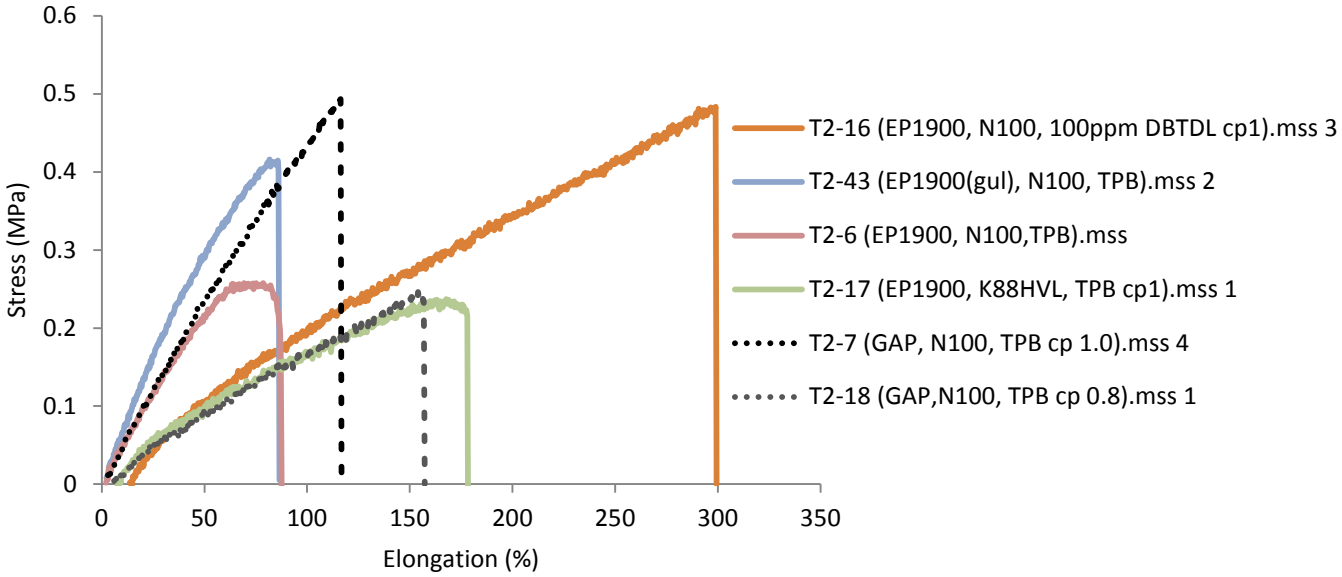

Figure 54. Collective plot of the median curves of four different EP1900-cures, compared to GAP/N100 at two different NCO:OH-ratios.

Regardless of color and texture, the mechanical properties altered dramatically when changing curing catalyst. Sample T2-16 represents EP1900/N100 cured with 100 ppm of DBTDL at 60 °C. The mixture had a pot life of 1 hour. A decline in hardness and stiffness (TABLE, FIG clustergraph and appended FIG) accompanied a surprisingly large increase in elongation. TPB is associated with a certain delay until activation, while DBTDL is recognized as a more effective curing agent. It should be briefly mentioned that a preliminary cure sample with about 350 ppm DBTDL led to an almost instantly cured sample after processing, and that a preliminary cure without curing agent resulted to a very slow cure.

a) 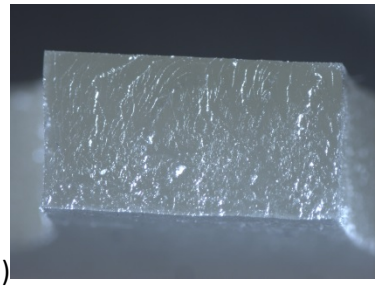 b) 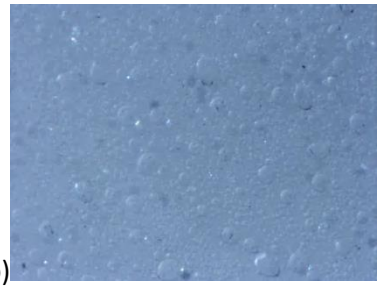 c) 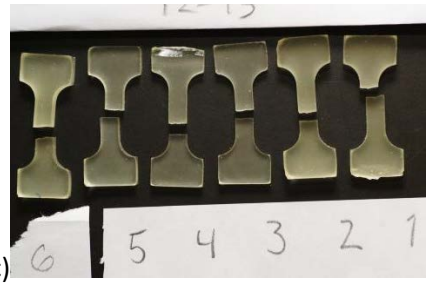

Figure 55. a) image of a broken dog bone, sample T2-43. b) The bottom-faced side of T2-43, showing some phase separation. c) the dog bone specimens of T2-43.

PPG-PEG

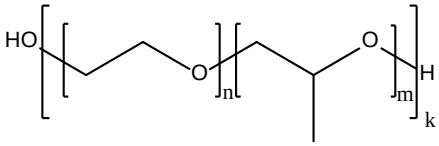

Figure 56. PPG-PEG (Clariant D21/150)

Preliminary experiments with PPG-PEG (sample T1F6c2) showed signs of migration difficulties when cured with N100. Droplets were observed at the bottom of the transparent sample vessel, as well as the cure being extremely slow and inhomogeneous. TPB seemed to sediment and cure the bottom layer only. Surprisingly, at an altered curing temperature of 80 °C, a homogenous and clear binder matrix was finished after two days, and applicable to tensile testing (sample T2-42).

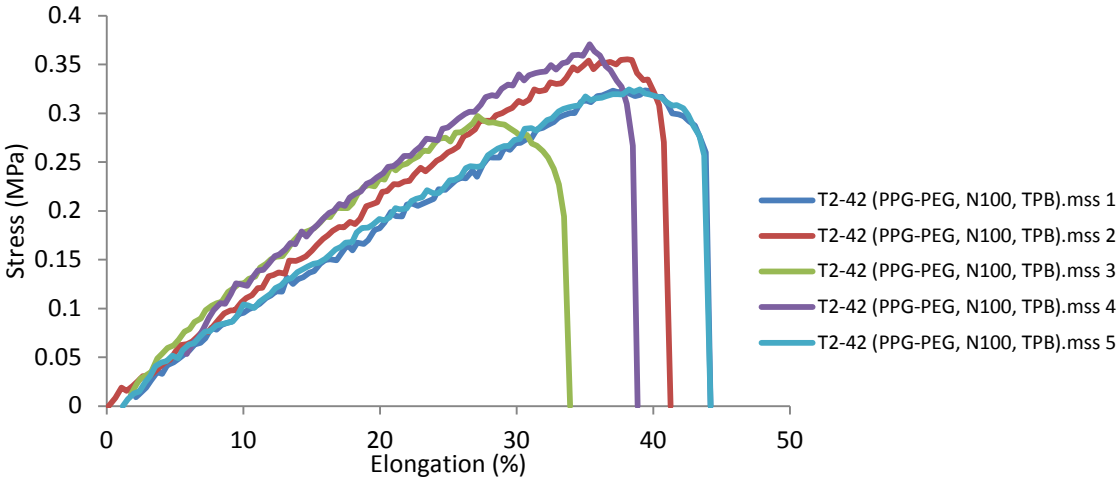

Figure 57. Tensile test results for PPG-PEG/N100 specimens.

Sample T2-42, containing PPG-PEG, N100 and TPB, showed rather poor mechanical properties. PPG-PEG is a random block copolymer of ethylene oxide and propylene oxide. The irregularity of a polymer with statistically distributed monomers could give less connectivity between the polyether chains than a block copolymer (or homopolymer). The propylene oxide has a methyl group branching out from the molecule. The branch is believed to contribute to the low T_g of Sample T2-42 (-67°C), since branching influences the prepolymer's melting point. Perceived as a long, irregular prepolymer, PPG-PEG could lack the presence of physical cross-linkage that the other tensile test specimen may have.

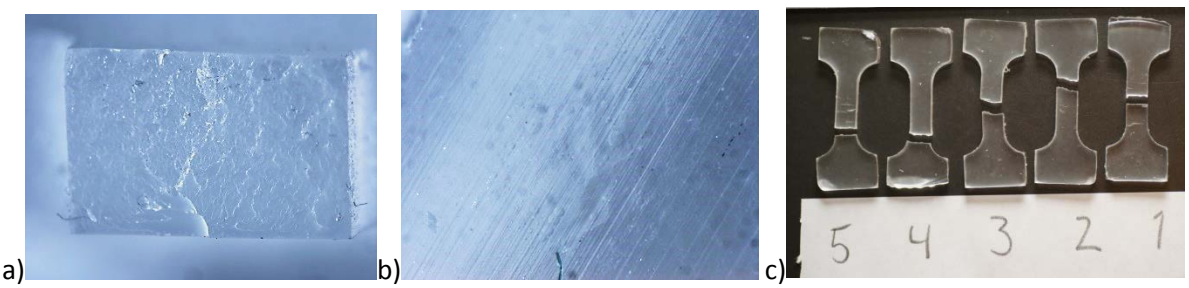

Figure 58. images of tensile tested dog bone specimens of T2-42. a) b) one can observe some phase separation close to the bottom-faced surface of T2-42. c) the dog bone specimens of T2-42.

HTPE

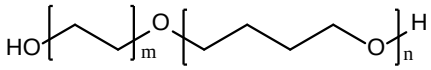

Figure 59. A hydroxyl terminated polyether (HTPE) unit (also called TPEG).

Sample T1F6d2 (see appended TABLE) concluded the investigation of HTPE in an N100 cure. Previous work at FFI {Knut Magne Hansen, 2003 #213}reported a T_g of -80 °C for an HTPE-matrix, a T_g of -45 °C for a GAP-matrix, and lastly a T_g somewhere in between for a 1:1 of GAP and HTPE, regarding molar amount of hydroxyl contribution. The positive influence HTPE showed on T_g, was promising results regarding low-temperature improvement of a GAP binder system.

HTCE

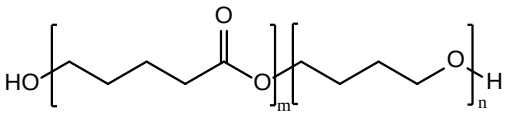

Figure 60. A hydroxy terminated caprolactone ether (HTCE).

From preliminary compatibility tests, HTCE showed to be the second most reactive of the inert prepolymers, with N100 (after TEG). A more polar nature, and relatively short chains are the properties that differentiate HTCE from HTPE, EP1900 and PPG-PEG. Sample T1f6e2 concluded research on HTCE, as further work was dedicated to GAP compositions (see appended TABLE for shore A hardness results). Other revelations regarding HTCE has been reported internally at FFI {Unneberg, 2006 #230}, where a T_g of -70 °C was reported. A simple miscibility test (figure 160, appended) showed better miscibility with GAP and HTCE, than of HTPE and EP1900. This is explained by the more polar nature of the ester group on HTCE.

Copolymeric binder systems

The implementation of a secondary prepolymer is a feasible approach for improving certain properties to an energetic binder, mainly T_g and mechanical properties. The secondary prepolymer is often inert, resulting in a dilution of energy.

Table 15. All the successfully cured mixes containing a secondary prepolymer, compared to GAP/N100.

Samples	Composition	po2/po1	T_g (°C)	Shore A hardness	Elastic modulus (MPa)	Peak stress (MPa)	Strain at break (%)
T2-7	GAP/N100	-	-43[a)]	31	0.47	0.50	122
T2-23	GAP/TEG/N100	0.90	-	55	1.70	1.04	66
T2-41	GAP/TEG/N100	2.44	-36[b)]	54	1.56	1.2	85
T2-32	GAP/1,4-butanediol/ N100	0.10	-37[a)]	38	0.74	0.59	90
T2-46	GAP/PPG-PEG/N100	0.10	-40[b)]	34	0.58	0.40	80

a) T_g for T2-7 and T2-32 is determined by DSC.

b) T_g for T2-41 and T2-46 is determined by DMA.

It can be revealed from TABLE that none of the additional prepolymers improved T_g, with respect to the benchmark sample of GAP/N100. The hardness and stiffness elevated for all copolymer samples. Even though the two GAP/TEG samples (T2-23 and T2-41) contain two very different po2/po1 ratios, they have practically the same stiffness and hardness. It could be speculated whether a plateau level is reached, as the polymer properties gets progressively dominated by TEG. A TEG/N100-polymer is drastically harder and stiffer than GAP/N100, with a shore A hardness of 86 for sample T1F6f2.

The results from TABLE are discussed in the following sections.

GAP/EP1900

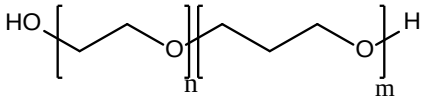

Figure 61. Voranol EP1900

EP1900 has been found to be insufficiently miscible with GAP diol. An early attempt of preparing a GAP/EP1900/N100 (po2/po1 = 0.20) copolymer mixture, recognized miscibility to be a potential problem. The sample had cured completely, but did also have a rough, moist surface. Investigation of the surface liquid by IR, revealed a region at 600-1500 cm^{-1}, identical to that of EP1900. Additionally, a small absorbance was found at around 2090 cm^{-1}, which represents the azide group in GAP. Ergo has some GAP dissolved in the EP1900 and did not participate in the copolymer matrix. Possible explanations for the compatibility issue could be the difference in polarity, density, and pot life – at which EP1900 is less polar, less dense and exhibits a considerably longer pot life at comparable concentrations of TPB (0.05 %). Plasticizers could possibly help

these otherwise immiscible prepolymers to participate in a homogenous binder system, but further research is discouraged.

GAP/PPG-PEG

A random block polyether could make a difference as an additive to improve low temperature properties. The producer of PPG-PEG highlights a high vaporization resistance, even at temperatures above 100 °C. T_m is independent of molar mass, due to their randomly distributed branched moieties. PPG-PEG has a molar mass of approximately 2700 g/mol while still being a low-viscosity liquid (pour point of -35 °C). In comparison, polyethylene glycols are waxes at roughly 600 g/mol (room temperature). PPG-PEG was used as an additive to GAP/N100/TPB formulations in order to examine whether the random copolymer could possibly lower T_g and also act as a reinforcing chain extender. Preliminary compatibility tests showed PPG-PEG to be completely miscible with GAP (FIG vial APP), and also readily cure to a random copolymer by N100 and TPB. FIG shows a modulus for GAP/PPG-PEG/N100 (T2-46, NCO:OH = 1.00, po2/po1 = 0.10) somewhat comparable to the benchmark formulation of GAP/N100 (T2-7, NCO:OH = 1.01). A fifth parallel was run, but excluded.

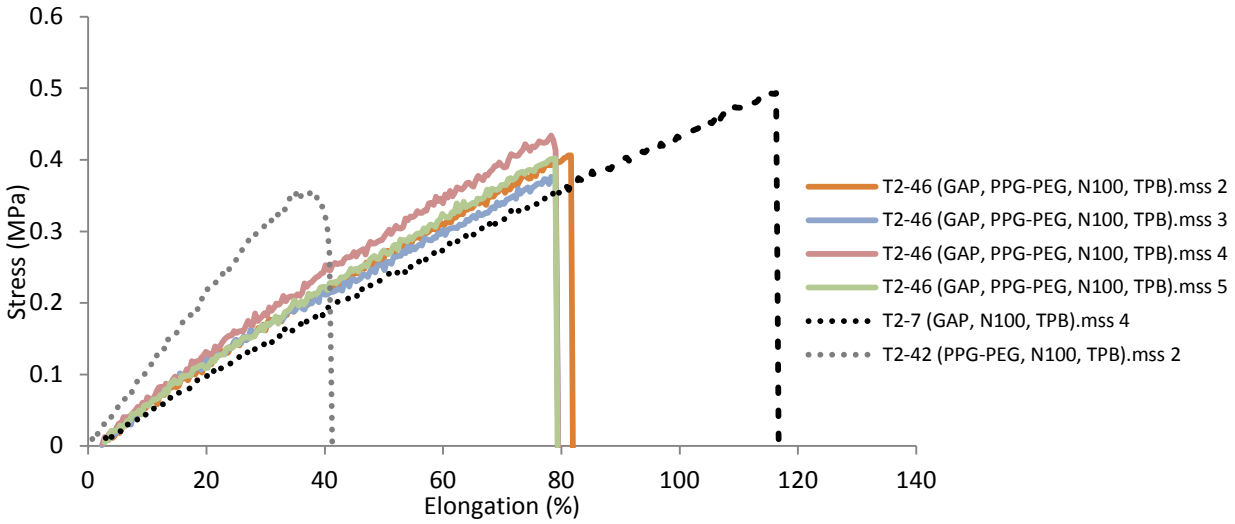

Figure 62. Tensile test results for T2-46, compared to the median curve of GAP/N100 and PPG-PEG/N100.

PPG-PEG is a relatively long molecule, so a po2/po1 ratio of 0.10 relates to a tenth of weighed GAP in sample T2-46. Since PPG-PEG/N100 (T2-42) exhibited a remarkably lower T_g, an overall lowering of T_g was expected for T2-46. However, T_g did not shift towards lower temperature when PPG-PEG was added to the GAP/N100 matrix in a po2/po1 ratio of 0.10 (TABLE). Therefore it may be concluded that the quantity of PPG-PEG is not sufficient to influence the glass transition region. Mechanically, T2-46 inherited a low maximum strain and an increase in stiffness from its parent PPG-PEG/N100 (T2-42) sample. The T_g of copolymers can be predicted through an empirically recognized relation, called the Fox's equation {McCrum, 1997 #205}.

$$\frac{1}{T_g} = \frac{w_1}{T_{g1}} + \frac{w_2}{T_{g2}}$$

Where w_1 and w_2 are weight fraction of the prepolymers in the copolymer, and T_{g1} and T_{g2} are their respective T_g as homopolymers (in kelvin). The predicted relationship suggests a T_g of -45 °C, which is lower than the observed Tg obtained from DSC (FIG). T_g remained unchanged.

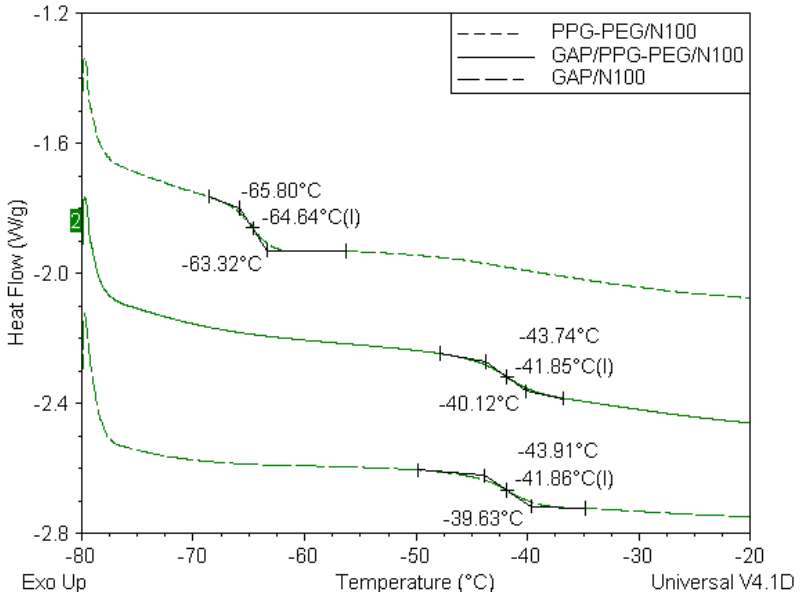

Figure 63. DSC of PPG-PEG/N100, GAP/N100 and the copolymer, with a po2/po1 of 0.10.

Some adjustments of curing conditions may influence the end-results of samples containing PPG-PEG, as a curing temperature of 80 °C (20 °C higher than normal) gave improved results. A further increase might help, but is considered impractical for larger scale processing. A change in curing catalyst would have been interesting, considering the attempt with EP1900 and 100ppm DBTDL (T2-16), which gave a highly improved strain at break, without compromising any obvious qualities.

GAP/TEG

The energetic plasticizer TMETN is stabilized with 20 wt % *polyethylene glycol* (PEG), for safer transportation and storage. The extraction of PEG is a fairly simple but cumbersome procedure with numerous repetitions. If the PEG stabilizer could prove itself valuable in a binder matrix, then such a time-consuming purification process would not be necessary. As an approach towards understanding how PEG would affect a GAP based binder matrix, notable experiments have been dedicated to TMETN/TEG, and PEG without the plasticizer. There is some uncertainty connected to the related safety data sheets, but PEG is believed to be *triethylene glycol* (TEG). The calculated amount of curing agent needed to react the hydroxyl groups of GAP and PEG, rely on the previous assumption. The cured molds have achieved satisfactory aesthetics.

Previous work by the author showed that TMETN/PEG could readily be incorporated in a GAP/N100 matrix without removing its polyethylene glycol stabilizer. Being a diol, PEG contributes as a chain extender to the polyurethane matrix. Also, simply unprocessed TMETN cured satisfactory with N100 at NCO:OH ratios of 1 and 1.5, without any need of curing catalyst.

The contribution of TEG in sample T2-41 was determined by its presence when introduced through TMENT/PEG, as used in a complete propellant formulation at FFI (po2/po1 = 2.44).

In spite of the fact that TEG was not soluble in GAP (SEE FIG, APP), the GAP/TEG/N100 matrix of T2-23 gave a clear, and apparently homogenous matrix, and was applicable to mechanical testing. The ideal ratio of 2.44 did not give a perfectly homogenous cure (T2-41), but a rather rough surface (FIG specimen APP). It is suggested that the system got saturated with TEG, which in turn agglomerated at the surface. Sample T2-23 had a reduced proportion of TEG relative to GAP, with a po2/po1 of 1.90. FIG shows strain at break comparable to GAP/N100, NCO:OH = 1.2, but a 40 % increase in strength (peak stress).

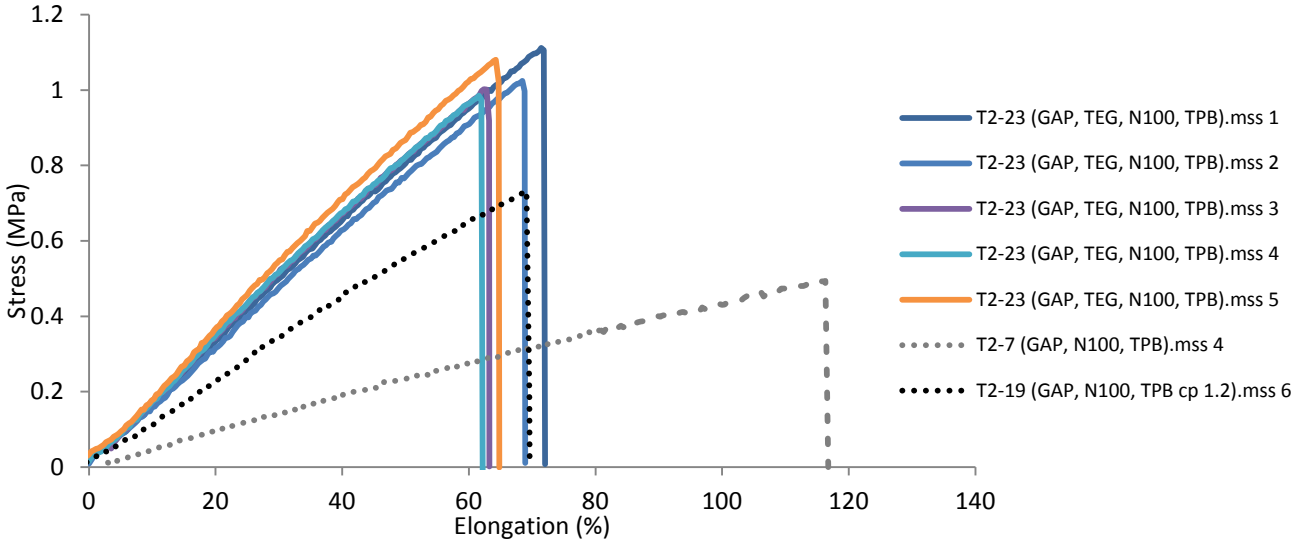

Figure 64. Tensile test results for GAP/TEG/N100 (sample T2-23) specimens.

Although T2-41 had a troublesome mold, the tensile test results came out surprisingly precise (FIG). The two strongest tensile curves (parallel 4 and 5) deviate somewhat from the rest of the specimens. This can be explained by the fact that parallels 4 and 5 got cut out almost perpendicular, relative to the others from the main sample, at which the irregular surface of sample T2-41 might have given the two some more surface area to comply with. The rough surface of T2-41 could be argued to give deviating and wrong values, but is backed up by precise shore A hardness measurements, which implies a homogenous matrix.

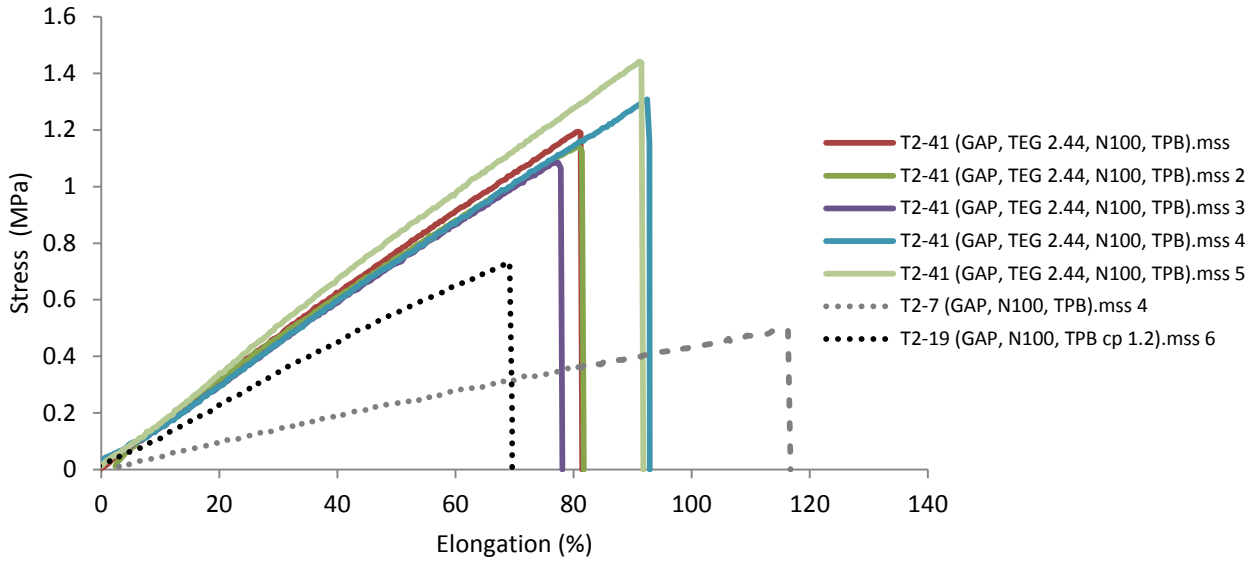

Figure 65. Tensile test specimens for GAP/TEG/N100 (sample T2-41) specimens.

Roughly one third of the mixture in sample T2-41 consists of N100 to attain equimolar proportions of isocyanate and hydroxyl groups (APP). That implies a binder system gradually moving away from being GAP based, and thereby getting less energetic. Considering solely the mechanical aspect, a modification of tunable parameters is a compromise between strength and strain. But when comparing the po2/po1 ratio 1.90 with that of 2.44, (FIG) an enhancement in strain is addressed, while still preserving the stiffness.

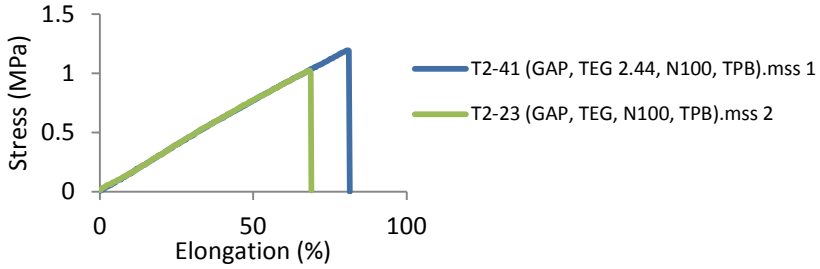

Figure 66. Median curves of T2-23 and T2-41.

Apparently, the overall mechanical abilities from TEG/N100 polyurethane outrun a GAP/N100 matrix regarding tensile strength. TEG/N100 was too stiff for the tensile test method. Considering implementation of nitrous plasticizers (migration and saturation), TEG is less polar and may thus have less affinity towards the plasticizer, but will perhaps provide a larger free volume than a GAP cross-linked polymer. The loss of overall energy when adding TEG could possibly be neglected when TMETN is implemented (see T3-5 in section 3.5). A tuning of cross-linkage would be interesting. An NCO:OH ratio below unity may give excess hydroxyl moieties and unlinked chains, thereby causing a softer, more compliant sample. If this is true, a GAP/TEG/N100 matrix could be tailored to meet various requirements.

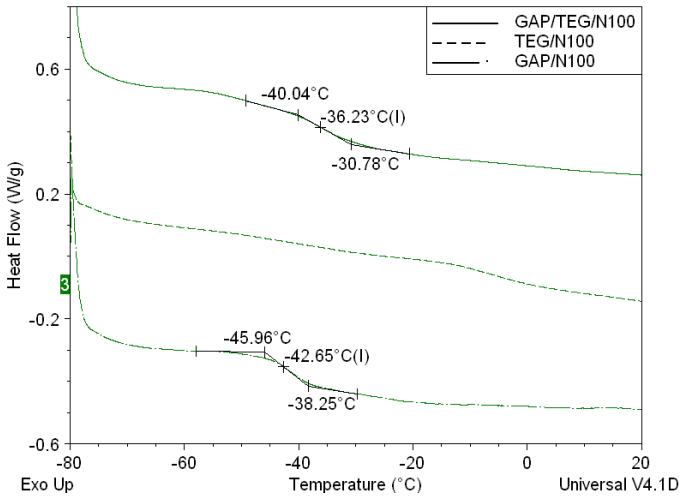

Figure 67. Glass transition temperature from DSC. The implementation of TEG influences T_g.
GAP/N100 is represented by sample T1F5c, TEG/N100 by sample T1F6f2, and the GAP/TEG/N100 by sample T2-41.

Figure FIG reveals how TEG drags T_g in an undesired direction. TEG/N100 (sample TiF6f2) exhibited a T_g of 10 °C, obtained from dynamic mechanical analysis. One can arguably consider TEG as evenly dispersed in the mold, as two separated polymer segments would reveal two glass transition regions. A prediction of where the theoretically T_g would be, was calculated (for equation, see APP). The calculation suggested a T_g of -38 °C, which is a sufficiently precise estimation, considering only 2 °C displacement. Estimation of copolymers by their parent homopolymers could prove to be a useful tool.

TGA of GAP/TEG/N100 (T2-41, FIG) highlights a substantial amount of TEG, being responsible of slowing down the weight plummet caused by scission of the azide group at 230 °C. Instead, what we see is arguably three disintegration steps towards 500 °C. 17 % of initial mass is left in the crucible, which is remarkably high relative to the other GAP based samples that were subjected to TGA (which ranged 7 – 3 %).

If one would assume only nitrogen gas to be produced at the first stage of decomposition, only 17 wt % would have declined. If one assumes the whole azide branch (N_3-CH_2), about 34 % would have declined – which is also within the integer value by which the TGA curve displays (FIG).

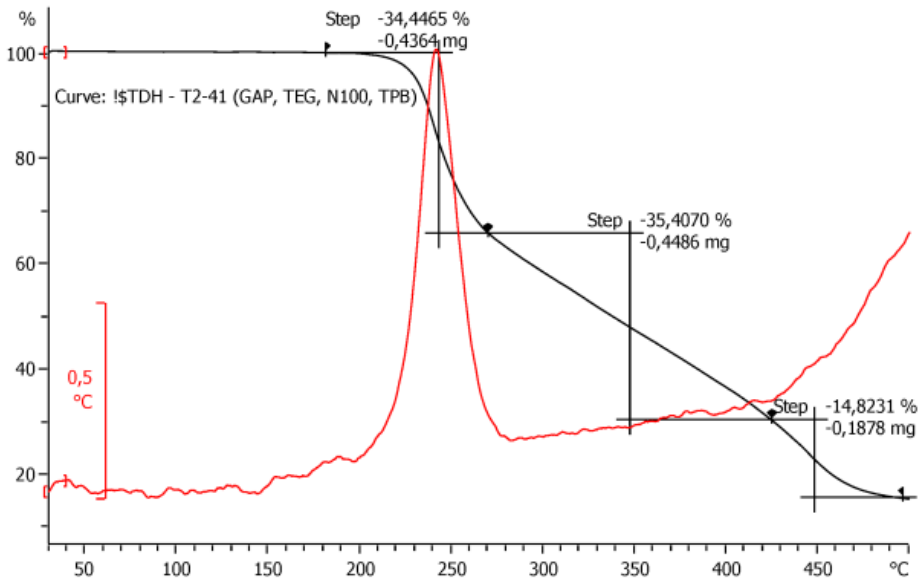

Figure 69. TGA of GAP/TEG/N100. The first step is GAP, second and/or third step has to be TEG. The second step is more of a steady decline than a notable reaction. The SDTA curve at 425 – 500 °C implies surpassing some sort of activation energy for the last disintegration.

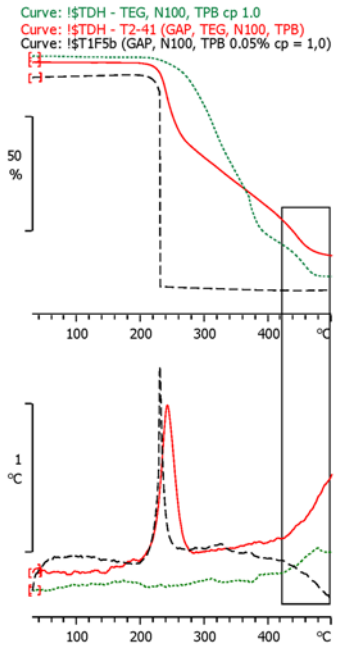

Figure 68. TGA, comparison of GAP, TEG and a combination (T2-41) in a polyurethane matrix. T2-41 compared with TEG/N100 and GAP/N100. TGA above, SDTA underneath. Scission of the azide moiety is delayed and spread out.

GAP/1,4-butanediol

Preliminary experiments showed 1,4-butanediol to have a limited miscibility in GAP (REF vial APP). Nevertheless, a successfully cure of a copolymer was accomplished, namely sample T2-32.

Sample T2-32 is a copolymer consistent of GAP and 1,4-butanediol at a po2/po1 ratio of 0.10, cross-linked with N100. 1,4-butanediol is considerably smaller than GAP. Therefore, only 4-5 droplets for 28.7 g of sample was needed to achieve a copolymer ratio of 0.10 (as the ratio is based on amounts of hydroxyl groups). Nevertheless, a change in mechanical behavior was revealed for T2-32. A sample of 1,4-butanediol/N100 was prepared for tensile testing, but was too stiff.

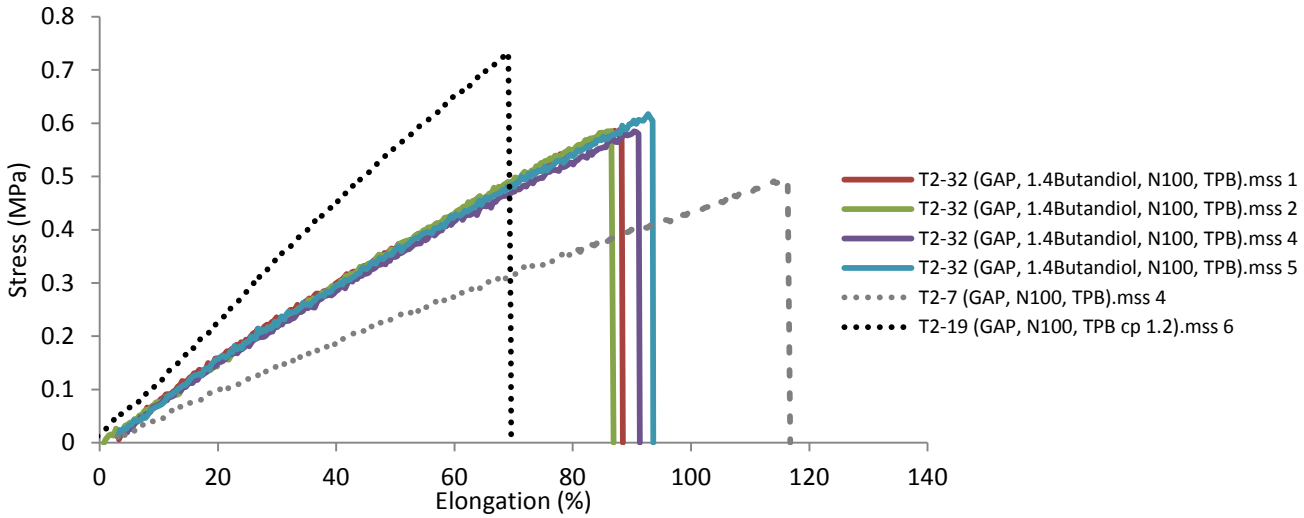

Figure 70. Tensile results of GAP/1,4-butanediol/N100/TPB. One parallel is removed, due to rough edges.

One could argue that 1,4-butanediol, since it is short and would arrange denser urethane regions, would promote physical cross-linkage, thus possibly resulting in a more stretchy polymer. The tensile results were either way predicted to display a stronger, stiffer nature than its comparable GAP/N100 elastomer, due to the closer arrangements of cross-links. An increase in elasticity and strength is observed, in combination with a compromise in elongation (FIG) – a trade-off that is associated with the tuning of NCO:OH ratio within the binder system. Tensile results of sample T2-32 is in fact located where the tensile curve of a GAP/N100 binder with a NCO:OH ratio of 1.1 is predicted to appear.

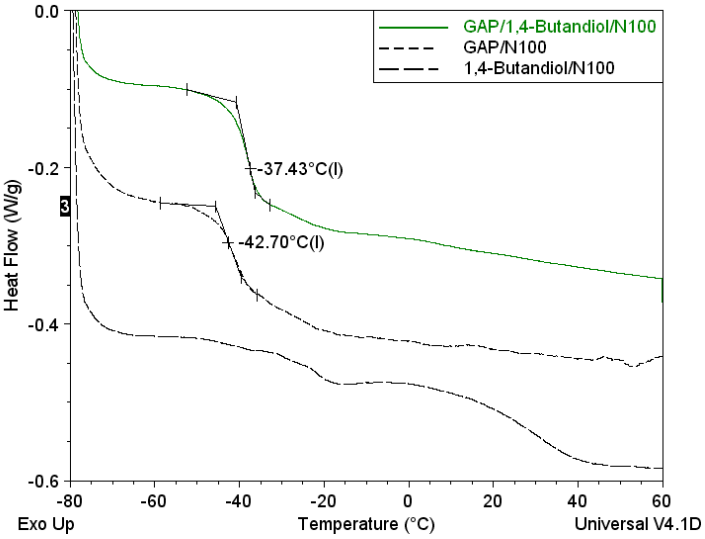

Figure 71. DSC curves of the GAP/1,4-butanediol/N100 copolymer and its parent homopolymers.

Any T_g region is problematic to read from the 1,4-butanediol/N100 in FIG. Results from DMA unveiled a T_g of +10 °C. The 1,4-butanediol sample is quite hard. Therefore a 3 point bend jig with an applied force of 0.05 N was used instead of the conventional 20mm dual cantilever.

A prediction of the T_g region was also attempted for sample T2-32, at which the results got very little accuracy with DSC results. The prediction did not differ from the integer value of -43 °C - identical to GAP/N100. The relationship (see appendix calculations) did not apply to the small weight fractions of 1,4-butandiol, specifically 0.4% of total prepolymer. Even though a small weight fraction, T_g was altered, although not in the preferred direction. Experiments with a larger fraction of 1,4-butanediol in a GAP based matrix would be interesting, but merely in the understanding of when a saturation point of miscibility of 1,4-butandiol might occur, and how the mechanical properties would be affected for sample combinations within that po2/po1-sector of 0.10 to saturation point.

Most relevant would be to create a block copolymer from GAP, 1,4-butanediol and N100, to investigate whether hard block moieties of urethane and 1,4-butanwediol would enhance the mechanical strength through physical cross-linkage. Also, an implementation of di-functional curing agents could possibly promote physical cross-linkage, especially if a block copolymer were to be synthesized. T_g would, sadly, most likely increase either way.

3.3 Triazole cross-linkage

Landsem (REF) published results of GAP cured with *bisphenol A bis(progargyl ether)* (BABE). However this was end-bonded tensile test samples, a method that is troubled with adhesive ruptures. Without further specification, she reported similar elastic modulus of a BABE cross-linked and a N100 cross-linked GAP system, implying similar mechanical properties. Merging BABE into a GAP mixture was reported to be somewhat problematic, when a relatively high melting point influenced its solubility at room temperature.

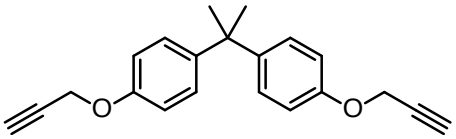

Figure 72. Bisphenol A bis(propargyl ether)

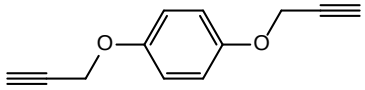

Figure 73. 1,4-bis(propyn-1-yloxy) benzene (BPOB)

Compared to polyurethanes (where at least one of the binder precursors need to be more than di-functional), di-propargyl curing agents connect to an abundance of azide groups on GAP. When expressing the proportion of curing agent in a triazole cross-linked matrix , one could adopt a term from the rubber vulcanization process: *pph* (parts curing agent per hundred parts polymer, by weight), as done by Byoung (Min, Park et al. 2012). But in order to relate to the NCO:OH ratio in compliance with previous work at FFI, a generalized «ALKYNE:AZIDE» ratio is used, introducing certain assumptions: GAP is considered di-functional, as the cross-linkage will be statistically distributed with the average of two alkyne moieties per GAP prepolymer (see REF c/p-calculation in APP). Ideally, some GAP could be unreacted, thus acting as plasticizer between the network chains.

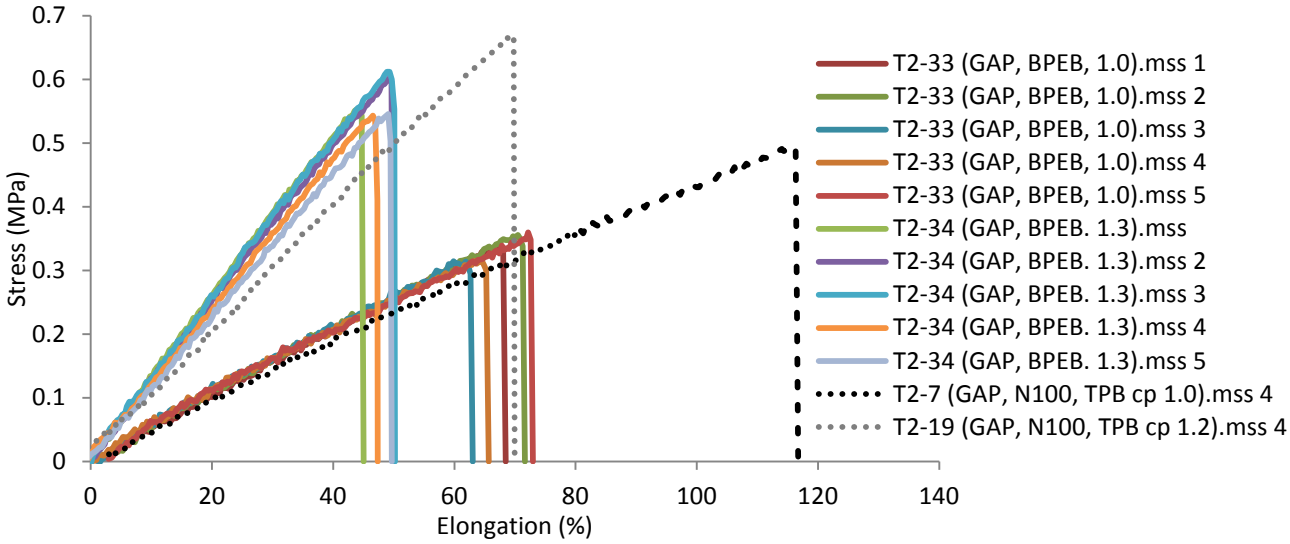

Figure 74. All of the GAP/BPOB tensile test specimen, compared to GAP/N100, NCO:OH ratios of 1.01 (T2-7) and 1.21 (T2-19). GAP/BPOB are in GAP/BPOB ratios of 1.00 (T2-33) and 1.30 (T2-34).

BPOB is smaller than BABE, and as a consequence, possesses a lower melting point. An ease in processing was predicted, and frankly: Stirring the solid flakes of BPEB into a GAP based solution was a treat. After some seconds of manual stirring with a glass rod, the initially fluffy powder merged readily into the solution. The isocyanate-free matrix of merely BPOB and GAP cured steadily over night at 60°C (at least 35-50 °C was necessary, argued in section 1.4). An increase in viscosity was discovered after 3.5 hours, and the viscosity appeared to be dependent on temperature: When shortly acclimated to ambient temperature, the hand stirring resistance increased additionally.

Table 16. shore A hardness and mechanical properties of GAP/BPOB, seen in perspective with GAP/N100.

Sample	Composition	BPOB:GAP	NCO:OH	Shore A hardness	elastic modulus (MPa)	Peak stress (MPa)	Elongation at break (%)
T2-7	GAP/N100	N/A	1.01	31	0.47	0.50	122
T2-33	GAP/BPOB	1	N/A	28	0.55	0.34	68
T2-34	GAP/BPOB	1.3	N/A	49	1.24	0.57	48

BPOB cross-linked GAP showed to be mechanically inferior in comparison with GAP diol in a polyurethane elastomer. A cross-linking ratio of BPOB:GAP = 1.0 (T2-33) gave a comparable stiffness with GAP/N100 at NCO:OH ratio of 1.0 (T2-7). This promotes the procedure of calculating triazole cross-linkage applicable as an analogue to NCO:OH ratios.

The glass transition of T2-33 is found to be -33 °C (FIG) by DSC, which is 10 °C higher than a conventional PUR matrix with comparable cross-linkage. The 1 Hz curve of a multi-frequency DMA run revealed a T_g of -36 °C, emphasizing that the glass transition is most of all a region, not a specified temperature.

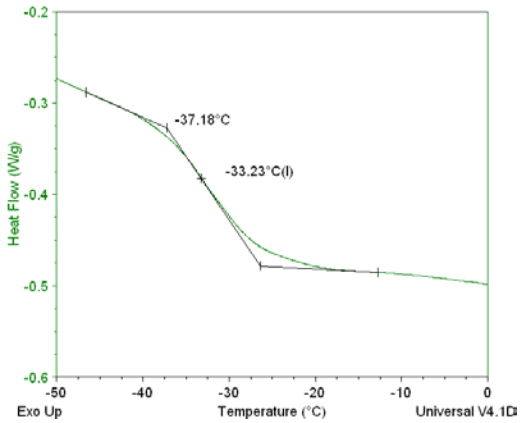

Figure 75. DSC analysis of T2-33, focused on what is proven (by DMA) to be the endotherm transition of T_g.

Ang et al. points out three disadvantages with triazole based curing: The depletion of energy when azide groups are consumed (since triazole groups provide much less energy), the difficulties in retaining energetic plasticizers in the polymer, and an erratic material rigidity (Ang 2012). As for the depletion of energy, DSC results of T2-33 (FIG) gave no apparent decrease in heat flow intensity, since the peak height for T2-33 (green curve) is between two parallels of GAP/N100 (T1F5b). Any significant energetic loss due to the utilization of

azide moieties is neglected because of an abundance of such. BPOB is a small molecule, which also is considered retarding the dilution of energy.

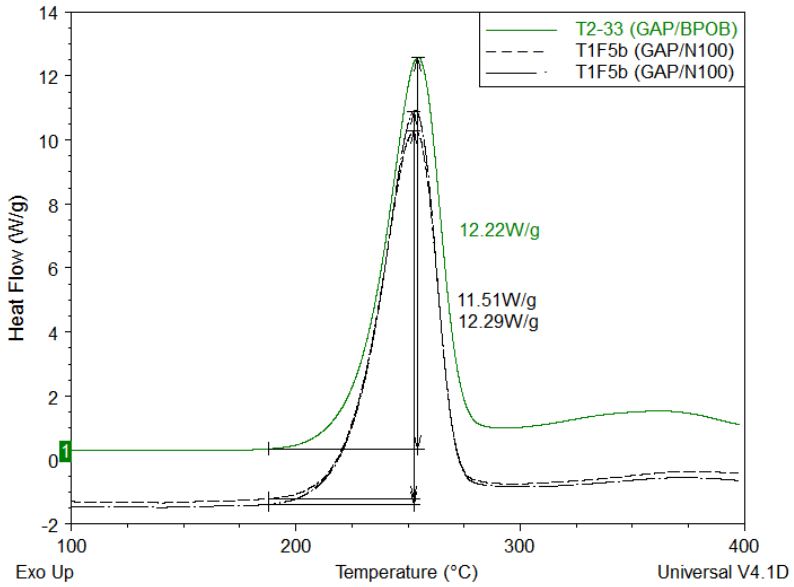

Figure 76. DSC of T2-33 compared with GAP/N100, comparable cross-linkage. Focused on the relevant temperature region where GAP disintegrates.

From FIG one can observe that BPOB does not inflict onset temperature from where the reaction of the azide moieties propagates. An integration of the heat capacity peak would suggest an enthalpy of the exothermal decomposition. The heat capacity peaks are similar, though opposite along the Y axis. According to the following interpretation of enthalpy: $\int C_p \, dT = \Delta H$. For GAP/BPOB (T2-33), a release of 1877 J/g is observed (see DSC APP). Enthalpy estimates from DSC tends to be somewhat lower than reported, which might origin from an insufficient sealing of the crucible lid.

Figure 77. a) Image of a ruptured specimen of T2-33. b) Specimens of T2-33, after tensile testing. c) T2-34.

The image taken of T2-34 (FIG), reveal small splinters due to cutting. Generally, when cutting highly cross-linked samples, a texture like this is normal.

The master curve plot of T2-33 reveals measurements of E modulus in angular frequency of about 1 000 Grad/s (≈ 160 GHz), at 20 °C as reference temperature, although the real response were measured only at temperatures from -36 °C (T_g) to about 50°C in steps of 2 °C/min. This illustrates the immeasurable regions a master curve can predict.

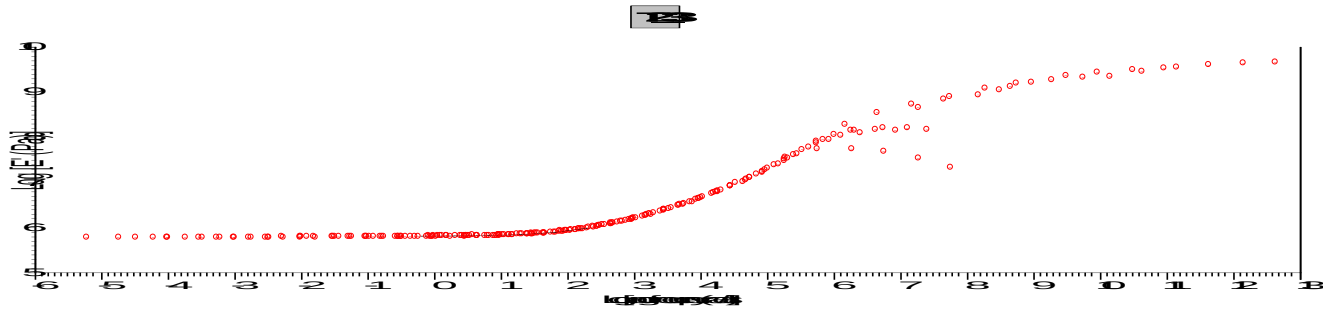

Figure 78. Shifted curves of T2-33. Some incompatibilities is found around the angular frequencies of log 6-8 rad/s. Other than that region, T2-33 complies with the time-temperature superposition principle.

Bluntly spoken, the specific material stiffness is given as Young's modulus (E'). The following master curves are constructed from the Storage modulus (G') of DMA, but converted to the elastic modulus (E') through the following relationship:

$$E' = 2G'(1 + \nu)$$

Where ν - the *poisson's ratio,* is a descriptive ratio of lateral contraction over the longitudinal extension. Poissons' ratio is fractionally below 0.5 for rubbers (McCrum, Buckley et al. 1997).

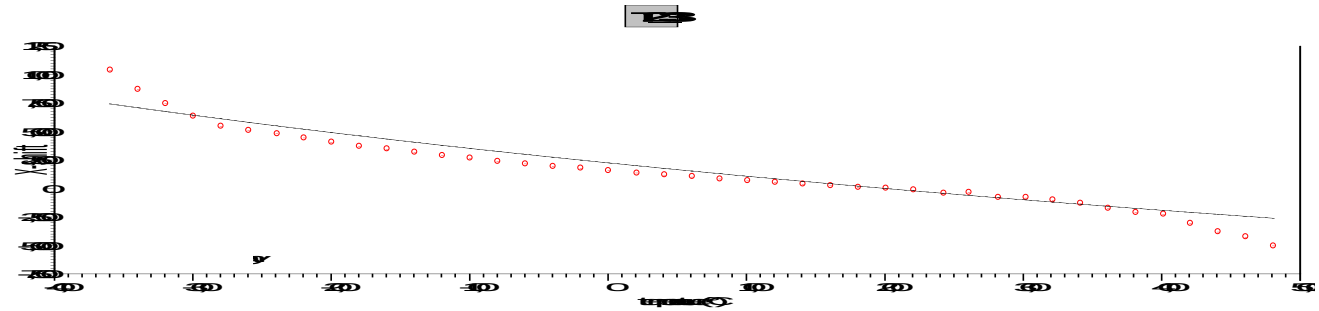

Figure 79. Shift function for T2-33. C1 is 26.35, C2 is 254.9, standard error of 61.26.

The WLF shift function of T2-33 is not completely correlating to the pattern of shift at the extreme ends of temperature. A relationship between temperature and shift factor is nevertheless obvious, if not optimized.

3.4 Dual cure

BPOB/IPDI

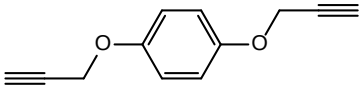

Figure 80. BPOB

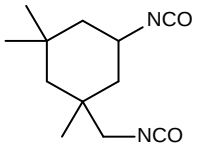

Figure 81. IPDI

What has been produced and characterized until now are matrices that contain one curing agent system. The introduction of an extra curing system to the binder synthesis could be beneficial in manners of controlling the curing process with two different reactions that takes place at the same time, but not interfering with each other. A dual cure could give enhanced mechanical strength above both of the parent binder systems.

The concept of dual curing in this work comprise of an isocyanate chain extender and a dialkyne cross-linking agent. The chain extender is specifically the diisocyanate IPDI. The cross-linking agent is in this case BPOB.

Processing the mixture and achieving a decent sample did not introduce any problems, on the contrary – all the dual cure samples of BPOB and IPDI went carelessly. Mechanically, the chain extender showed to improve significantly the mechanical strength, compared to its closest relatives from each curing system, GAP/BPOB and GAP/N100. Compared to the mechanical limitations of merely isocyanate curing, the dual cure highlights the importance of a chain extender as IPDI to accomplish favorable mechanical strength.

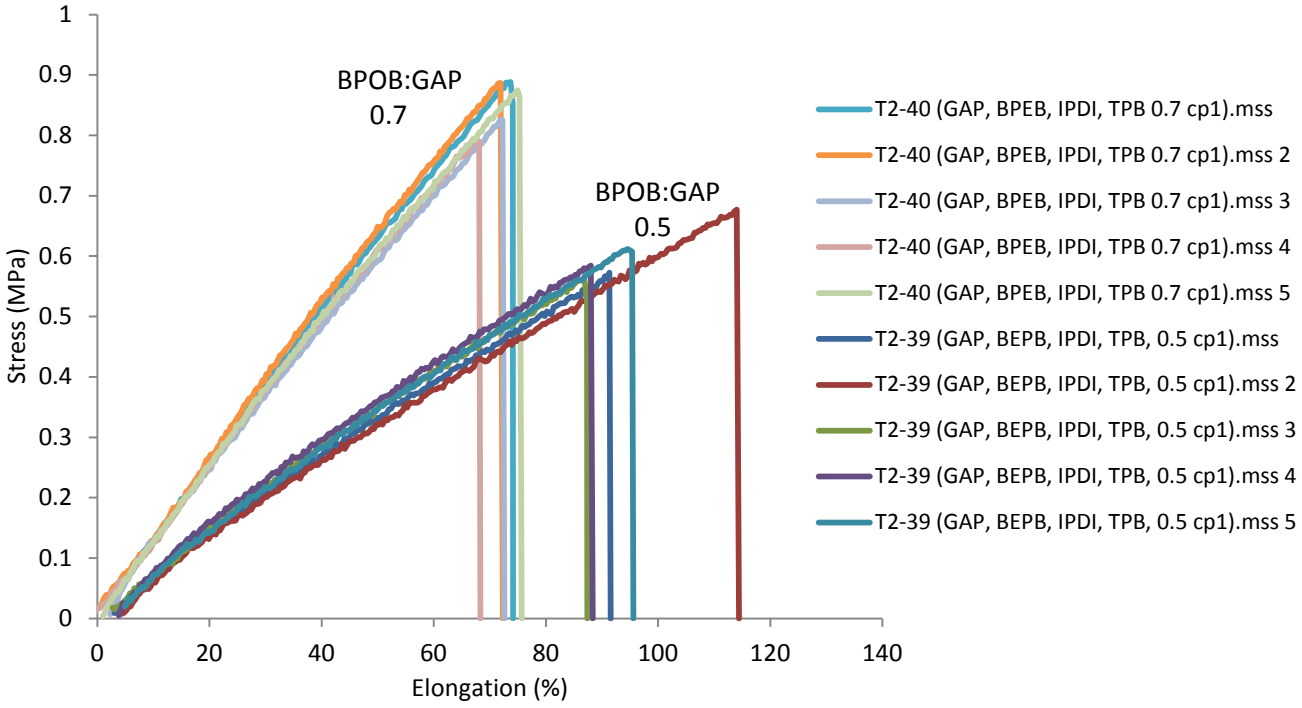

Figure 82. Tensile test specimens of the dual cured samples T2-39 and T2-40.

Two samples of different cross-linkage are shown in Fig, and one can appreciate the increase in stiffness as cross-linkage increases. For sample T2-39 and T2-40 the NCO:OH ratio is unity, as it could be argued that a di-

functional curing agent would not have an effect on mechanical properties when it became higher than one. However, an increase in stiffness and peak stress is shown when the NCO:OH ratio is elevated to 1.36. The behavior resembles the typical trade-off, regarding peak stress and elongation which any tuning of cross-linkage has given. The formation of allophanate cross-linkage is suggested. A comparison plot like FIG, of variation in NCO:OH ratio when BPOB:GAP is 0.70, would display a smaller change. Thus is an increasing cross-linkage by BPOB veiling for the mechanical influence of isocyanate curing.

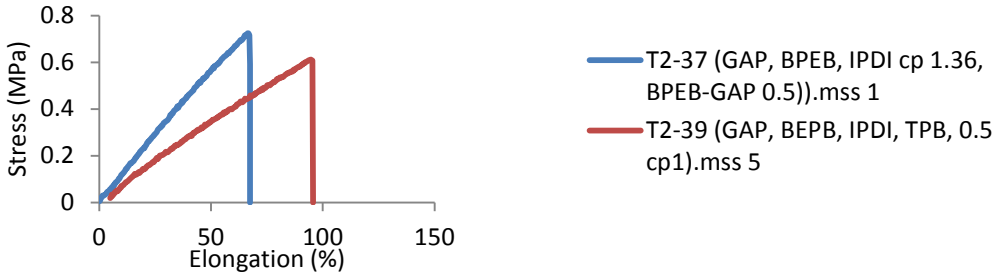

Figure 83. The response of varying NCO:OH.

BPOB is a relatively short cross-linker, which might not be optimal for cross-linkage. On the other hand, the curing agent offers an ease in preparation.

Figure 84. Image of the rupture of a T2-39-specimen. b) The dog bone specimens of T2-39. c) the dog bones specimens of T2-40.

Propargyl alcohol/IPDI

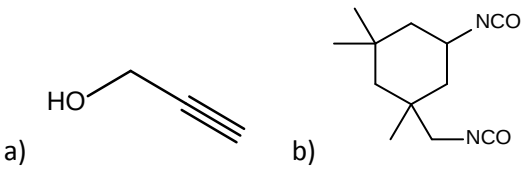

Figure 85. a) Propargyl alcohol b) IPDI.

The azide groups on GAP proved to be of use by isocyanate free curing with BPOB. Another way of cross-linking GAP diol through the azide moieties came to play, and involved two simple steps: First GAP diol was reacted with propargyl alcohol at 60°C for 22 h. If the propargyl alcohol had formed triazoles with the azide moieties by then, GAP diol became GAP polyol with a statistically distributed primary alcohol groups. A di-

functional isocyanate, namely IPDI, was introduced along with 0.05%TPB, to yield a flawless, cross-linked matrix, stating that a Huisgen cycloaddition did indeed occur. The detection of a downfall in the azide band on IR can possibly be observed along with an increase in urethane. See appended figure X in section 5.10.

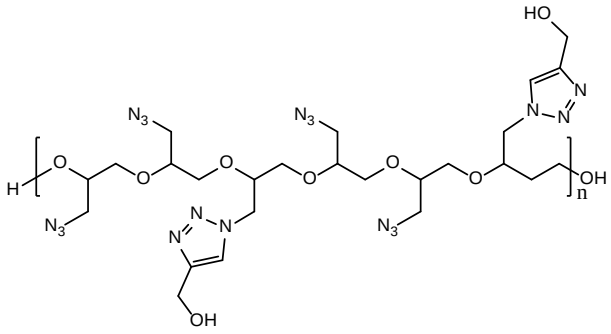

Figure 86. a GAP/propargyl alcohol prepolymer – a polyol.

According to Min et al. an aliphatic bis-propargyl curing agent (Bis(propargyl) Succinate, specifically) introduced better mechanical properties to a GAP binder matrix than the aromatic alternative, namely 1,4-Bis(1-hydroxypropargyl)benzene (Min, Park et al. 2012). The research could arguably be generalized towards following statement: Aliphatic alternatives of BPOB could introduce enhanced mechanical traits. The cross-linkage that is created by propargyl alcohol and IPDI is, in the end, aliphatic.

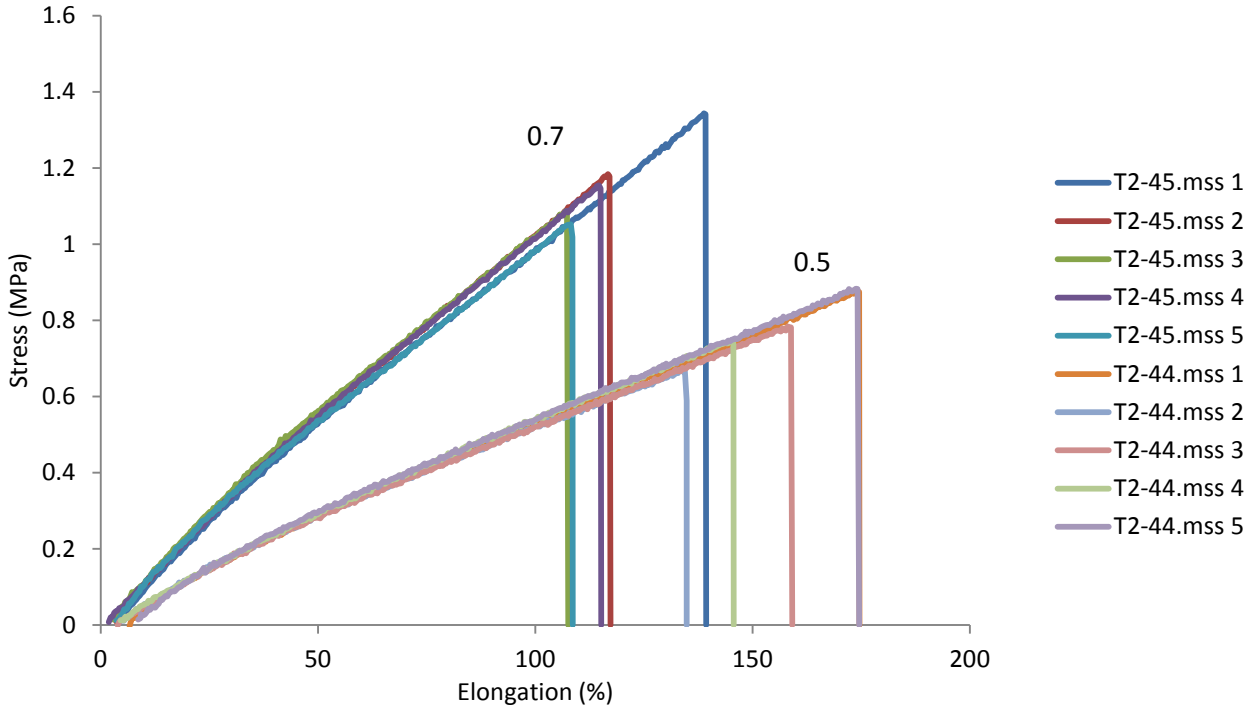

Figure 87. Tensile test results of T2-44 and -45.

Tensile test results of the GAP, extended with IPDI and cross-linked by both propargyl alcohol and IPDI, exhibited very promising mechanical strength. Comparable results are found in FIG CLUSTER, where the propargyl-alcohol shows remarkable strength, comparable to that of GAP/N100/IPDI. It would have been interesting to attempt a less cross-linked version of sample T2-44 and T2-45.

However, Propargyl alcohol has a T_g of around -25 °C, which is roughly 20 °C higher than GAP/N100. It could be speculated whether such a high T_g was caused by the triazole groups, or high content of IPDI, or something else.

Master curves of T2-44 are appended, and show to obey the time-temperature superposition principle. Additional master curves of T2-39 and T2-41 are also appended.

a)  b) 

c) 

Figure 88. images of broken dog bones a) the broken surface of T2-44. b) tensile tested dog bones of T2-44 c) T2-45.

Table 17. Shore A hardness and mechanical properties of dual cures, seen in perspective with GAP/N100.

Sample	Composition	BPOB:GAP	NCO:OH	Shore A hardness	elastic modulus (MPa)	Peak stress (MPa)	Elongation at break (%)
T2-7	GAP/N100	N/A	1.01	31	0.47	0.50	122
T2-37	GAP/BPOB/IPDI	0.50	1.36	47	1.11	0.69	67
T2-38	GAP/ BPOB/IPDI	0.70	1.36	52	1.6	0.9	57
T2-39	GAP/BPOB/IPDI	0.50	1.01	37	0.71	0.60	95
T2-40	GAP/BPOB/IPDI	0.70	1.01	50	1.28	0.85	72
T2-44	GAP/prop.alc./IPDI	0.5[a)]	1.0	35	0.57	0.79	157
T2-45	GAP/prop.alc./IPDI	0.7[a)]	1.0	46	1.11	1.2	117

a) Cross-linking agent is not BPOB, but in fact propargyl alcohol, reacted with IPDI to create a cross-linkage. ratios are comparable to those of BPOB:GAP.

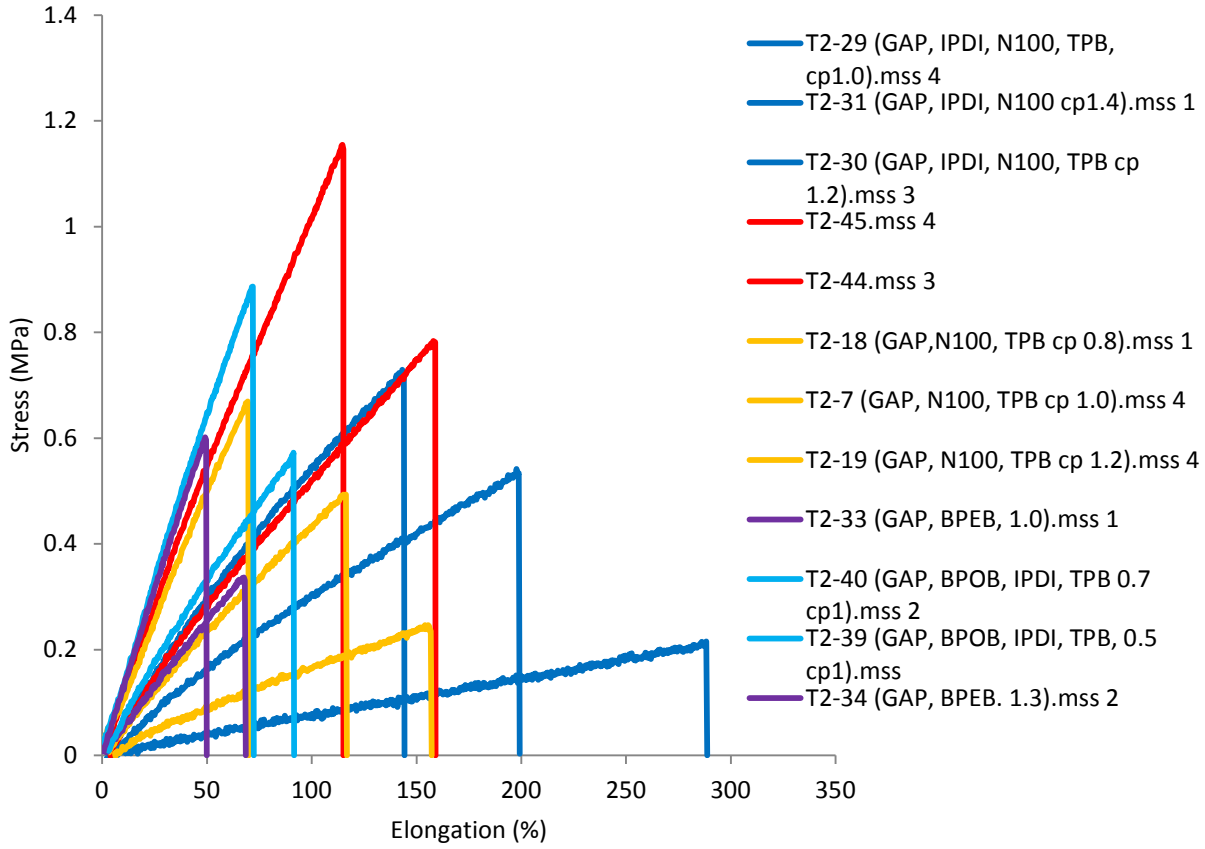

Figure 89. A clustered stress/strain plot over promising binder compositions, compared with their parent sample results.

The plot above (figure FIG) represents the promising binder combinations, although without T2-41. If T2-44 and T2-45 could be adjusted by ratio of cross-linkage, then they would seemingly mimic the behavior of GAP/N100/IPDI (dark blue).

3.5 Plasticizer

The introduction of a plasticizer will naturally decrease the stiffness in a cross-linked binder. As the plasticier content increases, a decrease in mechanical performance is expected. That does not necessarily mean a weakening of the binder matrix, but more a dilution. Five promising, GAP based, binder systems were introduced to plasticizer. One would sometimes try to implement as much plasticizer as possible, since a plasticizer would lower T_g, as well as introduce more energy to the combustion. The use of energetic plasticizer would ease the processing of a solid propellant formulation, as an introduction of filler crystals would increase viscosity.

BuNENA

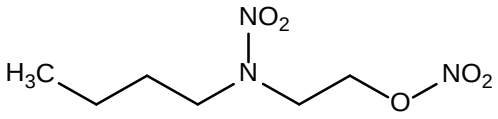

Figure 90. BuNENA

BuNENA is less sensitive than TMETN, and could, unlike TMETN, be conveyed without inert diluents. The use of NENAs gives high burning rates and reductions in flame temperature (Provatas 2000). Then again it provides less propulsive performance compared to more sensitive plasticizers (as NG, TMETN). BuNENA has a negative O_2 balance of -104 %, and decomposes exothermically at 210 °C. One disadvantage of NENAs as plasticizers is their possible long-term migration from the polymeric system (Simmons 1994), being relatively small molecules (although BuNENA is the larger among its family). NENAs are synthesized by nitration of alkyl ethanolamines, in yields of 80 %.(Provatas 2000)

a) 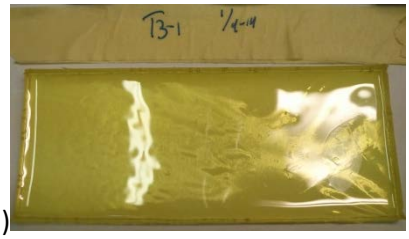 b) 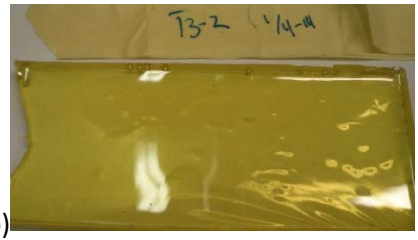

Figure 91. finished samples of BuNENA-Plasticized binders. a) T3-1 b) T3-2.

Tensile tests of plasticized binder systems displayed the borders of how robust the tensile test method was. Not regarding sensitivity (a burden handed to the tensile test machine itself), but regarding the clamp's ability to fixate any form of relatively soft rubber samples with the shape of dumbbells, comparable to each other. T3-1 approached the edge of sensible tensile results, a the sample thickness was exceptionally thin - only 1.8 mm thick. The respective peak load of T3-1 was 1.3 Newton, which translates to only 130 g of resistance until breakage. The tensile test curves (FIG) constitutes of remarkably intense noise. Nevertheless, an elastic modulus can be clearly read, and is uniform for all five specimens.

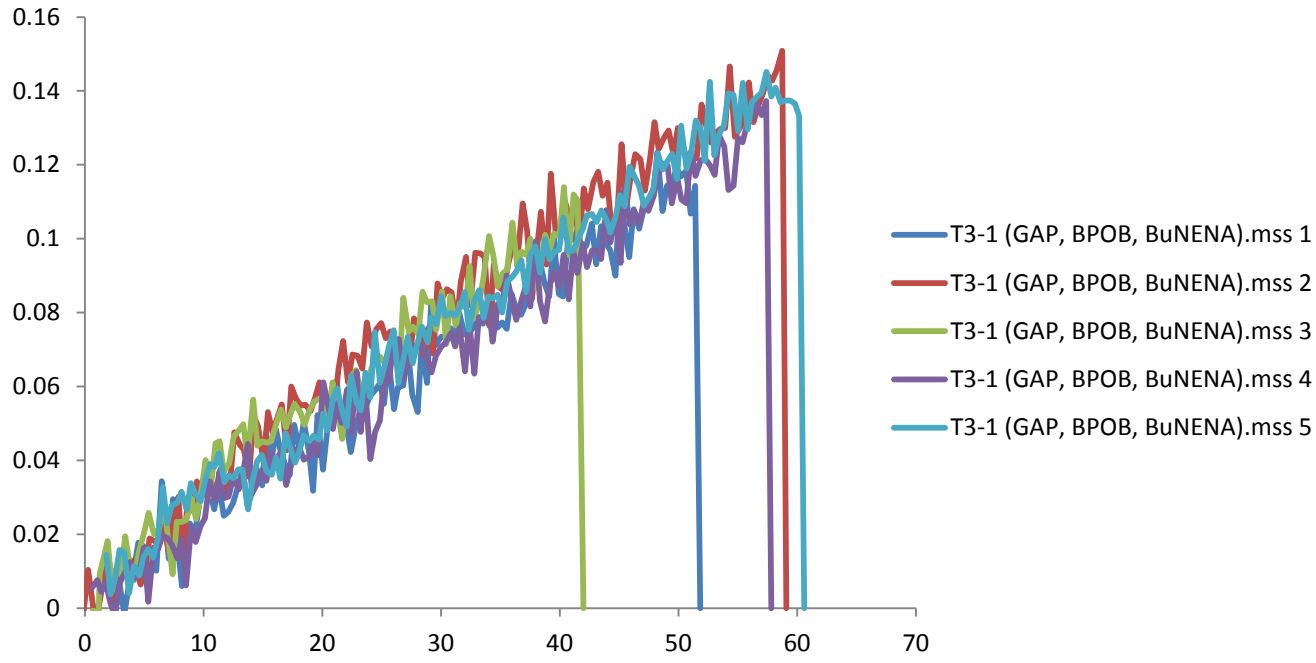

Figure 92. Stress-strain curve of GAP/BPOB/BuNENA (T3-1).

The plasticized GAP matrix, cross-linked with solely BPOB, did display relatively poor mechanical strength, which might be due to the exceptionally thin sample – but as poor mechanical strength also is the situation for the parent binder system T2-33, the sample size is believed to be within the method applicability.

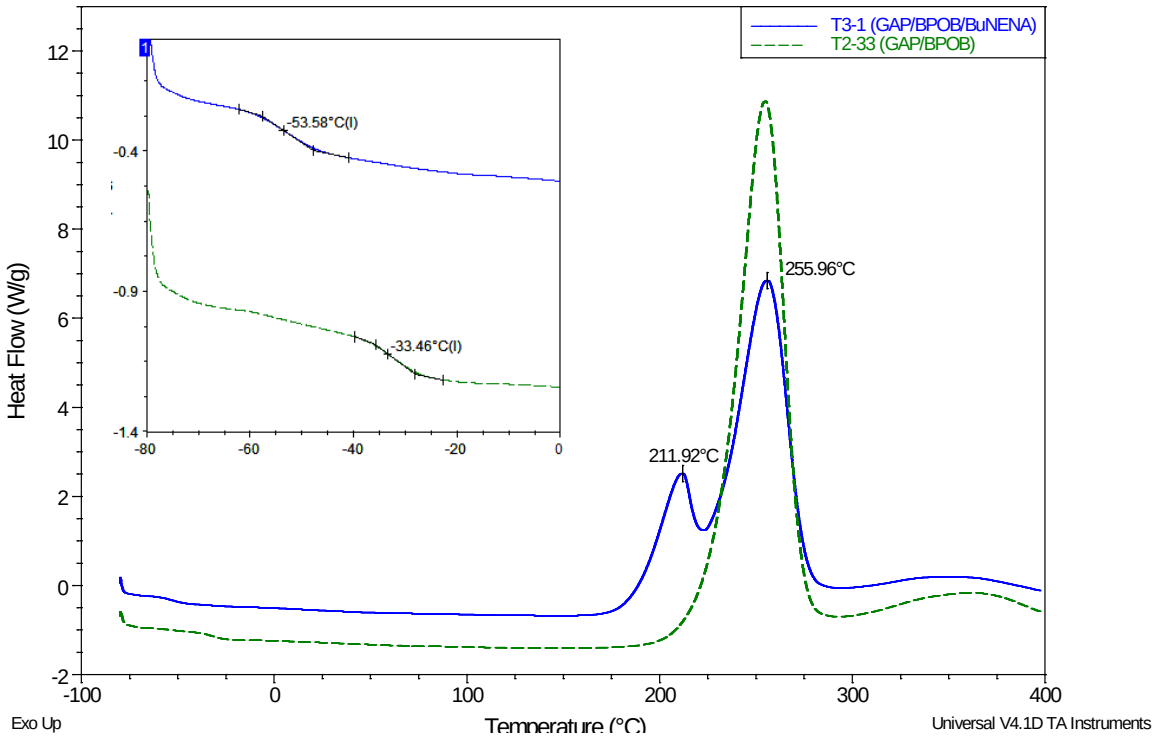

Figure 93. DSC curve of GAP/BPOB and its plasticized relative.

Table 18 shows how a plasticizer can inflict on physical and mechanical properties. The stiffness is almost halved in all cases.

Table 18. Summary table. Mechanical and physical properties of plasticized binder systems, and their un-plasticized comparisons. T3-1 was too thin for Shore A measuring. T_g is determined from DMA.. Elastic modulus is given automatically by Testworks 4. (Note: T_g for T2-30 is, in fact from T2-31 (a NCO:OH ratio raised by 0.2, determined by DSC).

	BuNENA				Mechanical Properties		
Sample	**Composition**	**(pl/po)**	**T_g (°C)**	**Shore A hardness**	**Elastic modulus (MPa)**	**Peak stress (MPa)**	**Strain at break (%)**
T2-33	GAP/BPOB	0	-36	28	0.55	0.34	68
T3-1		0.46	-55	N/A	0.28	0.13	53
T2-39	GAP/BPOB/IPDI	0	-35	37	0.71	0.60	95
T3-2		0.46	-57	21	0.42	0.21	57
T2-44	GAP/prop.alc/IPDI	0	-25	35	0.57	0.79	157
T3-3		0.46	-56	21	0.37	0.22	68
T2-30	GAP/N100/IPDI	0	-37	25	0.315	0.52	192
T3-4		0.46	-58	12	0.15	0.19	148

When a plasticizer is introduced, the T_g falls down to practically the same temperature. When a plasticizer is introduced, the properties that originally influenced T_g, is suppressed, and instead, the plasticizer now governs where T_g occur. This recognition is of high interest to the binder systems that originally had poor thermal properties – the plasticizer rules out the imperfections. A bottom level at about -55 °C is perceived from the collected data, at which the binder sample is responsible.

A IPDI/N100 cross-linked GAP matrix, plasticized with BuNENA produced a soft sample that were sticky towards the aluminum foil that surrounded it while being stored, which may relate to a saturation of plasticizer. Elongation was, however superior to the other BuNENA plasticized sample results.

Fig shows an enhanced illustration of the T_g of T2-33 and its plasticized parallel T3-1. The peak at 211 °C is the combustion of BuNENA. Since the Azide peak has not shifted, BuNENA is considered not to destabilize GAP. Similar DSC curves for the other BuNENA plasticized compound is appended in section 5.7.

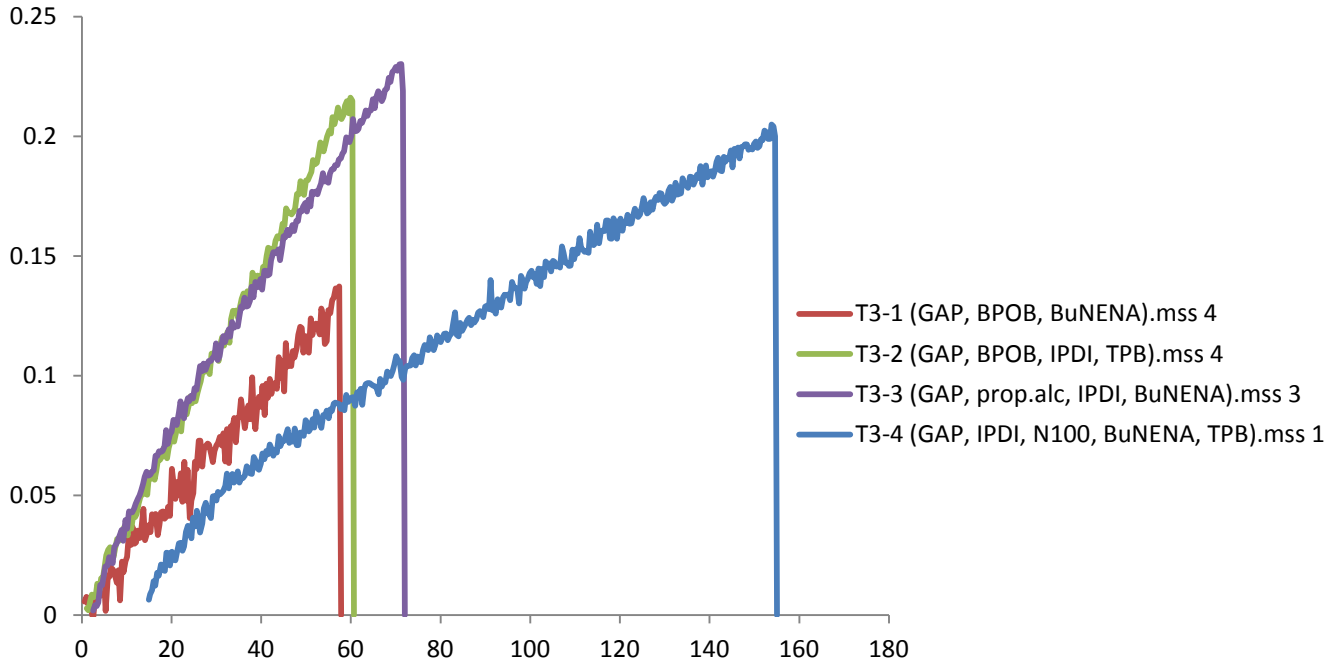

Figure 94. A collective plot of the median curve of all BuNENA-plasticized binder systems.

Figure shows the graphical tensile test results for BuNENA plasticized binders.

TMETN

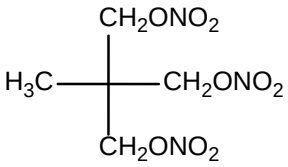

Figure 96. TMETN

Figure 95. Dog bone samples of T3-5 (GAP/N100/TMETN/PEG). The samples showed some perspiration of TMETN.

TMETN is a plasticizer that resembles NG, but is less sensitive. It is more energetic than BuNENA. Sample T3-5 contains unprocessed TMETN, as a closure of the investigations from T2-23 and -41, where TEG was added to mimic how a binder with the stabilizer PEG – but without plasticizer would behave.

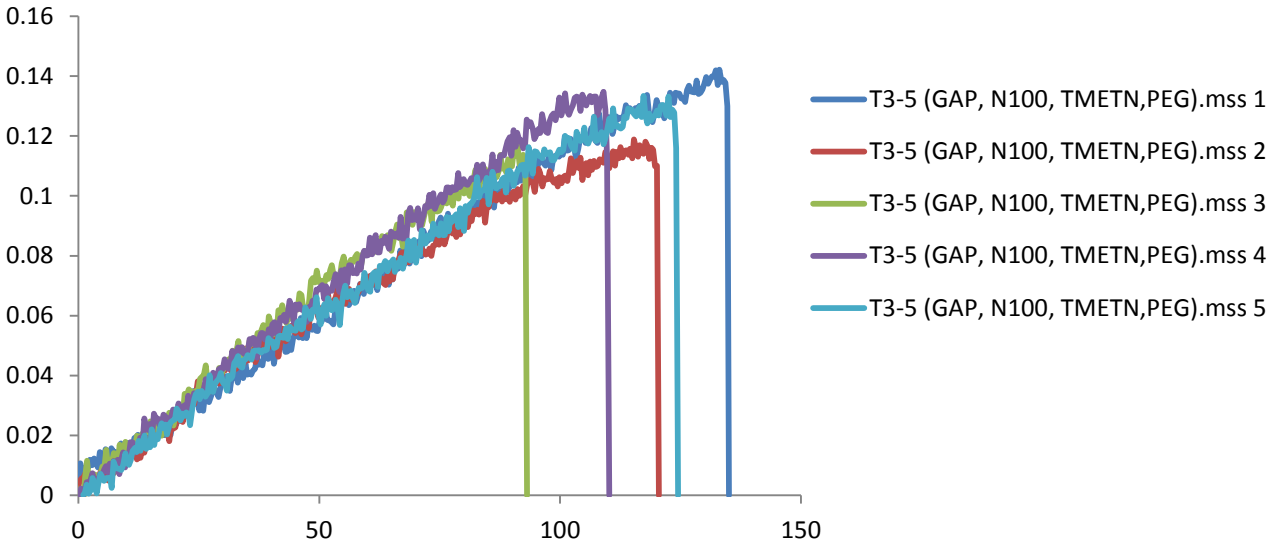

Figure 97. Plot of GAP/N100/TMETN/PEG

The sample specimens were remarkably thick (5mm). The thickness suppressed the noise of the curve some, in the sense of requiring a stronger load. The thickness is of course taken in account when displaying the results in Pascal.

Table 19.Table that describes how the unprocessed plasticizer TMETN(/PEG) influences a GAP/N100 binder.

	TMETN				Mechanical properties		
Sample	**Composition**	**(pl/po)**	**T_g (°C)**	**Shore A hardness**	**Elastic modulus (MPa)**	**Peak stress (MPa)**	**Strain at break (%)**
T2-41	GAP/TEG/N100	0	-36	54	1.56	1.2	85
T3-5	GAP/N100/TMETN/PEG	0.55	-54	0	0.13	0.13	116

The introduction of plasticizer undoubtedly lowered hardness (beyond measurable by Shore A hardness method). The stiffness declined by a factor of ten.

Also T_g was lowered. From comparing the decline in T_g for TMETN with those of BuNENA (prev. TABLE), it is suggested that BuNENA is a more effective plasticizer, even though less plasticizer was introduced. DSC of a similar sample with purified TMETN from previous work by the author (REF), revealed a T_g identical to T3-5. Therefore does PEG not influence T_g when plasticizer is involved.

In harmony with the four other plasticized compositions (T2-1,2,3,4), the T_g went down to a level where the plasticizer supposedly governed T_g. The binder was perhaps approaching a saturation point for the amount of plasticizer it could withhold. The sample had a sticky, moist surface.

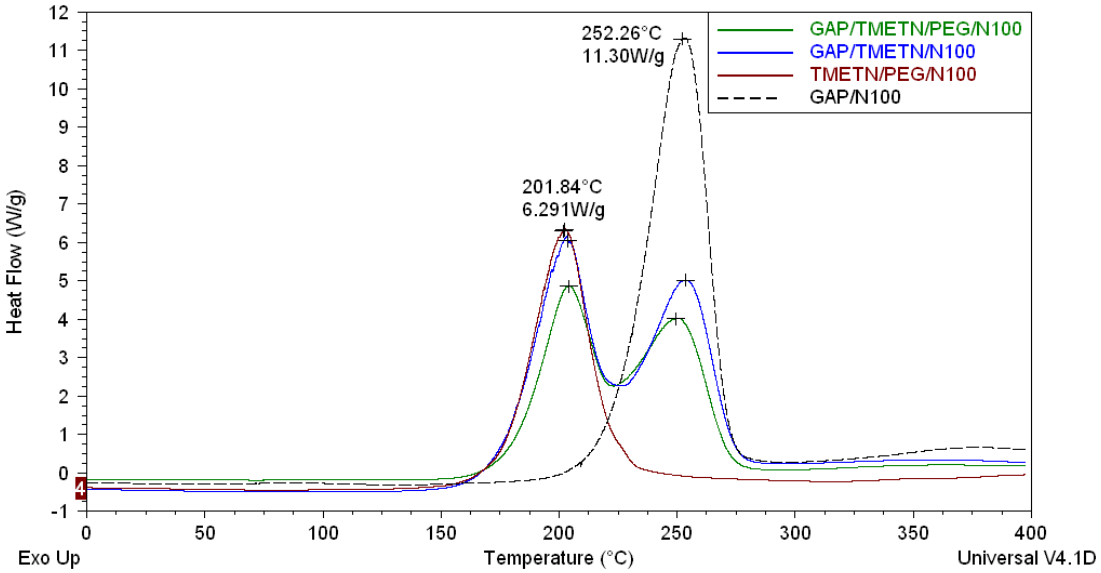

Figure 98. multiple DSC curves layered to show the occurrence of nitrous (onset 170 °C) and azide (onset 230 °C) triggered combustion processes. GAP/TMETN/N100 is taken from previous work by the author.

Figure FIG displays a peak where TMETN is degrading (200 °C), and a peak where GAP is degrading (250°C). The blue curve is obtained by previous work by the author (REF prev), and represents a sample similar to T3-5 (green), but where TMETN has been extracted. TMETN does not destabilize the initial combustion of GAP, and vice versa. Unprocessed TMETN is very similar, but a little less energetic than its purified twin, where the PEG stabilizer is removed.

4. Conclusions

A fairly comprehensive preparation and analysis of prepared binder systems for use in solid propellant formulations has been performed, with regards to mechanical tensile testing an thermal characterization.

The versatility of cross-linkage has been clearly addressed. The NCO:OH ratio could seemingly be tuned to fit the mechanical properties of a isocyanate cured polymer sample.

Prepolymers that are not initially miscible with GAP can still produce a homogeny copolymer when cured with N100. Specifically produced TEG, 1,4-butanediol and PPG-PEG a successful cure with GAP, cured with N100 and catalyzed by TPB.

PPG-PEG/N100 exhibited inferior mechanical strength, but a satisfactory T_g. An incorporation PPG-PEG to form a GAP/PPG-PEG/N100 copolymer corrupted the mechanical properties of GAP/N100. A favorable T_g for the copolymer was predicted, but not shown.

1,4-butanediol did not improve the mechanical properties of GAP/N100 when introduced as a random chain extender in a GAP/1,4-butanediol/N100 copolymer binder system. 1,4-butanediol did also provoke a raise in T_g.

Miscibility issues combined with a slow pot life is believed to be the reason for erratic results with Voranol EP1900 and Desmodur N100. A change of curing catalyst resulted in a major increase in elongation at break. Separately, the change in curing conditions gave a stiffer harder and stronger sample. Pot life is crucial for achieving a homogenous matrix of EP1900/N100. Voranol EP1900 was not willingly compatible to an energetic GAP/N100 matrix.

Propargyl alcohol did, with the aid of IPDI, readily produce a dual cured binder sample with GAP. The preparation method was uncomplicated and yielded a mechanically strong binder.

The combined cure of N100/IPDI isocyanate together with GAP, gave a mechanically very strong binder.

Master curves were successfully created for four different curing systems, specifically GAP/BPOB, GAP/TEG/N100, GAP/prop.alc/IPDI, and GAP/BPOB/IPDI. The samples showed to obey the time temperature superposition principle.

Plasticizer

The implementation of BuNENA plasticizer recapitulates the initially promising features of propargyl alcohol, as a T_g of -25 ° descends down to -56 °C when BuNENA is introduced.

When a plasticizer is introduced to a GAP binder, T_g drops to about -55 °C, regardless of what the previous T_g without plasticizer was. The plasticizer governs T_g when implemented.

BuNENA is a more effective plasticizer than TMETN, regarding T_g. The BuNENA samples from which the statement derives, also contained less plasticizer (pl/po) than the relevant TMETN plasticized binder.

A GAP based binder system, plasticized with unprocessed TMETN (containing 20 wt % PEG), provided an adequate matrix at a pl/po ratio of 0.55. PEG, supposedly TEG, interacted with the curing agent to provide a mechanically enhanced binder, from the following logic: We know that the PEG stabilizer reacts with the curing agent N100 in a mixture dominated by TMETN, sufficient to create a sustainable plasticized matrix alone. TEG in solitude interacts actively in a GAP/N100 matrix, giving a stronger matrix without the expected loss in strain, only a depletion of energy potential. A stiffer, but also more stretchable sample might imply a promotion of physical cross-linkage when TEG is introduced.

T_g increased 7 °C at a po2/po1 ratio of 2.44. TMETN lowered it to -54 °C. Some perspiration of TMETN was observed, and a large quantity of N100 was required to attain a NCO:OH of 1. A slightly reduced amount of unprocessed TMETN might combine the best from mechanical strength and energy output.

method applicability (tensile strength)

The personally developed clamps were most applicable to a wide range of cross-linked polymer matrices. The method, as a unity, delivered precise tensile test results for all given challenges. The method is perhaps especially applicable to the enquiry of very soft binder systems, e.g. with a high plasticizer content (as the T3-samples) or a low cross-linkage (as T2-29). For these soft samples conventional, static fixation jigs may induce a considerate error, as mass from the outer dog bone regions could contribute to the elongation, or even allow the dog bone ends to slip out. Deductively, the teeth on the dynamic clamps do not apply more compressive load than the stiffness of the sample provides. This feature makes the method versatile to a large range of elastomeric materials.

Being only 4 cm long, the dog bones could be machine pressed from rather small samples, demanding only about 30 g of total sample mass to acquire 5 to 6 parallels. Such a small sample mass should be recognized as a material-efficient, and also a safety-oriented approach towards a comprehensive investigation of mechanical properties.

None of the promising binder systems revealed problems in manners of thermal stability. The same can be stated for the plasticized sample containing GAP/N100/TMETN/PEG.

5. Appendix

5.1 Temperature and humidity measurements

Table 20. Temperature and relative humidity at the laboratory. The dates are directly connected to experimental work.

Date (2013-14)	Time	Relative air moisture	Temperature
05.nov	-	26.4 %	21.0 °C
11.nov	13:14	23.0 %	20.4 °C
12.nov	09:40	34.4 %	20.0 °C
12.nov	10:00	33.8 %	20.3 °C
13.nov	10:30	23.9 %	20.3 °C
13.nov	13:20	24.0 %	21.0 °C
15.nov	10:30	28.2 %	20.9 °C
18.nov	11:00	32.8 %	20.2 °C
20.nov	09:50	17.2 %	20.0 °C
22.nov	-	14.0 %	20.8 °C
25.nov	10:30	15.7 %	20.6 °C
27.jan	-	17.6 %	19.8 °C
28.jan	18:32	18.5 %	22.6 °C
03.feb	09:30	28.3 %	19.4 °C
04.feb	13:00	22.8 %	20.3 °C
10.feb	15:53	28.9 %	19.7 °C
11.feb	16:00	25.6 %	20.8 °C
12.feb	13:45	26.0 %	20.3 °C
18.feb	13:30	19.8 %	20.3 °C
19.feb	13:25	20.8 %	19.9 °C
20.feb	11:00	19.4 %	19.9 °C
26.feb	15:30	26.0 %	20.8 °C
27.feb	18:40	28.6 %	20.7 °C
28.feb	11:42	27.0 %	20.4 °C
03.mar	13:30	26.8 %	20.9 °C
10.mar	09:40	30.7 %	20.2 °C
13.mar	11:30	24.7 %	22.0 °C
14.mar	12:40	19.0 %	20.9 °C
01.apr	18:19	17.5 %	20.8 °C
02.apr	16:30	19.4 %	20.7 °C

5.2 Sample compositions

Table 21. Sample compostions of «T1» samples.

sample	Composition	Fraction of substance		
T1	**Prepolymer/Curative/curing agent**	**NCO:OH**	**TPB (wt %)**	**Comments**
T1F6a2	EP1900/N100/TPB	0.9	>0.05	
T1F6a2	EP1900/N100/TPB	1.0	>0.05	
T1F6b2	EP2010/N100/TPB	0.8	>0.05	not cured
T1F6b2	EP2010/N100/TPB	1.0	>0.05	not cured
T1F6c2	PPG-PEG/N100/TPB	0.9	>0.05	
T1F6c2	PPG-PEG/N100/TPB	1.0	>0.05	formally identical to T2-42
T1F6d2	HTPE/N100/TPB	0.8	>0.05	
T1F6d2	HTPE/N100/TPB	1.0	>0.05	
T1F6e2	HTCE/N100/TPB	0.8	>0.05	
T1F6e2	HTCE/N100/TPB	1.0	>0.05	
T1F6f2	TEG/N100/TPB	0.8	>0.05	
T1F6f2	TEG/N100/TPB	1.0	>0.05	
T1F1P2	TEG/N100/TPB	1.4	>0.05	
T1-1,4But0.8	1,4-butanediol/N100/TPB	0.8	>0.05	
T1-1,4But1.0	1,4-butanediol/N100/TPB	1.0	>0.05	
T1-1,4But1.2	1,4-butanediol/N100/TPB	1.2	>0.05	
T1F4a4	GAP/K88/TPB	0.79	0.051	
T1F4a4	GAP/K88/TPB	1.02	0.049	
T1F4a4	GAP/K88/TPB	1.20	0.051	
T1F4b4	GAP/K88HVL/TPB	0.82	0.050	
T1F4b4	GAP/K88HVL/TPB	1.00	0.050	
T1F2f	GAP/N100/TPB	1.26	0.049	
T1F3	HTPB/IPDI/TPB	1.59	0.049	
T1F3b	HTPB/IPDI/TPB	1.13	0.050	
T1F3c	HTPB/IPDI/TPB	0.80	0.042	

Table 22. Compositions of «T2» samples.

Sample	Composition	Fraction of substance					
T2	**Prepolymer/Curative/ Curing agent**	**IPDI: N100 (^{n}NCO)**	**po2/ po1 (^{n}OH)**	**BPOB: GAP (n)**	**NCO: OH (n)**	**TPB (wt %)**	**Comments**
T2-6	EP1900/N100/TPB				1.00	0.048	
T2-7	GAP/N100/TPB				1.01	0.048	
T2-8	HTPB/IPDI/TPB				1.00	0.050	
T2-12	GAP/K88HVL/TPB				1.00	0.048	formally identical to T2-21
T2-16	EP1900/N100/DBTDL				1.00		100ppm DBTDL

T2-17	EP1900/N100/TBL				1.01	0.050	
T2-18	GAP/N100/TPB				0.80	0.048	
T2-19	GAP/N100/TPB				1.21	0.048	
T2-21	GAP/K88HVL/TPB				1.01	0.049	formally identical to T2-12
T2-23	GAP/TEG/N100/TPB		1.90		1.00	0.051	
T2-24	EP1900/N100/TPB				1.04	0.049	75°C cure
T2-29	GAP/N100/IPDI/TPB	0.95			1.02	0.052	
T2-30	GAP/N100/IPDI/TPB	0.99			1.21	0.050	
T2-31	GAP/N100/IPDI/TPB	1.00			1.40	0.049	
T2-32	GAP/1,4-butandiol/TPB		0.100		1.01	0.049	
T2-33	GAP/BPOB			1.00			
T2-34	GAP/BPOB			1.30			
T2-37	GAP/BPOB/IPDI/TPB			0.50	1.36	0.052	
T2-38	GAP/BPOB/IPDI/TPB			0.70	1.36	0.050	
T2-39	GAP/BPOB/IPDI/TPB			0.50	1.01	0.051	
T2-40	GAP/BPOB/IPDI/TPB			0.70	1.01	0.050	
T2-41	GAP/TEG/N100/TPB		2.44		1.00	0.050	
T2-42	PPG-PEG/N100/TPB				1.00	0.050	Formally identical to T1F6c2. 80 °C cure.
T2-43	EP1900/N100/TPB				1.00	0.050	New batch of EP1900. 80°C cure
T2-44	GAP/prop.alc/IPDI/TPB					0.049	
T2-45	GAP/prop.alc/IPDI/TPB					0.051	
T2-46	GAP/PPG-PEG/N100/TPB		0.100		1.00	0.049	

Table 23. Compositions of «T3» samples.

Sample	Composition	Fraction of substance						
T3	Prepolymer/Curati - ve/Curing agent	IPDI:N100 (nNCO)	pl/po (wt)	po2/po1 (^{n}OH)	BPOB:GAP (n)	NCO: OH (n)	TPB (wt %)	Comm.
T3-1	GAP/BPOB/BuNENA		0.46		1.00			thin sample
T3-2	GAP/BPOB/IPDI/ BuNENA/TPB		0.46		0.50	1.00	0.049	
T3-3	GAP/prop.alc/IPDI/ BuNENA/TPB		0.46				0.050	
T3-4	GAP/N100/IPDI/ BuNENA/TPB	0.99	0.46			1.21	0.050	
T3-5	GAP/N100/ TMETN/PEG/TPB		0.55	2.43*		1.00	0.047	

5.3 Quality control at Nammo

OH-level quantification

Table 24. Table of titration volumes for OH-level determination in GAP diol lot # 06S12. Three parallels.

GAP diol sample	Weighed (g)	Titrant consumed (mL)	OH levels (meq/g)
1	2.0300	26.377	0.800
2	2.0125	26.314	0.823
3	2.0195	26.325	0.817
Blind 1		29.539	
Blind 2		29.714	
Blind average		29.627	

Table 25. Table of titration volumes for OH-dtermination in EP1900 lot # WH20091503. Three parallels.

EP1900 sample	Weighed (g)	Titrant consumed (mL)	OH levels (meq/g)
1	2.0111	27.855	0.345
2	1.9987	28.556	0.171
3	1.9991	28.122	0.280
Blind 1		29.283	
Blind 2		29.199	
Blind average		**29.241**	

NCO-level quantification

Table 26. Table of titration volumes for NCO-level determination in Desmodur N100 (lot # ABL-4823) and Baymidur K88 (lot # not available). Two parallels each.

N100 sample	Weighed (g)	Titrant consumed (mL)	% NCO
1	5.0058	23.744	22.03
2	5.0287	23.816	21.87
K88 sample			
1	3.0169	27.588	31.20
2	2.9918	27.274	31.91
Blind 1		49.981	
Blind 2		50.021	
Blind average		**50.001**	

5.4 Shore A

Note that presented values are the shore A hardness-results from 5 seconds after indentation, average values of 5 parallel measurements. Where possible, the numbers represent random indentations of top and bottom of the sample material.

Table 27. Shore A hardness measurements from T1-samples. the values origin from 5 parallels, presented as mean hardness and standard deviation of selected samples. T1F6c2 were too thin for Shore A measurement, but T2-43 is formally equal.

Sample	Composition	NCO:OH	Shore A Hardness				Comments
			0 sec	σ	5 sec	σ	
T1F6a2	EP1900/N100/TPB	0.9	N/A	N/A	N/A	N/A	thin sample
T1F6a2	EP1900/N100/TPB	1.0	23	1.5	22	1.5	
T1F6c2	PPG-PEG/N100/TPB	0.9	24	4.1	23	3.9	
T1F6c2	PPG-PEG/N100/TPB	1.0	N/A	N/A	N/A	N/A	thin sample
T1F6d2	HTPE/N100/TPB	0.8	41	3.3	39	2.7	
T1F6d2	HTPE/N100/TPB	1.0	51	2.2	48	1.9	
T1F6e2	HTCE/N100/TPB	0.8	62	2.1	58	1.8	
T1F6e2	HTCE/N100/TPB	1.0	67	1.5	65	1.5	
T1F6f2	TEG/N100/TPB	0.8	82	2.9	75	4.3	
T1F6f2	TEG/N100/TPB	1.0	93	1.5	86	3.8	
T1F1P2	TEG/N100/TPB	1.4	93	3.6	91	4.1	
T1-1,4But0.8	1,4-butanediol/N100/TPB	0.8	84	2.6	79	2.5	
T1-1,4But1.0	1,4-butanediol/N100/TPB	1.0	86	7.1	82	9.1	
T1-1,4But1.2	1,4-butanediol/N100/TPB	1.2	89	4.7	87	5.1	
T1F4a4	GAP/K88/TPB	0.79	0	0.0	0	0.0	
T1F4a4	GAP/K88/TPB	1.02	12	0.7	10	0.5	
T1F4a4	GAP/K88/TPB	1.20	29	1.5	25	1.3	
T1F4b4	GAP/K88HVL/TPB	0.82	1	1.3	1	1.3	
T1F4b4	GAP/K88HVL/TPB	1.00	17	0.9	17	0.5	
T1F2f	GAP/N100/TPB	1.26	47	1.4	45	2.1	
T1F3	HTPB/IPDI/TPB	1.59	61	1.3	55	0.8	
T1F3b	HTPB/IPDI/TPB	1.13	43	0.8	38	0.9	
T1F3c	HTPB/IPDI/TPB	0.80	46	1.7	10	0.4	

Table 28. Shore A hardness measurements from samples subjected to tensile tests. the values origin from 5 parallels, presented as mean hardness and standard deviation of selected samples.

Sample	Composition	NCO:OH	Shore A Hardness				Comments
			0 sec	σ	5 sec	σ	
T2-6	EP1900/N100/TPB	1.00	34	0.0	25	0.0	
T2-7	GAP/N100/TPB	1.01	33	3.2	31	3.5	
T2-8	HTPB/IPDI/TPB	1.00	43	1.8	36	1.4	

T2-10	GAP/N100/TPB	-	33	0.8	31	1.7
T2-12	GAP/K88HVL/TPB	1.00	18	1.0	17	0.5
T2-16	EP1900/N100/DBTDL	1.00	23	0.9	21	1.0
T2-17	EP1900/N100/TBL	1.01	19	2.8	15	1.9
T2-18	GAP/N100/TPB	0.80	17	0.9	16	0.8
T2-19	GAP/N100/TPB	1.21	44	5.1	44	5.3
T2-21	GAP/K88HVL/TPB	1.01	24	1.3	23	0.8
T2-23	GAP/TEG/N100/TPB	1.00	58	1.6	55	1.6
T2-24	EP1900/N100/TPB	1.04	26	1.5	24	1.3
T2-29	GAP/N100/IPDI/TPB	1.02	8	2.3	7	2.1
T2-30	GAP/N100/IPDI/TPB	1.21	27	2.0	25	2.5
T2-31	GAP/N100/IPDI/TPB	1.40	39	2.3	36	3.0
T2-32	GAP/1,4-butandiol	1.01	39	1.8	38	1.4
T2-33	GAP/BPOB	-	29	1.7	28	1.3
T2-34	GAP/BPOB	-	49	0.9	49	1.3
T2-37	GAP/BPOB/IPDI/TPB	1.36	49	0.5	47	1.1
T2-38	GAP/BPOB/IPDI/TPB	1.36	53	1.8	52	1.5
T2-39	GAP/BPOB/IPDI/TPB	1.01	38	2.3	37	2.8
T2-40	GAP/BPOB/IPDI/TPB	1.01	51	1.6	50	1.3
T2-41	GAP/TEG/N100/TPB	1.00	60	4.0	54	1.3
T2-42	PPG-PEG/N100/TPB	1.00	39	5.6	38	4.0
T2-43	EP1900/N100/TPB	1.00	38	3.6	33	2.1
T2-44	GAP/prop.alc/IPDI/TPB		36	4.7	35	4.1
T2-45	GAP/prop.alc/IPDI/TPB		49	2.5	46	4.1
T2-46	GAP/PPG-PEG/N100/TPB	1.00	35	1.9	34	2.5

Table 29. Shore A hardness measurements from samples containing plasticizer. the values origin from 5 parallels, presented as mean hardness and standard deviation of selected samples.

Sample	Composition	NCO:OH	Shore A Hardness				Comments
			0 sec	σ	5 sec	σ	
T3-1	GAP/BPOB/BuNENA/TPB	1.00	N/A	N/A	N/A	N/A	thin sample
T3-2	GAP/BPOB/IPDI/BuNENA/TPB	1.00	25	1.4	21	3.2	
T3-3	GAP/prop.alc/IPDI/BuNENA/TPB		23	1.2	21	1.5	
T3-4	GAP/N100/IPDI/BuNENA/TPB	1.21	12	1.3	12	1.1	
T3-5	GAP/N100/TMETN/PEG/TPB	1.00	10	2.4	0	0.0	

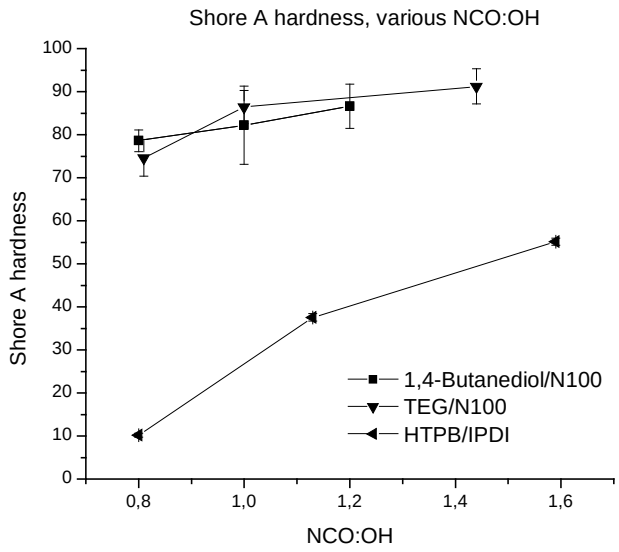

Figure 99. illustrative shore A hardness for different inert binder systems, when varying NCO:OH.

5.5 Mechanical performance

Table 30. Tensile test. Each result is the mean value of 5 parallels (if not commented otherwise). Standard deviation values of the specimen groups are attached.

Sample	Elastic modulus (MPa)	σ	Peak stress (MPa)	σ	Strain at break (%)	σ	Comments
T2-6	0.48	0.05	0.258	0.008	88	8	
T2-7	0.47	0.03	0.50	0.03	122	15	
T2-8	0.44	0.02	0.91	0.06	348	32	
T2-12	0.22	0.02	0.26	0.01	132	3	2 parallels
T2-16	0.20	0.01	0.48	0.01	295	6	4 parallels
T2-17	0.21	0.02	0.24	0.01	178	1	3 parallels
T2-18	0.180	0.002	0.26	0.02	161	13	
T2-19	1.09	0.07	0.7	0.1	69	9	
T2-21	0.30	0.01	0.27	0.04	138	14	3 parallels
T2-23	1.70	0.09	1.04	0.05	66	4	
T2-29	0.082	0.004	0.23	0.03	285	23	
T2-30	0.315	0.008	0.52	0.02	192	7	4 parallels
T2-31	0.60	0.01	0.76	0.06	147	11	
T2-32	0.74	0.02	0.59	0.02	90	3	
T2-33	0.55	0.02	0.34	0.02	68	4	
T2-34	1.24	0.07	0.57	0.03	48	2	
T2-37	1.11	0.05	0.69	0.06	67	5	
T2-38	1.6	0.1	0.9	0.1	57	7	6 parallels
T2-39	0.71	0.04	0.60	0.05	95	11	
T2-40	1.28	0.03	0.85	0.04	72	3	
T2-41	1.56	0.08	1.2	0.1	85	7	
T2-42	1.1	0.1	0.33	0.03	40	4	
T2-43	0.61	0.05	0.41	0.04	88	5	
T2-44	0.57	0.01	0.79	0.09	157	18	
T2-45	1.11	0.04	1.2	0.1	117	13	
T2-46	0.58	0.03	0.40	0.02	80	1	

Table 31. Tensile test. The results are average values of 5 parallels with their related standard deviation value for the sample specimen.

Sample	Elastic	σ	Peak	σ	Strain at	σ	Comments

	modulus (MPa)		stress (MPa)		break (%)		
T3-1	0.28	0.04	0.13	0.02	53	8	1.8mm thick
T3-2	0.42	0.06	0.21	0.02	57	9	
T3-3	0.37	0.03	0.22	0.02	68	8	
T3-4	0.15	0.01	0.19	0.02	148	16	
T3-5	0.13	0.01	0.13	0.01	116	16	

Table 32. Method precision of tensile tests. Elastic modulus measurement of sample T2-42, T2-41 and T2-8 gave the most deviating results out of 5 parallels, regarding elastic modulus, peak stress and elongation at break, respectively.

	Elastic modulus	MPa	Peak stress	MPa	Strain at break	(%)
Max σ	0.1	(T2-42)	0.1	(T2-41)	32	(T2-8)
Min σ	0.002		0.008		1	
Average σ	0.04		0.04		9	

Tensile test curves

Curing agent

GAP/N100

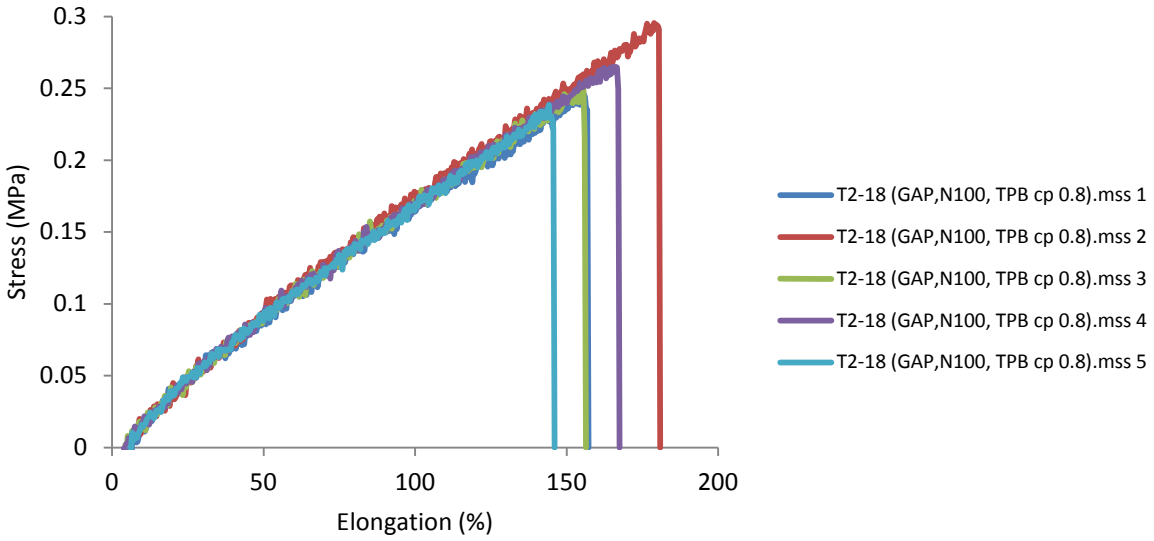

Figure 100. tensile test results of T2-18.

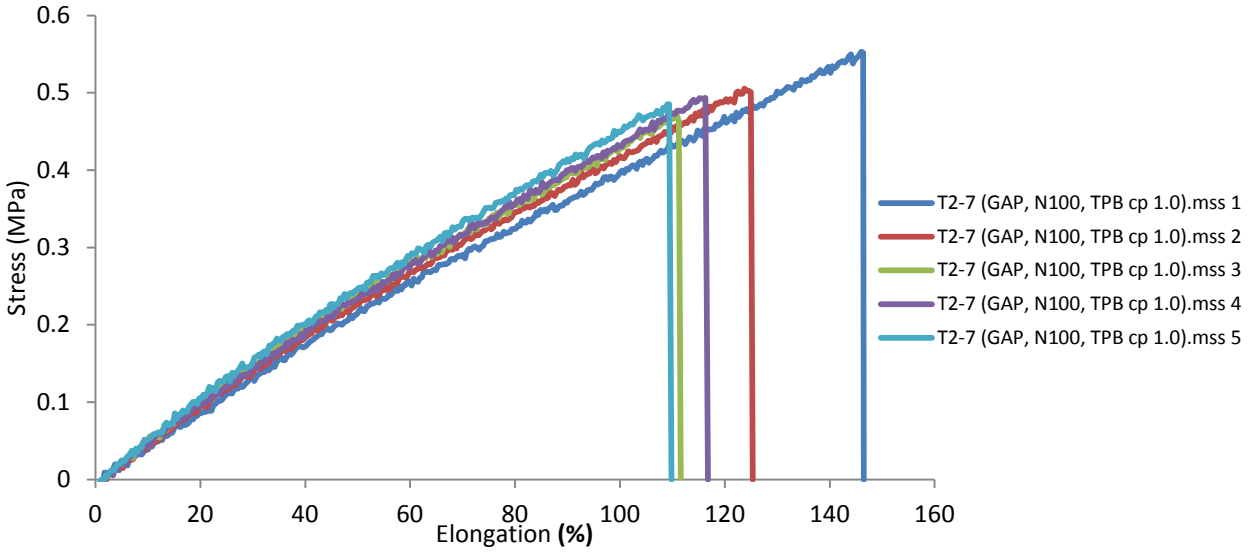

Figure 101. Tensile test results of T2-7

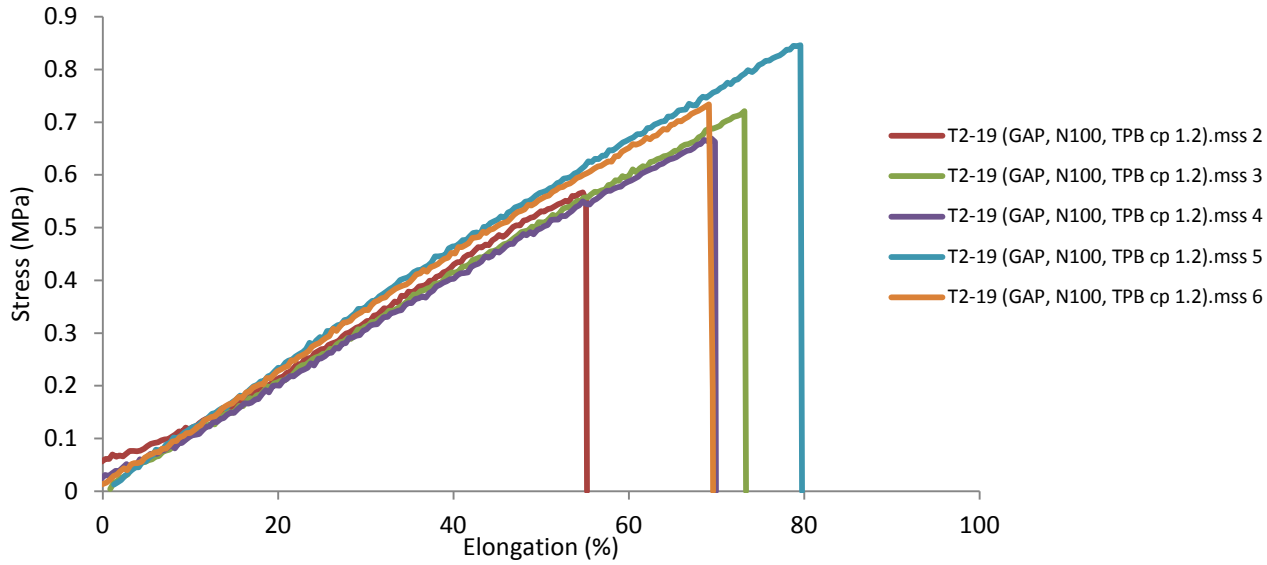

Figure 102. Tensile results of T2-19.

GAP/K88HVL

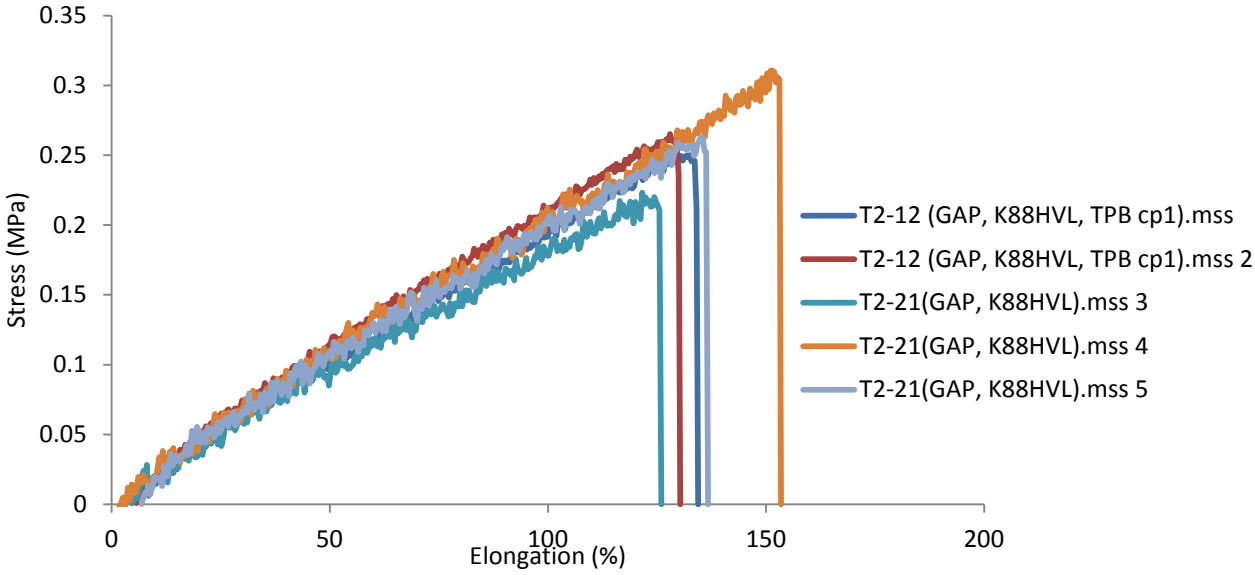

Figure 103. GAP, cross-linked with the aromatic curing agent K88 HVL.

GAP/IPDI/N100

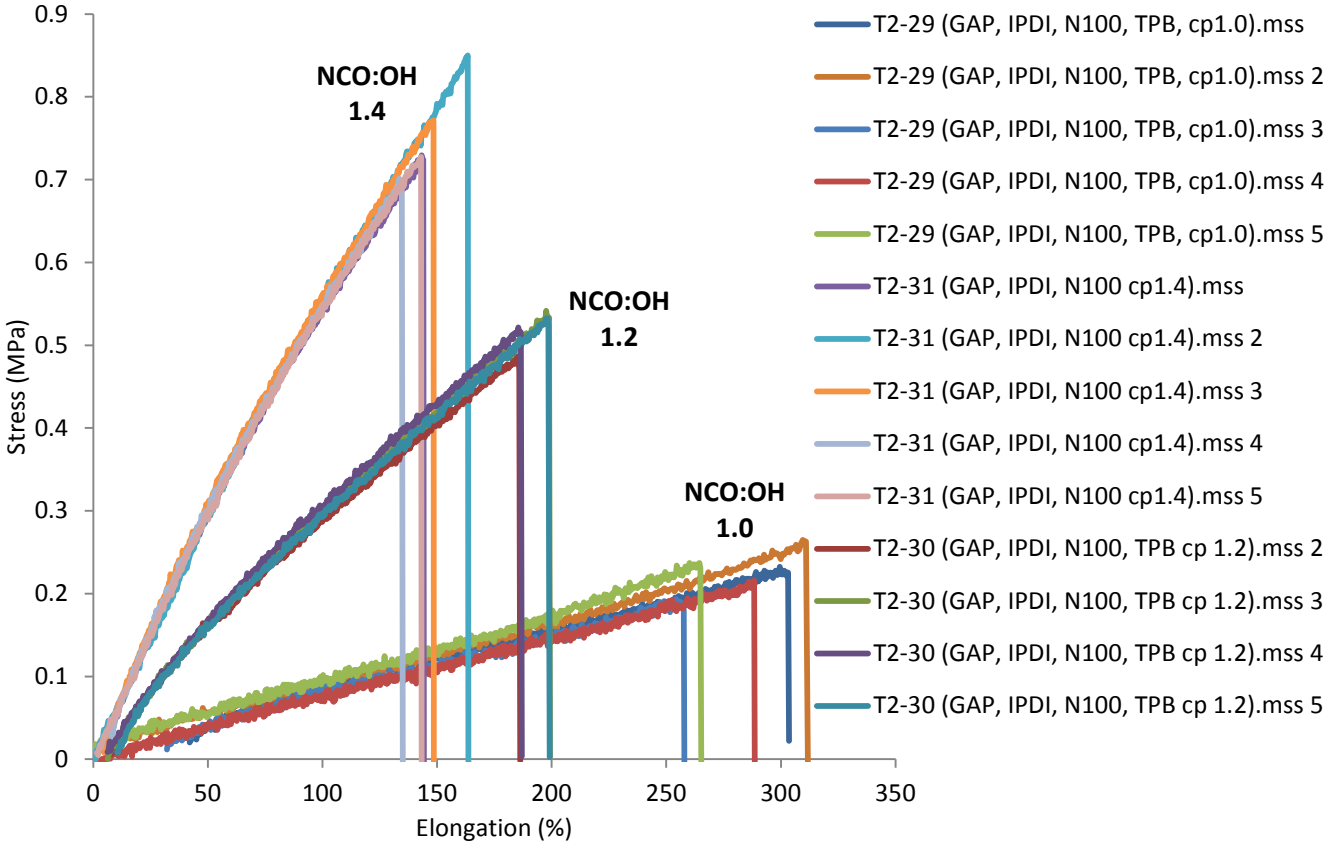

Figure 104. tensile test curves of GAP/IPDI/N100, three different cross-linkage ratios.

EP1900

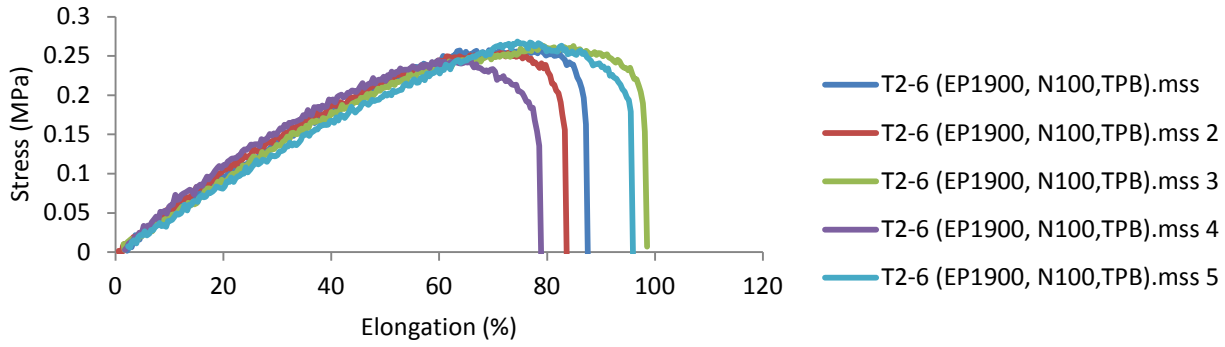

Figure 105. Tensile test results of T2-6.

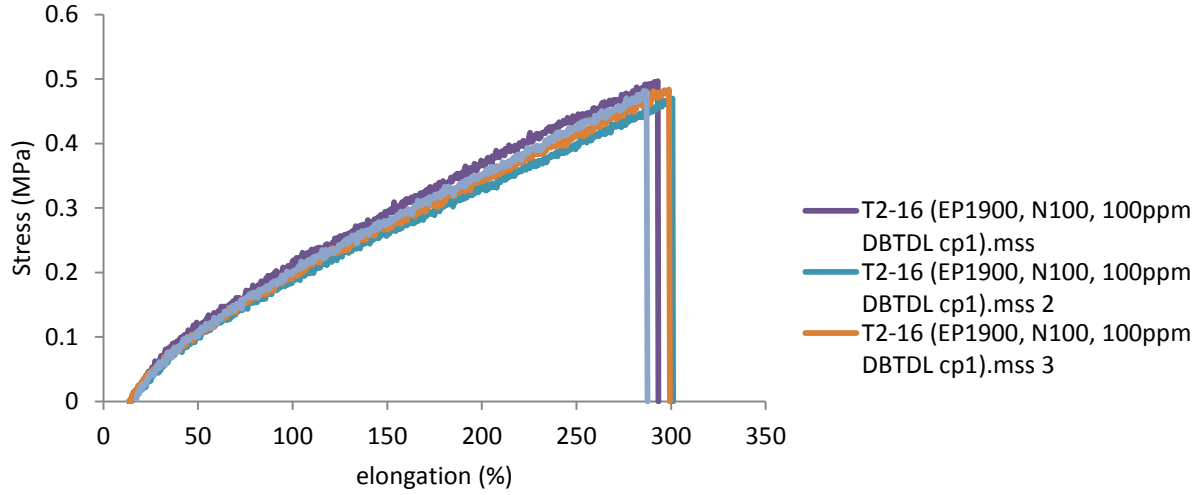

Figure 106 Tensile test results of T2-16.

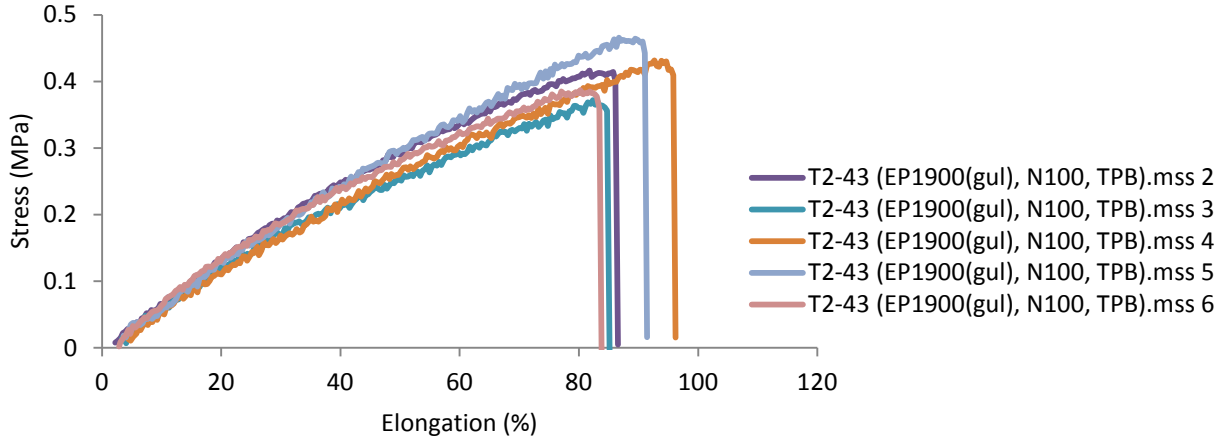

Figure 107. Tensile test results of T2-43.

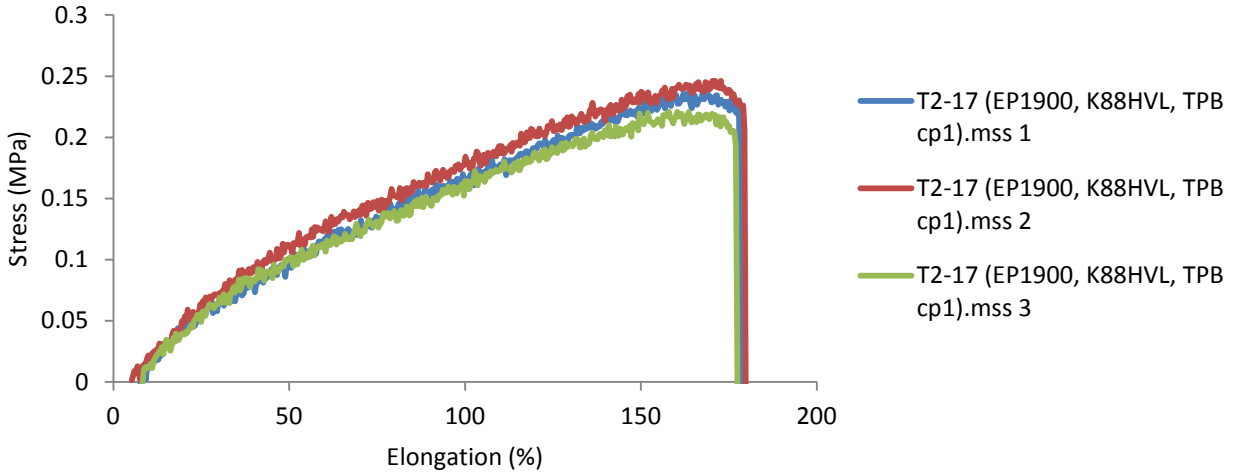

Figure 108. Tensile test results of T2-17.

Dual cure

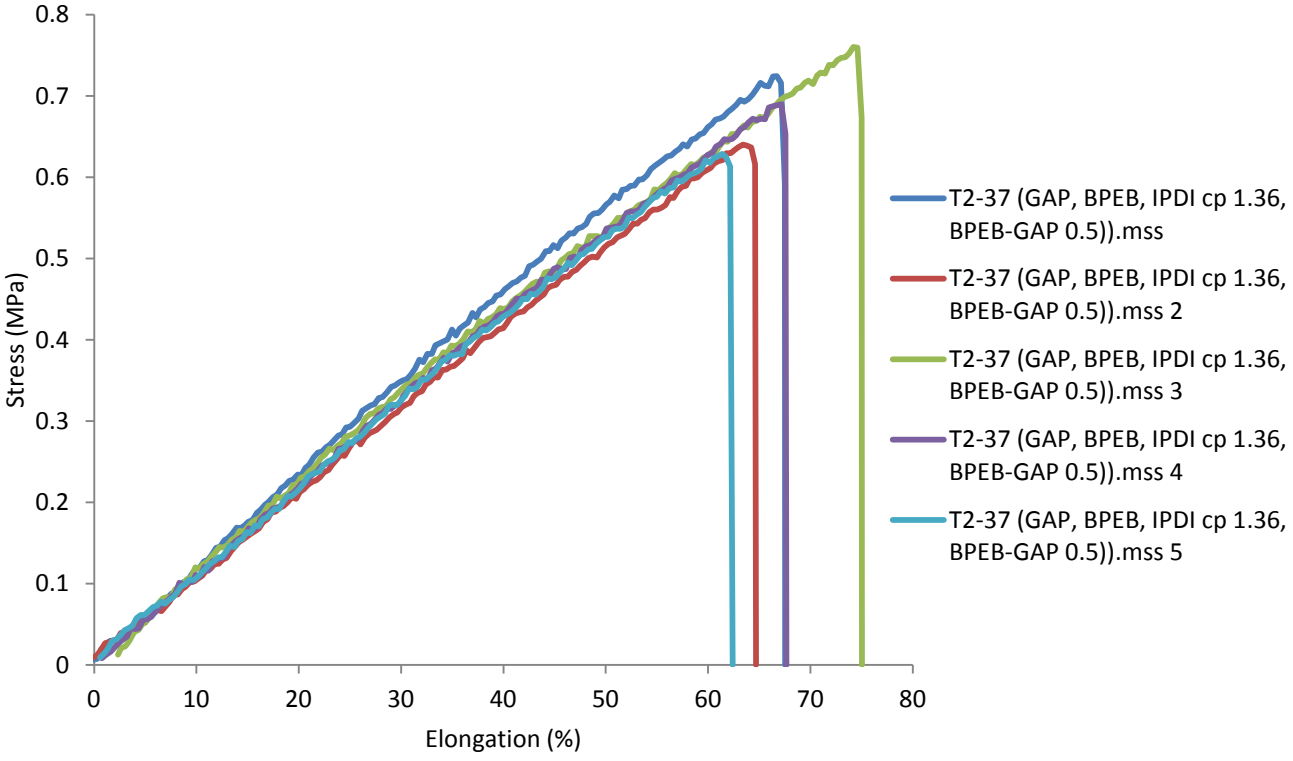

Figure 109. tensile test results of T2-37.

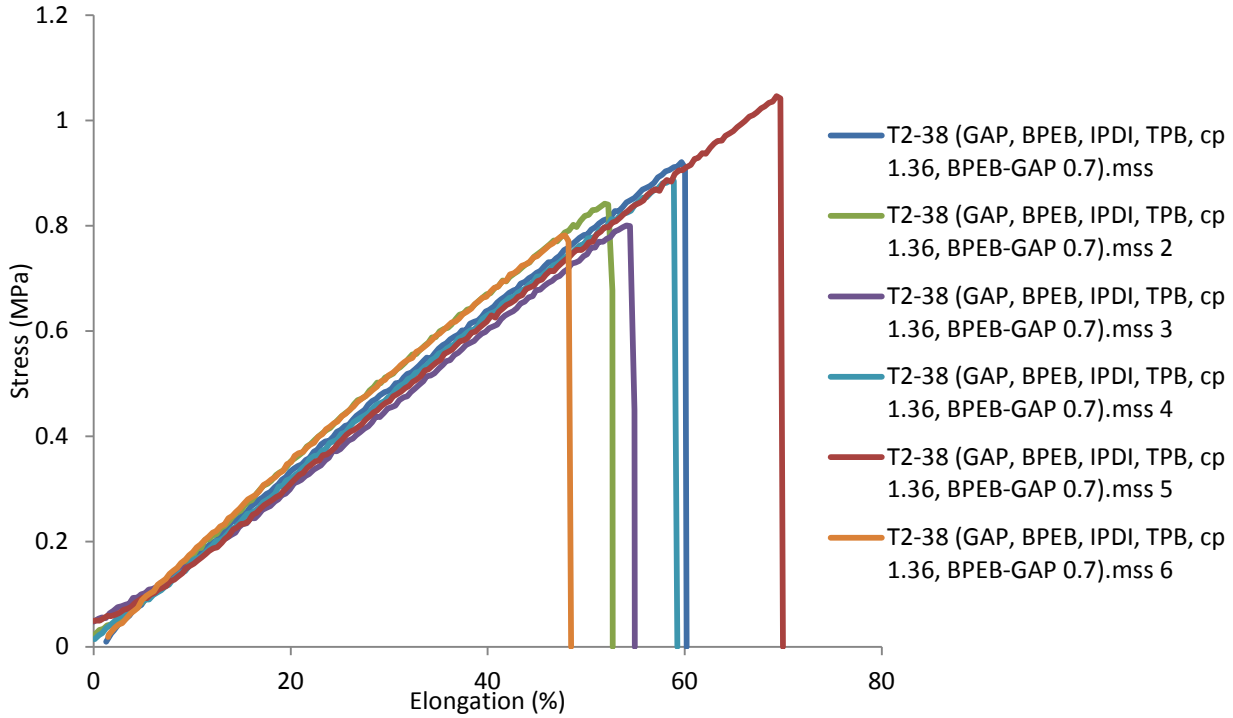

Figure 110. tensile test results of T2-38.

Plasticizer

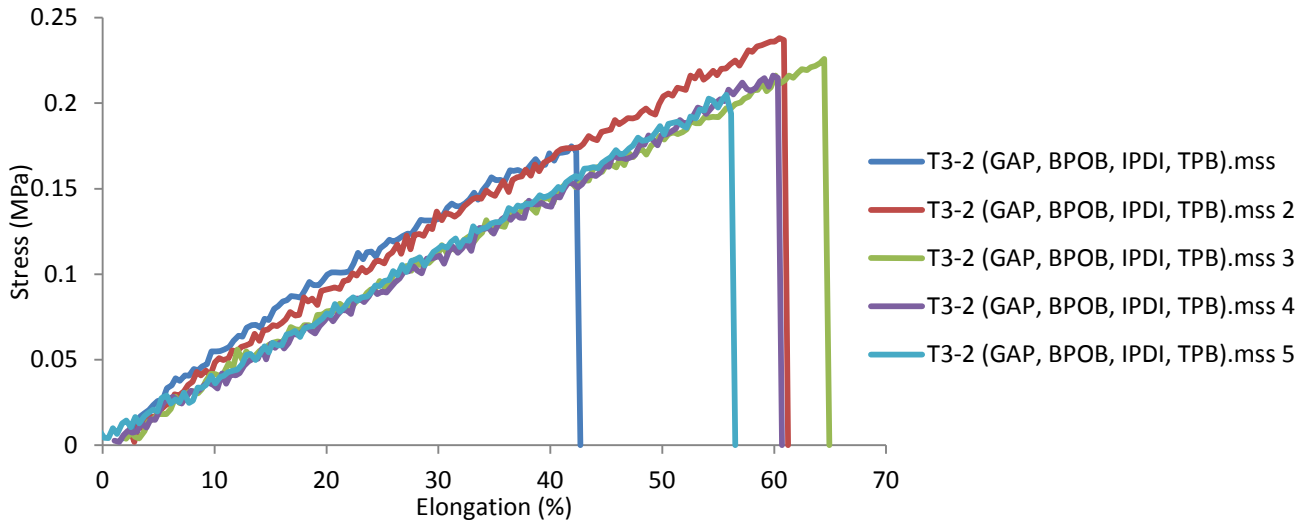

Figure 111. Tensile test results of T3-2.

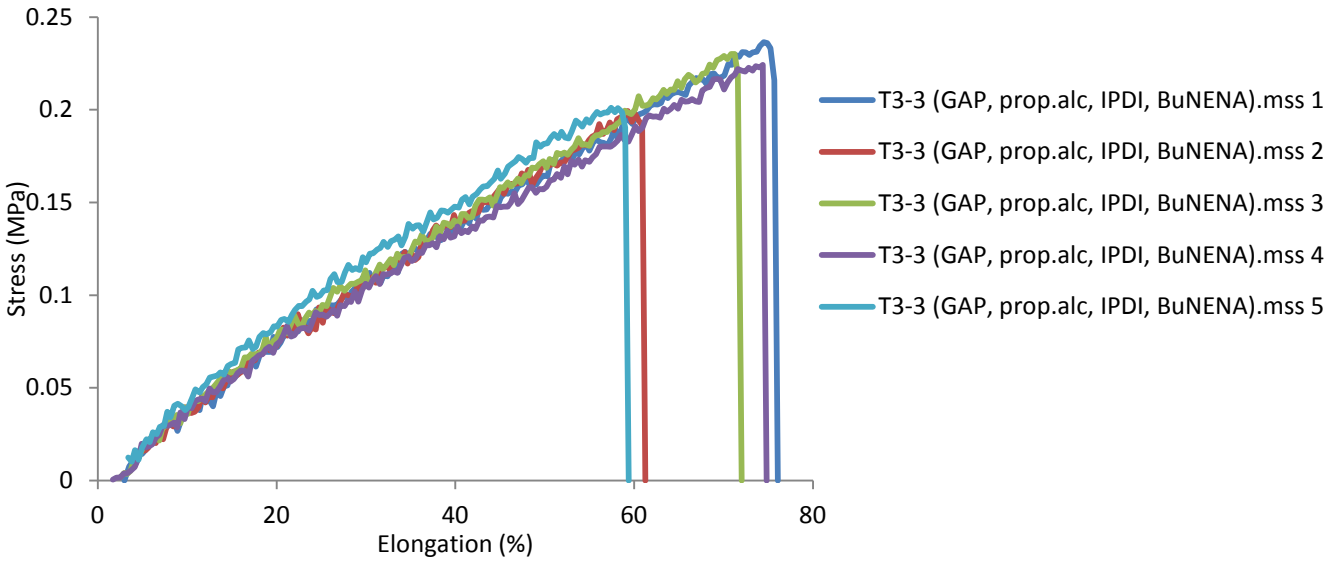

Figure 112. Tensile test results of T3-3.

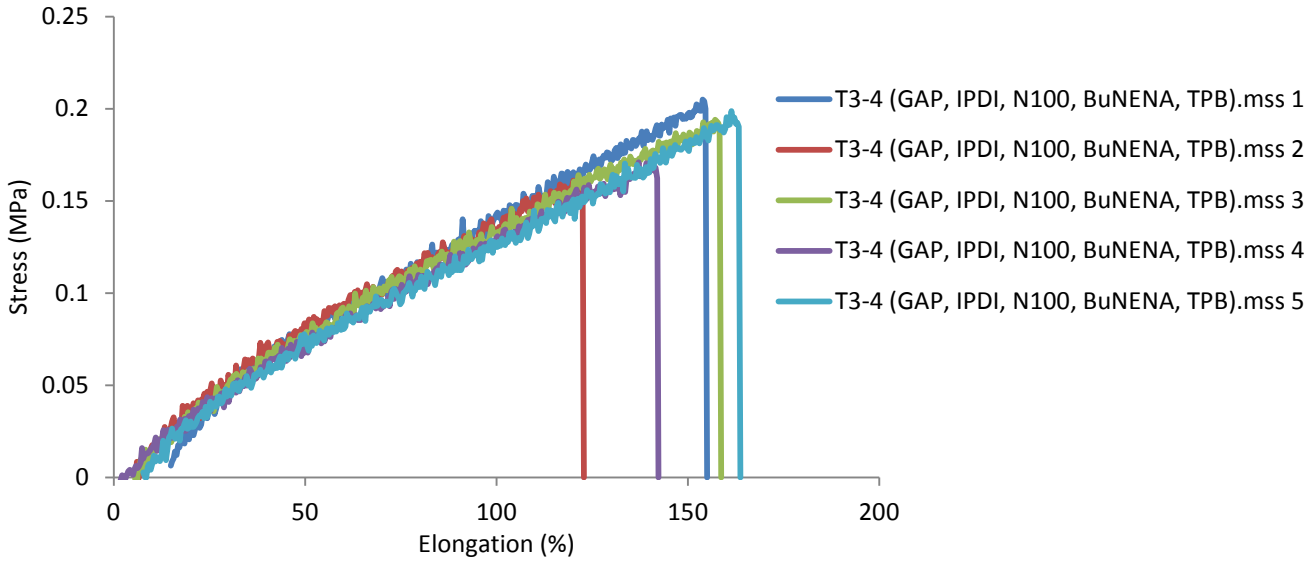

Figure 113. Tensile test results of T3-4

5.6 TGA

GAP-based binders

Table 33. TGA. Summary of weight loss steps for GAP based binders. The top three are GAP/N100 at various NCO:OH ratios, in order to rule out any cross-linkage dependency.

			weight loss step			
Sample	**Composition**	**NCO:OH**	**1st**	**2nd**		**Residue**
			200-240 °C	235-500 °C		
TiF2f	GAP/N100	1.2	89 %	4 %		7 %
T1F5b	GAP/N100	1	93 %	2 %		5 %
T1F5c	GAP/N100	0.8	89 %	5 %		6 %
T2-31	GAP/IPDI/N100		92 %	5 %		3 %
T2-32	GAP/1,4-butanediol/N100		87 %	8 %		5 %
T2-33	GAP/BPOB		93 %	4 %		3 %
T2-39	GAP/BPOB/IPDI		89 %	6 %		5 %
T2-45	GAP/prop.alc./IPDI		92 %	4 %		4 %
T2-46	GAP/PPG-PEG		91 %	6 %		3 %
			1st	2nd	3rd	
			200-270 °C	270-425 °C	425-500 °C	
T2-41	GAP/TEG/N100		34 %	35 %	14 %	17 %

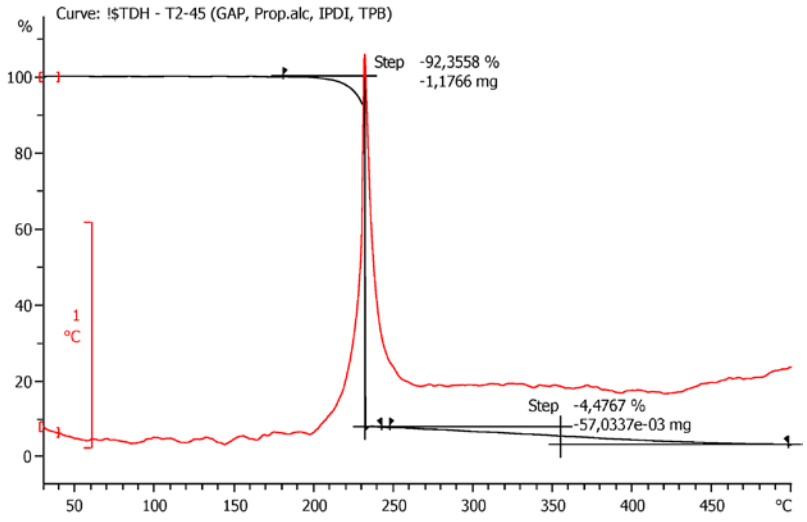

Figure 114. Thermo-gravimetric analysis of GAP/prop.alc./IPDI

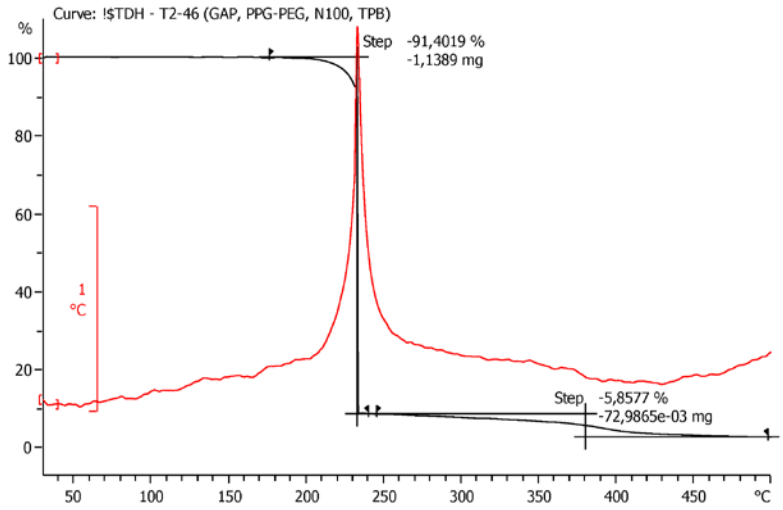

Figure 115. Thermo-gravimetric analysis of GAP/PPG-PEG/N100.

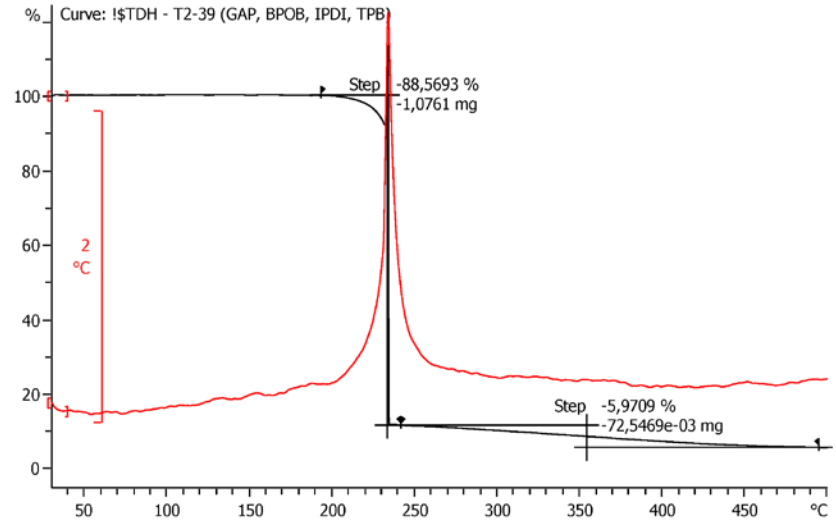

Figure 116. Thermo-gravimetric analysis of GAP/BPOB/IPDI.

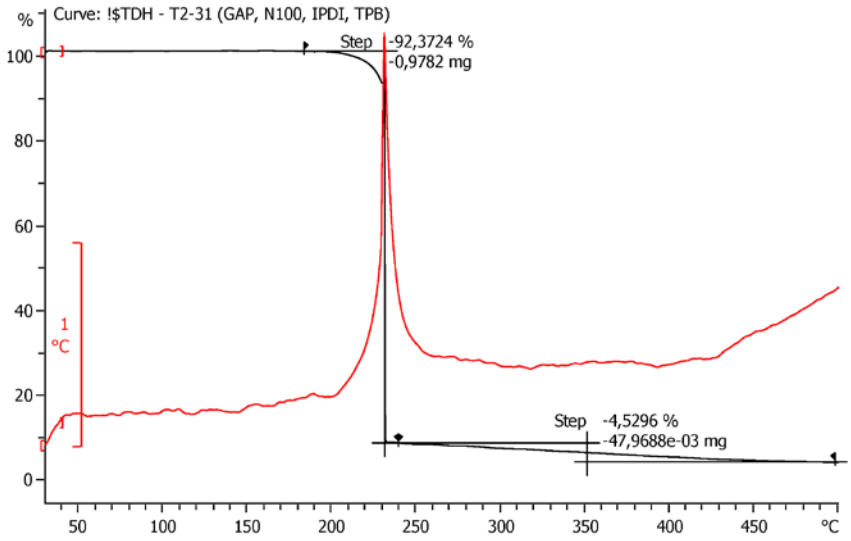

Figure 117. Thermo-gravimetric analysis of GAP/IPDI/N100

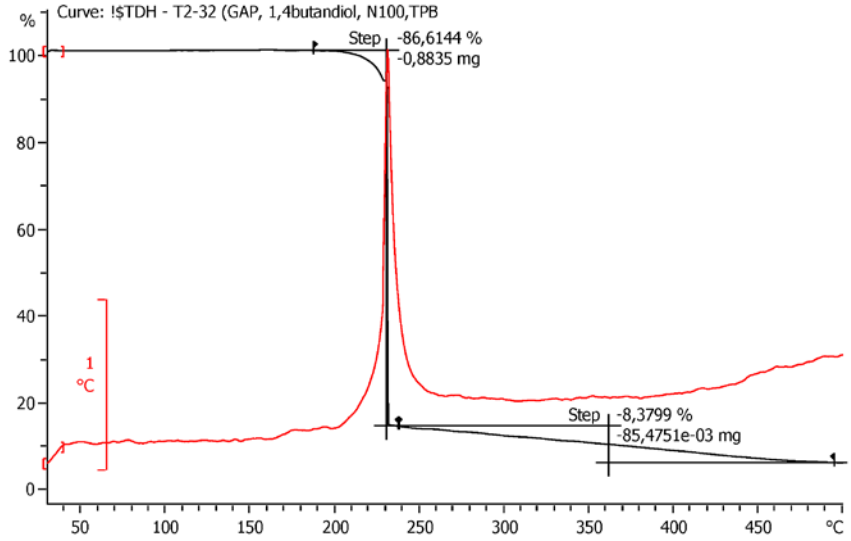

Figure 118. Thermo-gravimetric analysis of GAP/1,4-butanediol/N100.

T2-32 contains a small fraction of 1,4 Butandiol. The second loss step is somewhat larger than of other GAP-based TGA sequences, which is believed to origin from 1,4-butandiol.

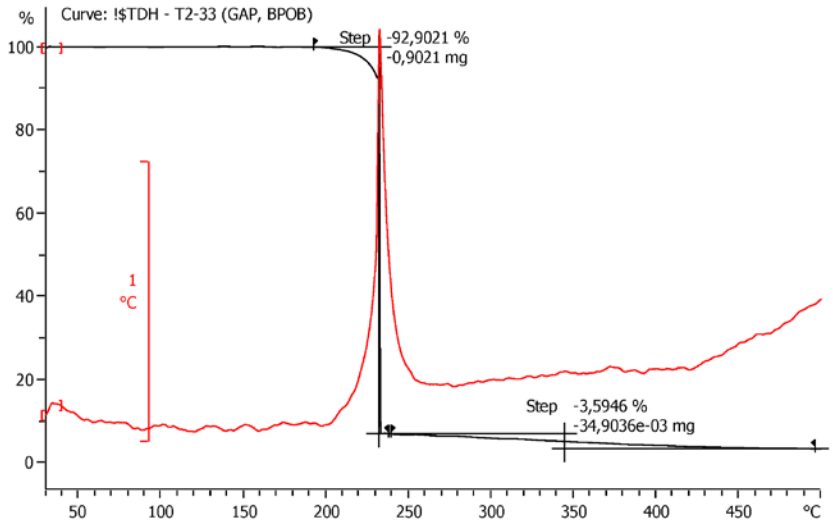

Figure 119. Thermo-gravimetric analysis of GAP/BPOB.

Inert binders

Table 34. Summary of TGA results for samples that did not contain GAP. Relative weight loss and estimated residual mass.

Sample	Components	weight loss step		Residue
		1st	2nd	
		260-410 °C	410-500 °C	
T1F3c	HTPB/IPDI	19 %	75 %	6 %
		200-500 °C		
T2-42	PPG-PEG/N100	99 %		1 %
T1F6a2	EP1900/N100	100 %		0 %
T1F6d2	HTCE/N100	99 %		1 %
T1F6f2	TEG/N100	97 %		3 %

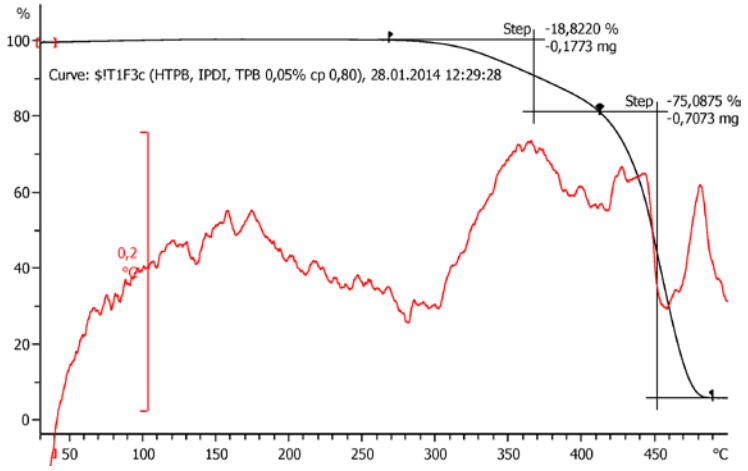

Figure 120. TGA of HTPB/IPDI (sample T1F3c) NCO:OH ratio of 0.8.

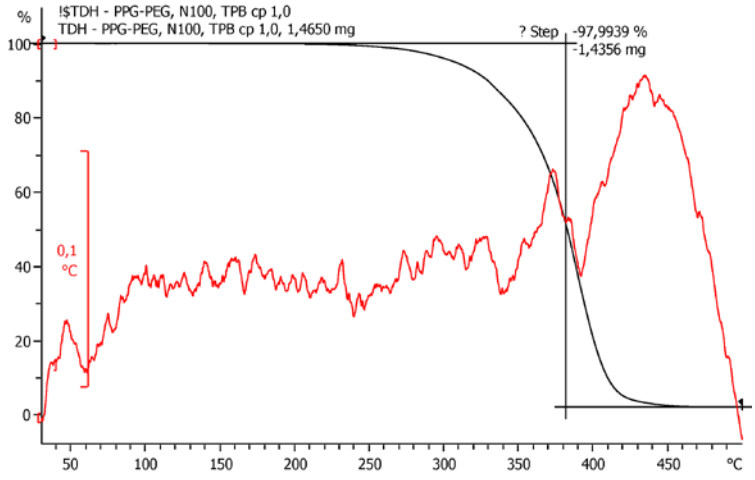

Figure 121. TGA of PPG-PEG/N100, sample T1F6c2. NCO:OH ratio 1.0.

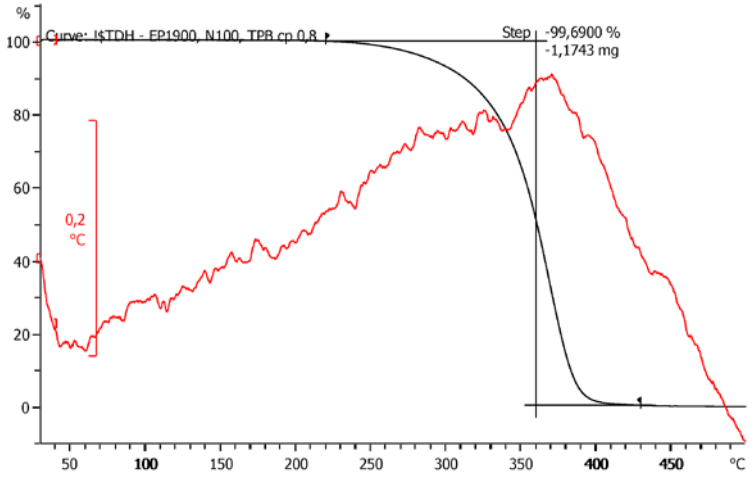

Figure 122. TGA of EP1900/N100, sample T1F6a2. NCO:OH ratio of 0.8.

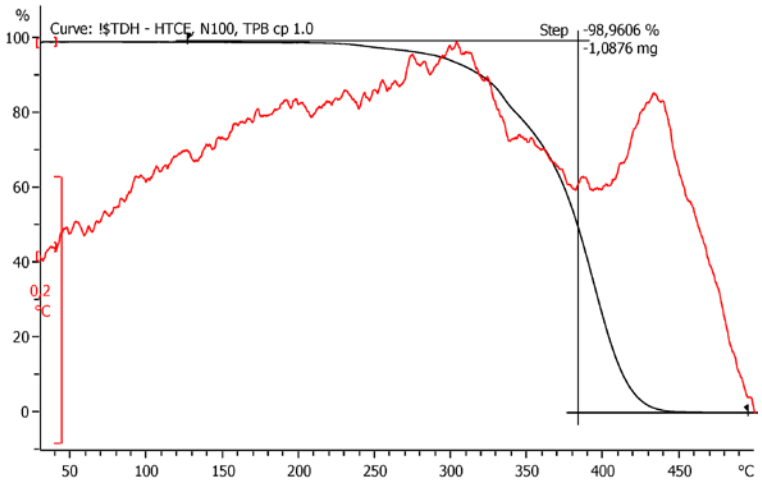

Figure 123. TGA of HTCE/N100, sample T1F6e2. NCO:OH ratio of 1.0.

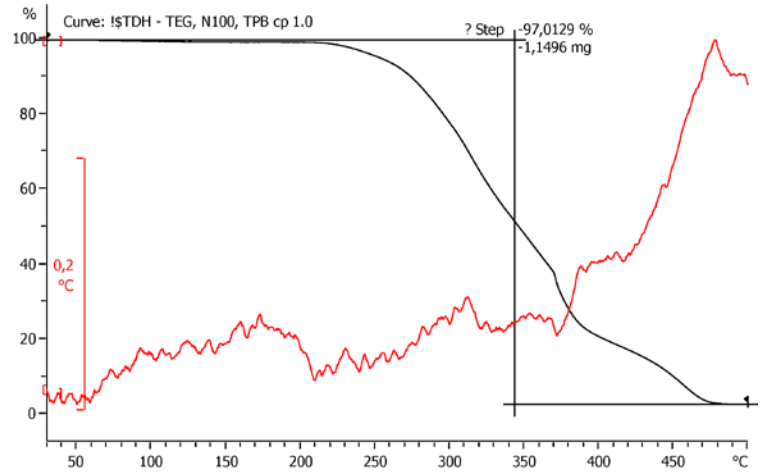

Figure 124. TGA of TEG/N100, sample T1F6f2. NCO:OH ratio of 1.0.

5.7 DSC

Inert prepolymers

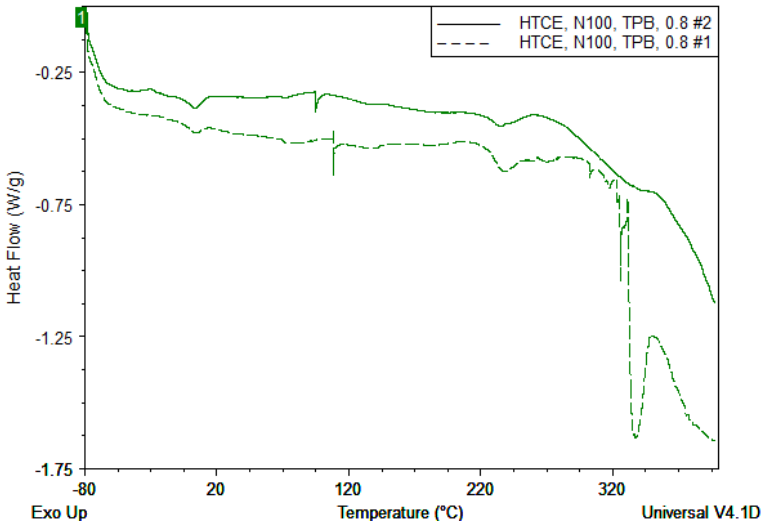

Figure 125. DSC curve of HTCE/N100. The deviations at elevated temperatures are believed to be caused by poor contact of sample crucible and instrument.

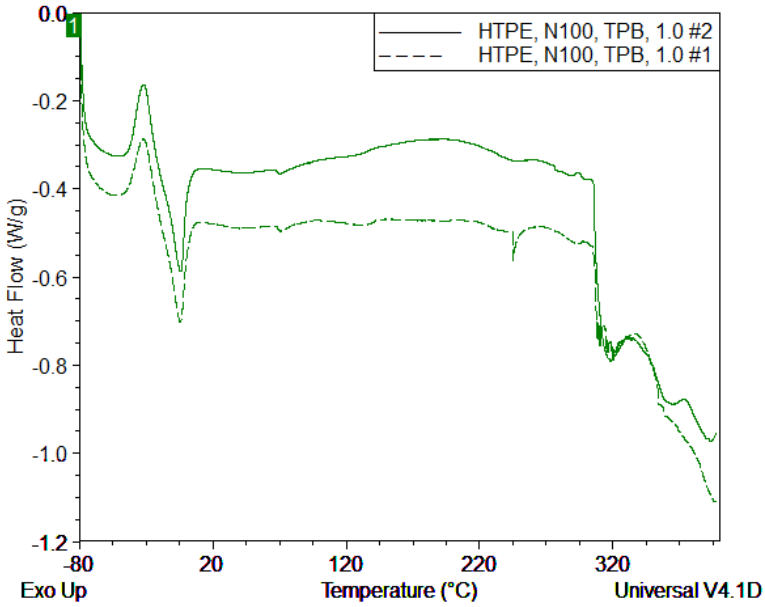

Figure 126. DSC of HTPE/N100. The prominent signal change around 0 °C is not the Tg region for HTPE, which has been found to be around -77 °C by Haugmo (REF), and -80 ° by Hansen (REF).

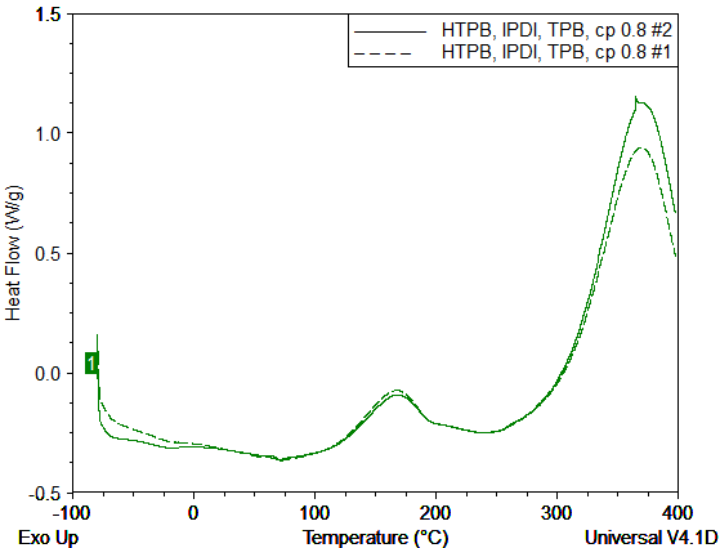

Figure 127. DSC figurative data of HTPB/IPDI show a good reproducibility of two parallels.

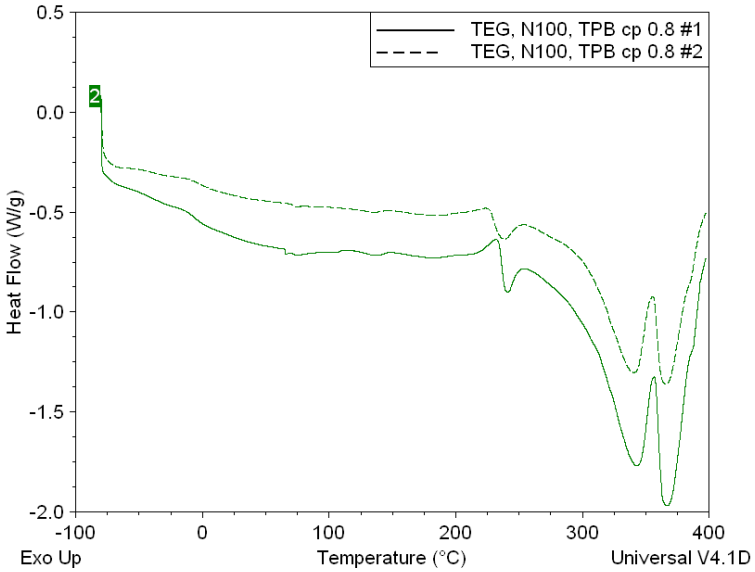

Figure 128. DSC of TEG/N100. The precision is considered as adequate for DSC measurement, but two parallels are adviced, in order to rule out errors.

Aromatic isocyanates

BPOB

T2-33

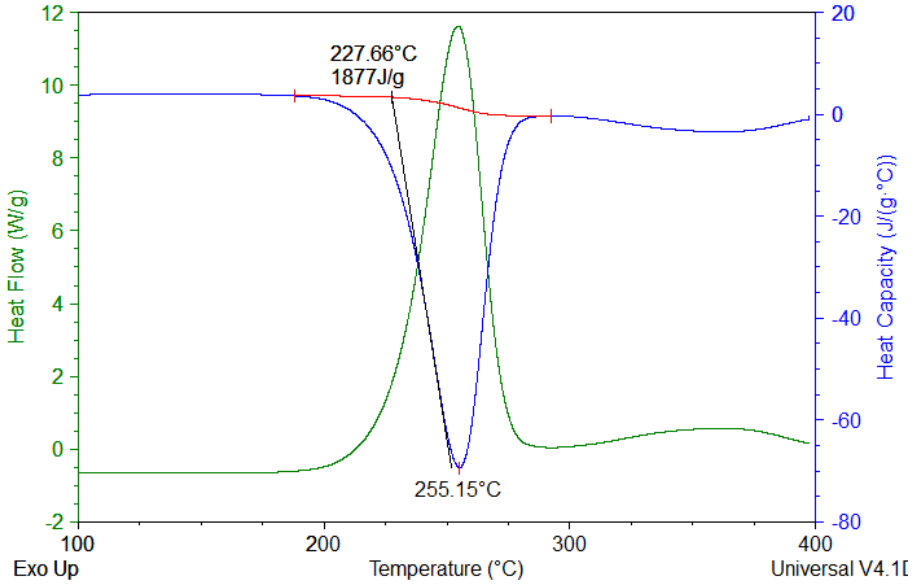

Figure 129. DSC of T2-33, with emphasis on the heat capacity of the major exothermic signal.

Propargyl alcohol

T2-45

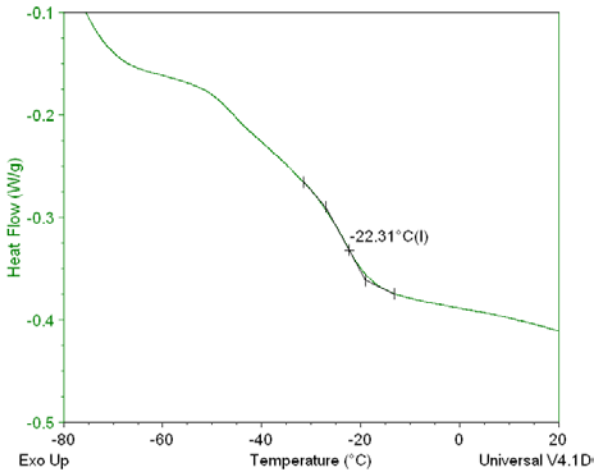

Figure 130.DSC of T2-45. T_g is a couple degrees Celsius above the DMA multi-frequency curve.

TMETN

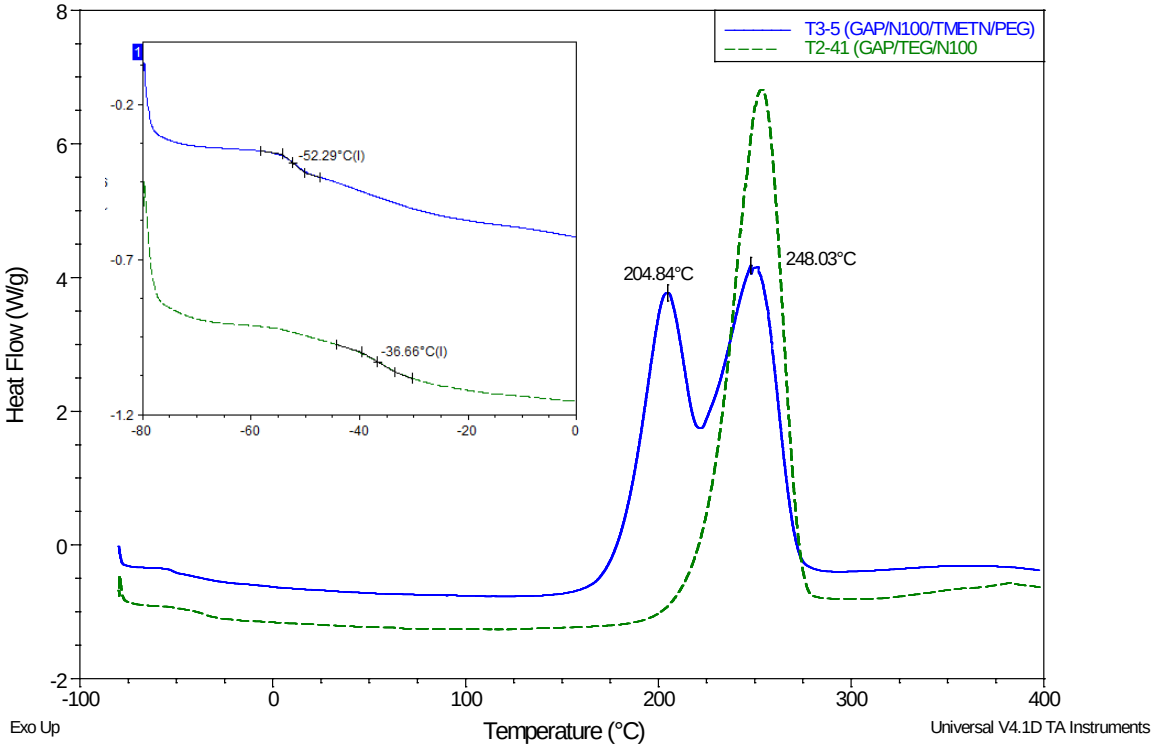

Figure 131. Plasticized and non-plasticized, comparable samples. The heat flow as a function of temperature. GAP/N100/TMETN/PEG (T3-5) compared with an interpreted version of the same , but without TMETN (T2-41).

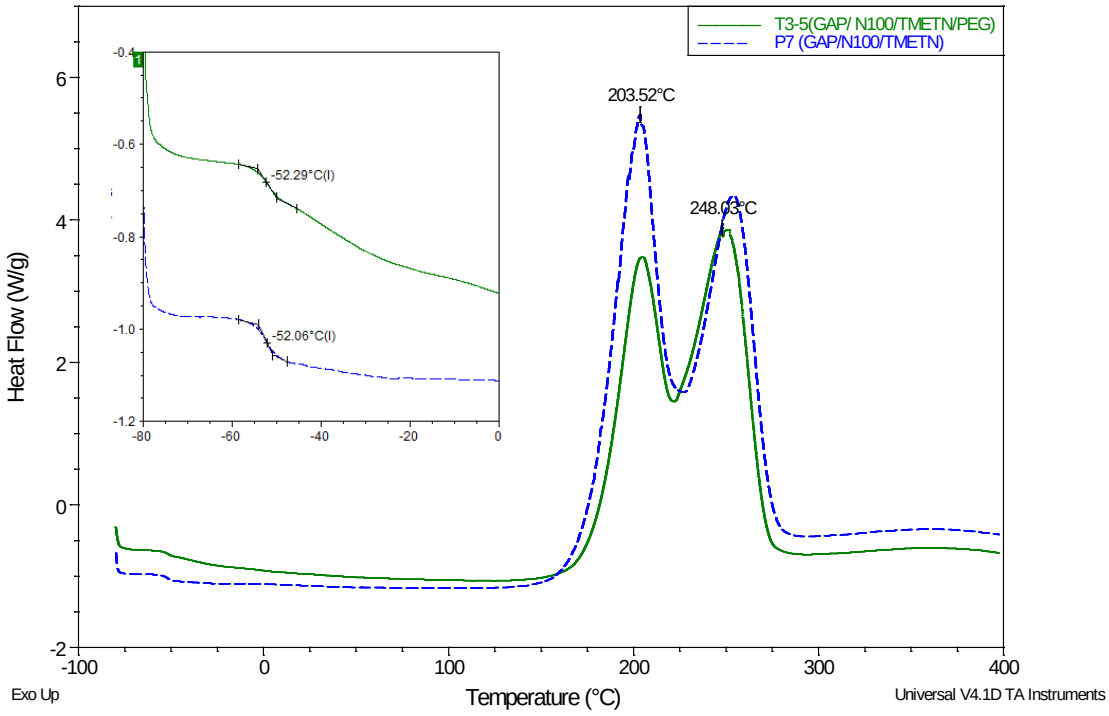

Figure 132. DSC curves. Comparison GAP/N100 containing the conventional TMETN (PEG is extracted, blue curve) and one with unprocessed TMETN (containing 20 wt % PEG, green curve). P7 was made in the summer engagement.

BuNENA

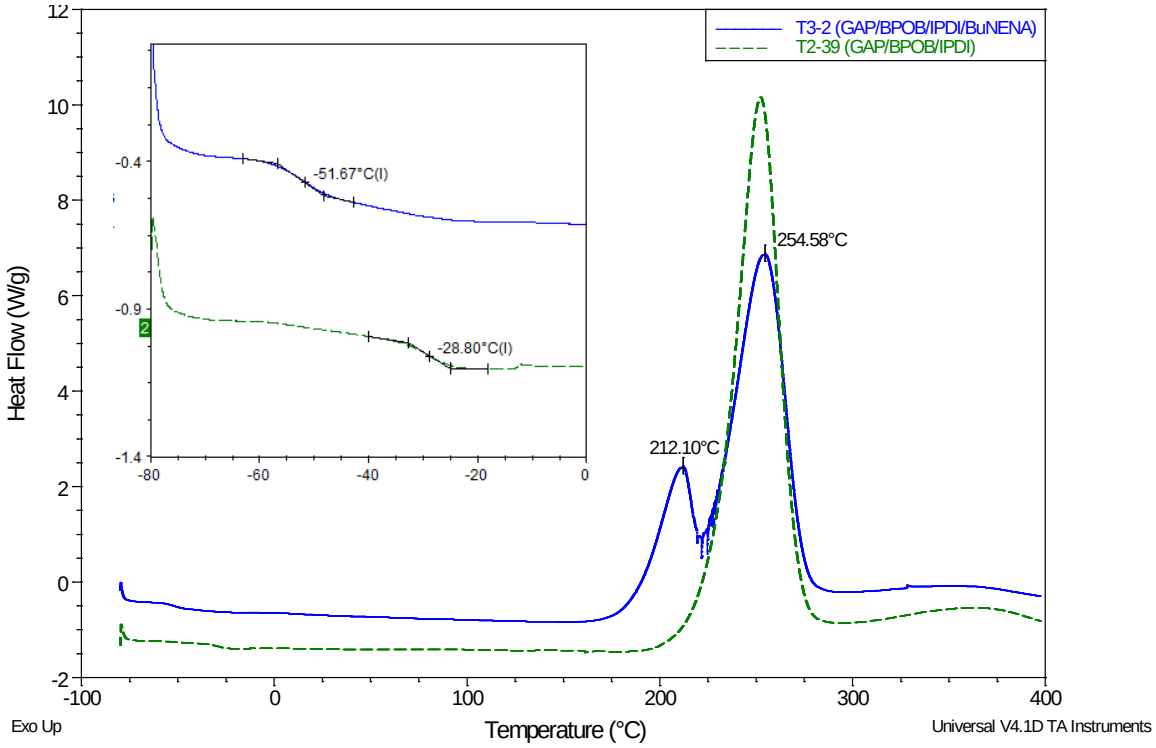

Figure 133. . Plasticized and non-plasticized, comparable samples.

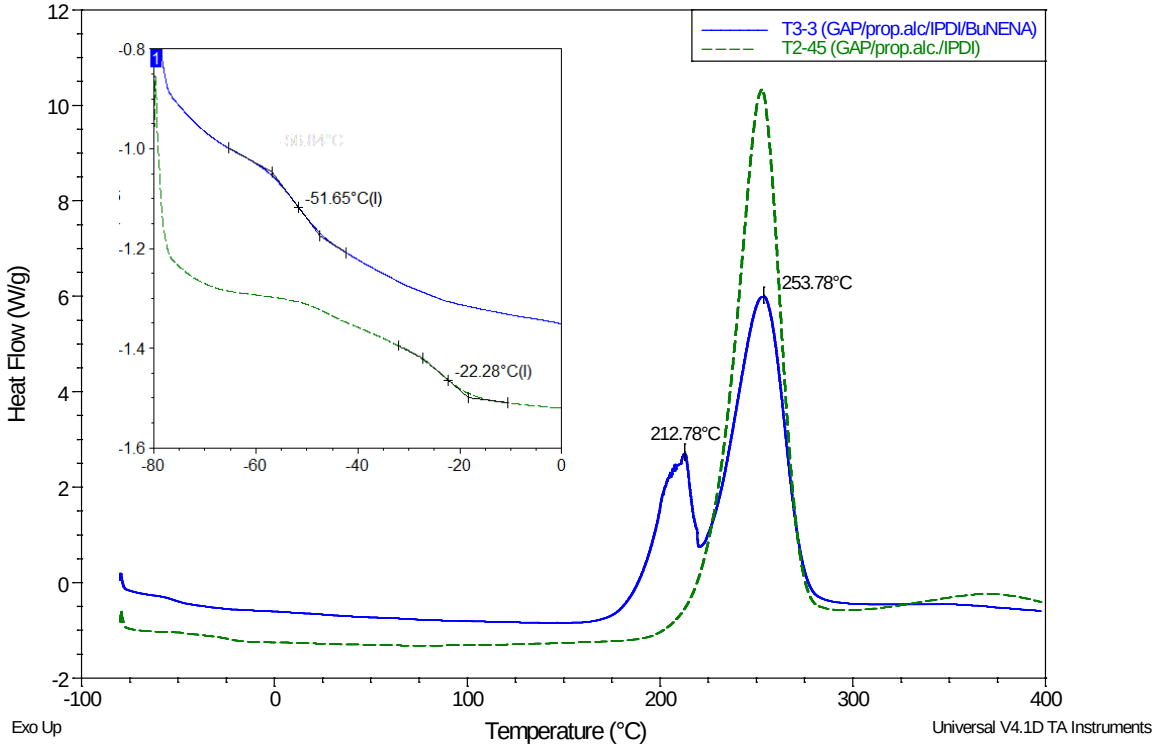

Figure 134. . Plasticized and non-plasticized, comparable samples.

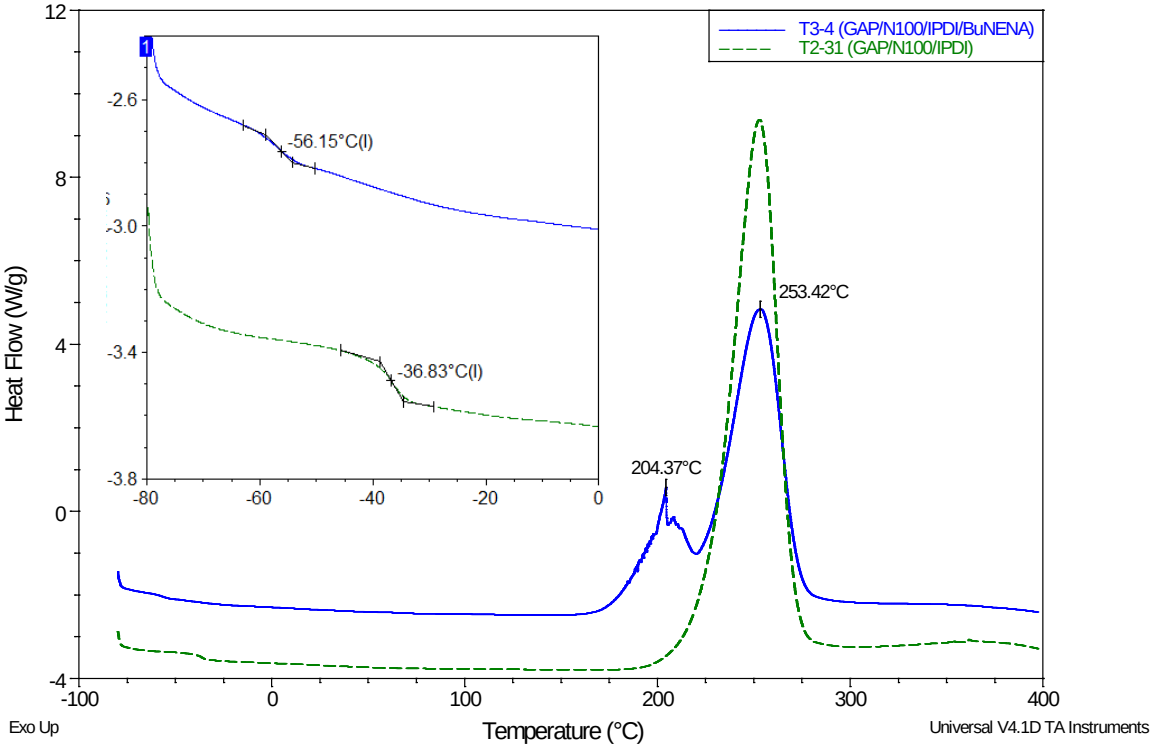

Figure 135. . Plasticized and non-plasticized, comparable samples.

5.8 DMA

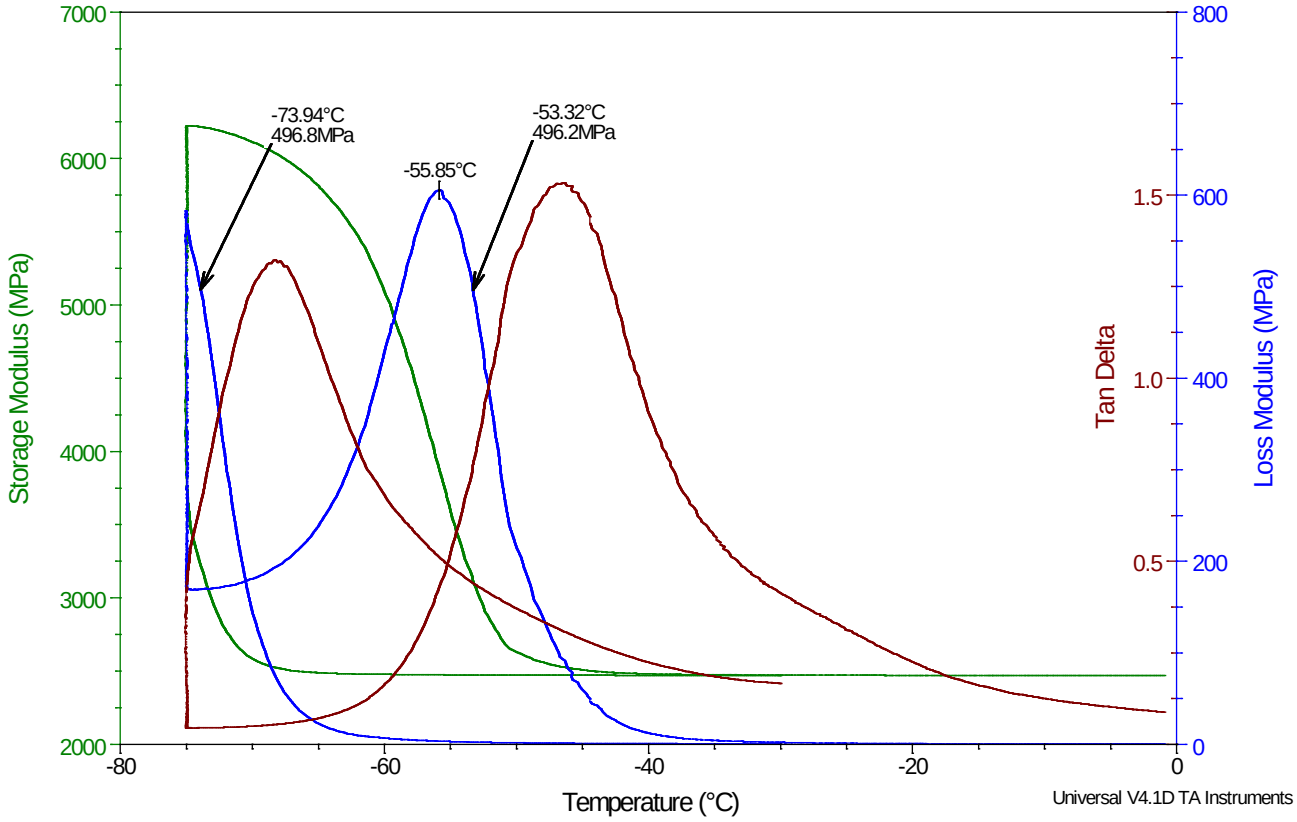

Figure 136. DMA of T2-42. On of the loss modulus peaks are not apparent. Therefore, a feasible estimate is made.

$$T_{g(T2-42)} = \left(\frac{-53.32°C - 73.94°C}{2}\right) + 53.32°C - 55.85°C = -66.16°C$$

DSC = -64 .64 °C

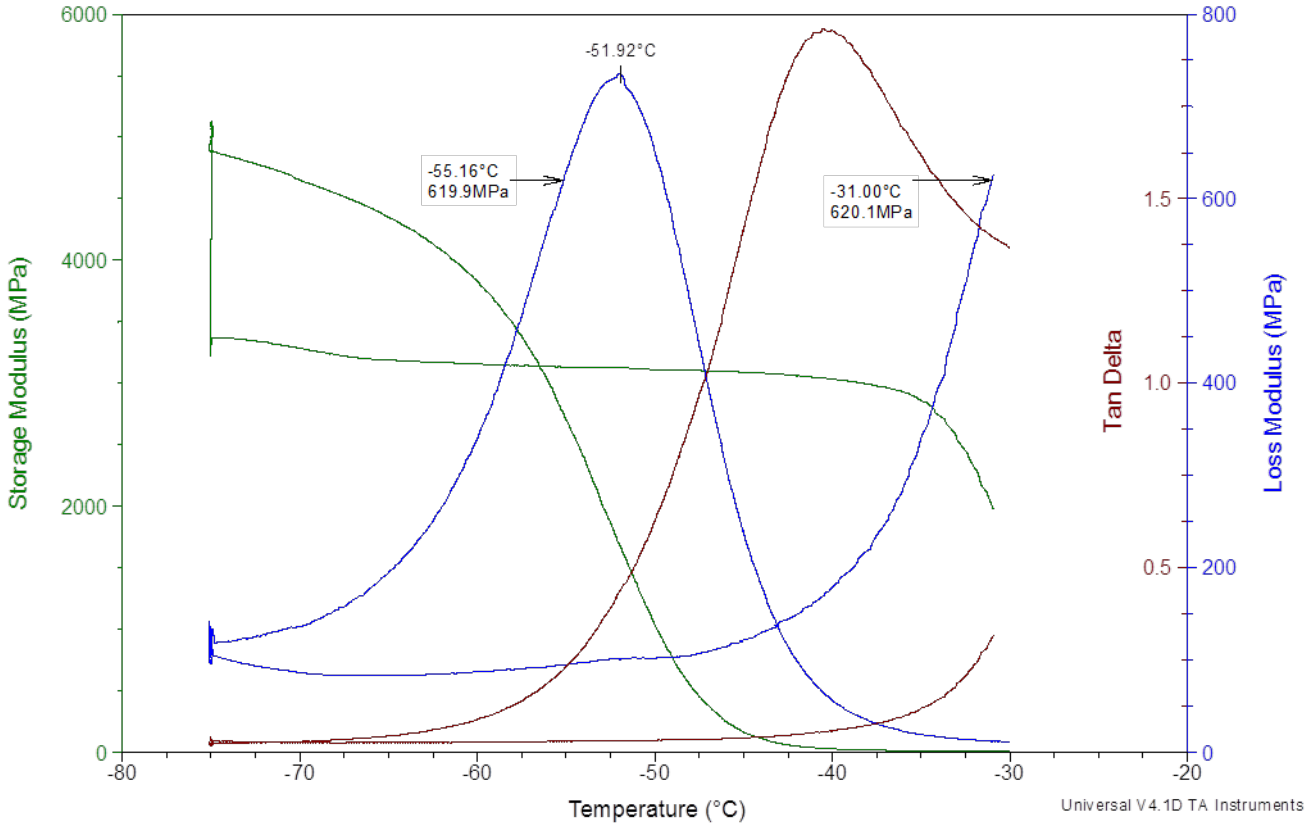

Figure 137. DMA of sample T2-46 (GAP/PPG-PEG/N100). One of the loss modulus peaks did not include in this region. Therefore, a feasible estimate is made.

$$T_{g\ (T2-46)} = \left(\frac{-55.16°C - 31.00°C}{2}\right) + 55.16°C - 51.92°C = -39.84°C$$

DSC = -41.86 °C

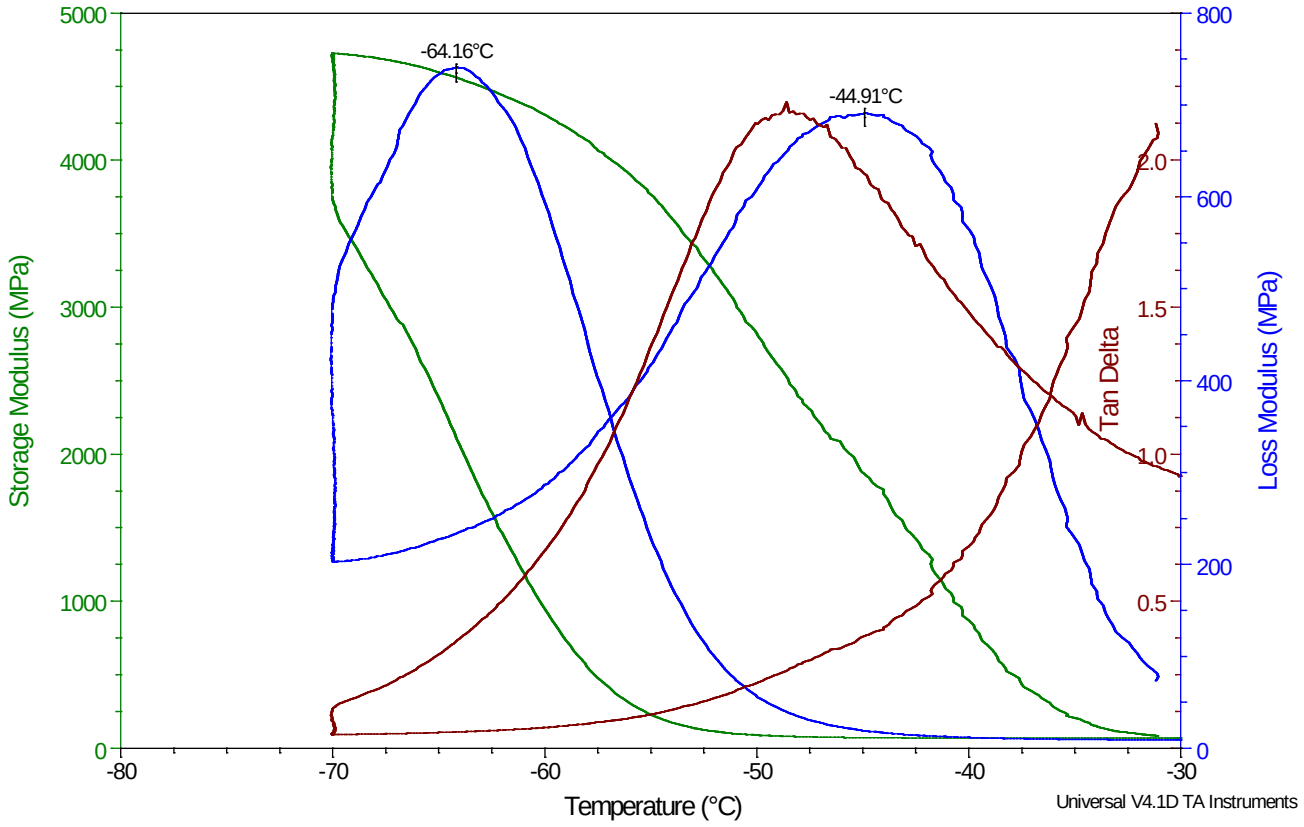

Figure 138. DMA of T3-1.

$$T_{g\ (T3-1)} = \left(\frac{-64.16°C - 44.91°C}{2}\right) = -54.54°C$$

DSC= -53.58 °C

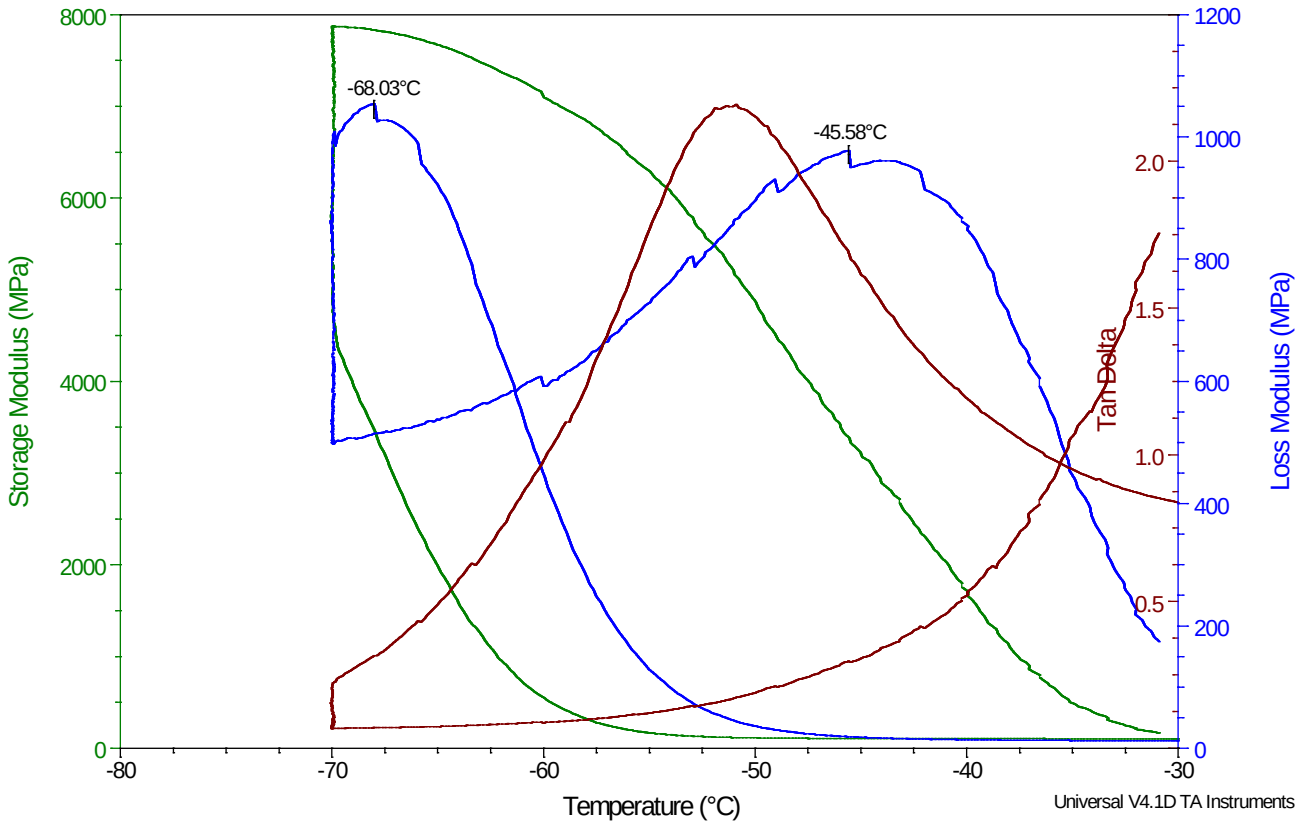

Figure 139. DMA of T3-2.

$$T_{g\ (T3-2)} = \left(\frac{-68.03°C - 45.58°C}{2}\right) = -56.81°C$$

DSC = -51.67 °C

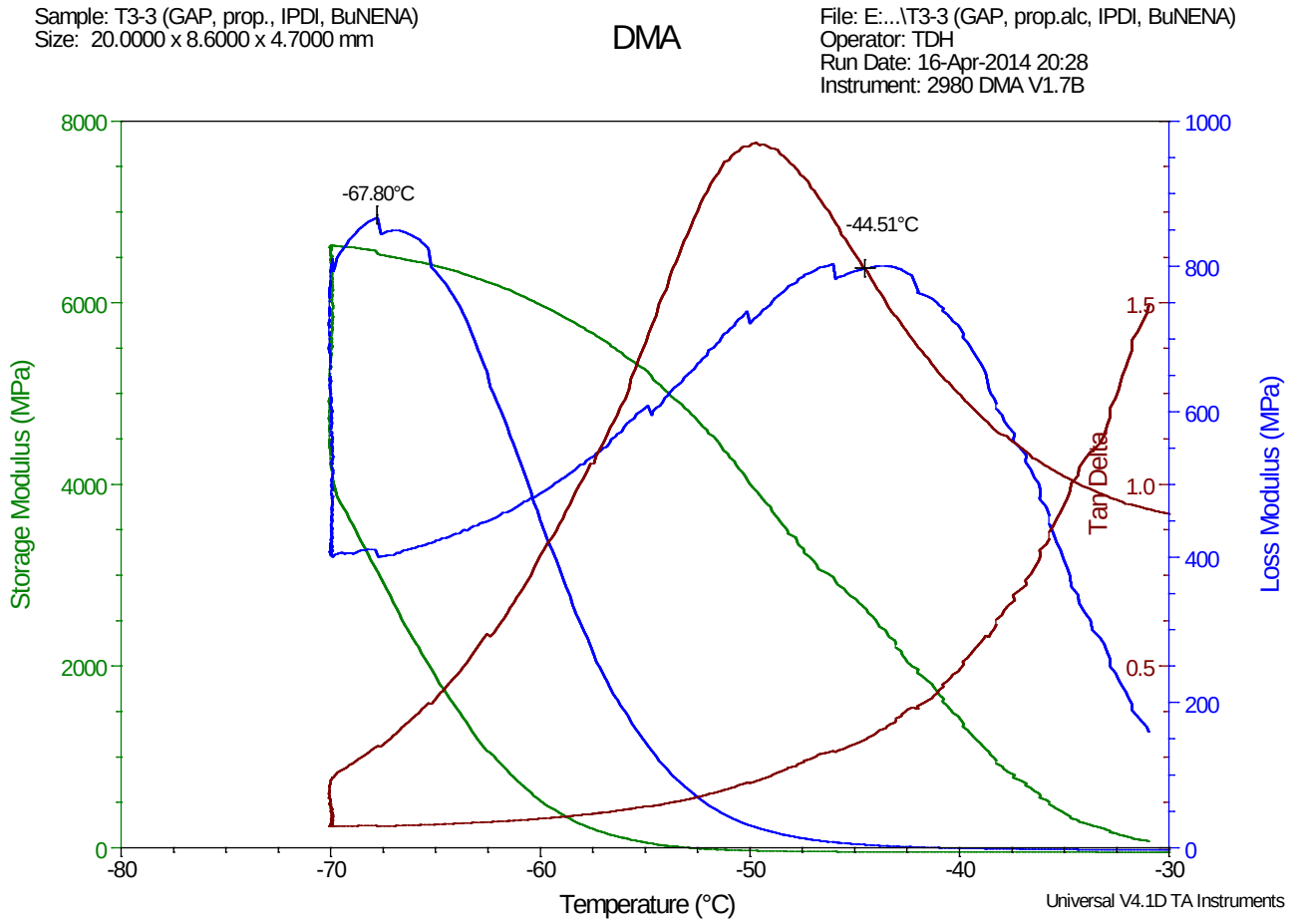

Figure 140. DMA of T3-3.

$$T_{g\ (T3-3)} = \left(\frac{-67.80°C - 44.51°C}{2}\right) = -56.16°C$$

DSC = 51.65 °C

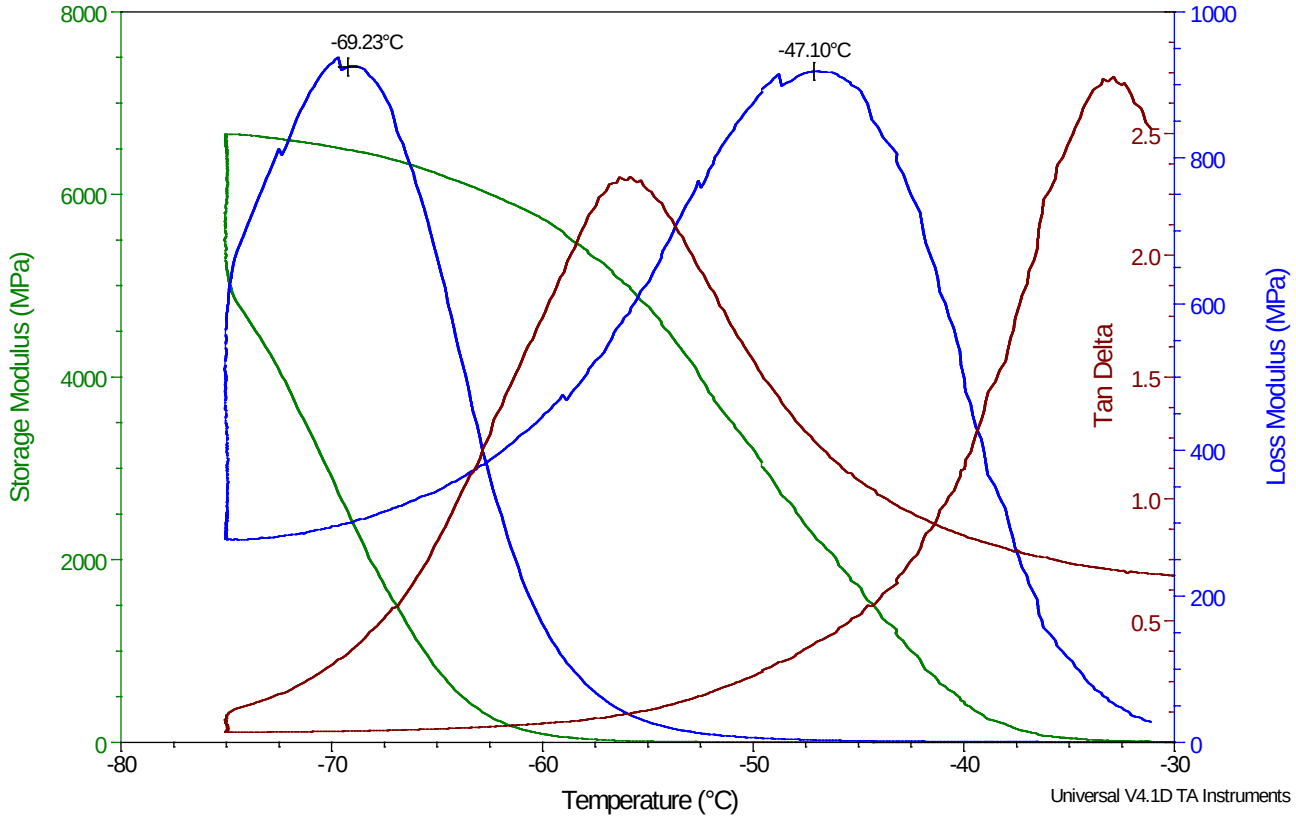

Figure 141. DMA of T3-4

$$T_{g\,(T3-4)} = \left(\frac{-69.23°C - 47.10°C}{2}\right) = -58.17°C$$

DSC = -56.15

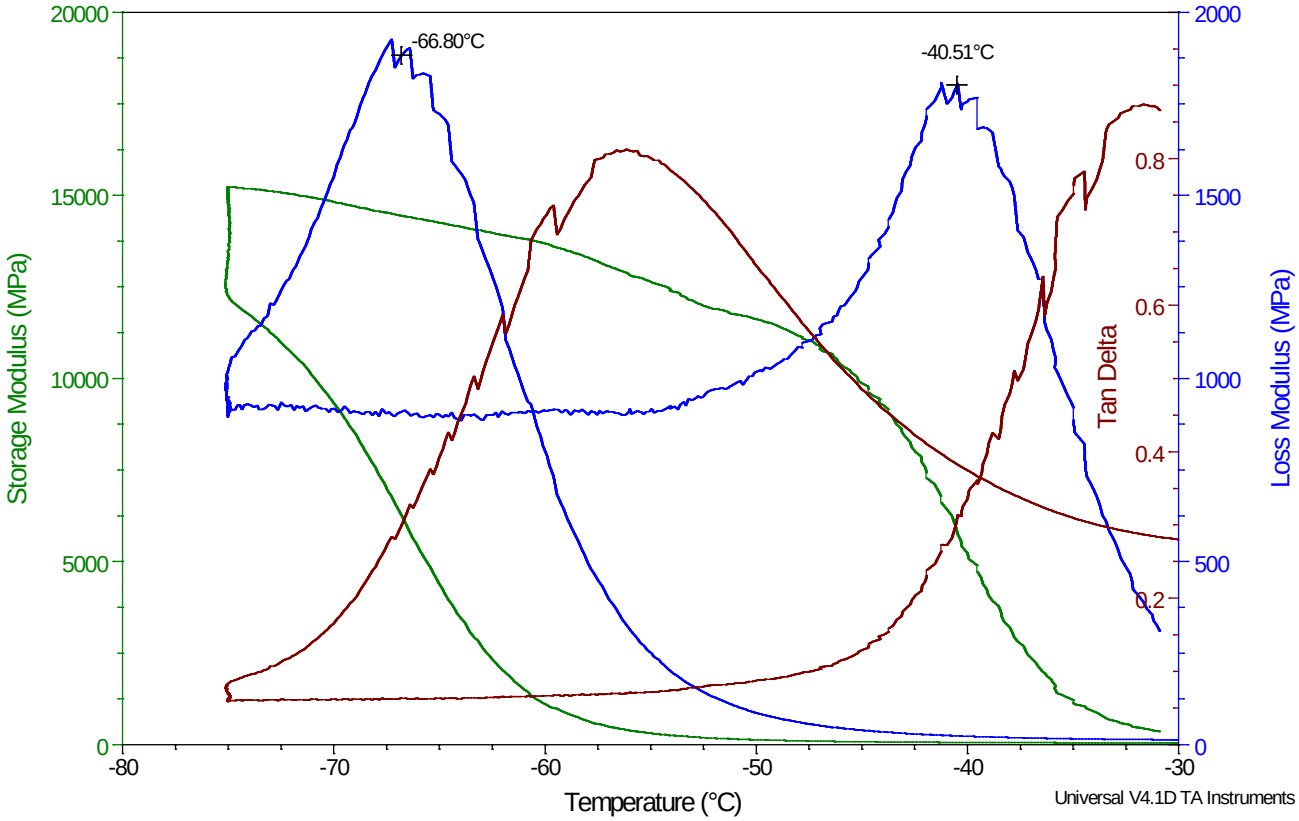

Figure 142. DMA of T3-5.

$$T_{g\ (T3-5)} = \left(\frac{-66.80°C - 40.51°C}{2}\right) = -53.66°C$$

DSC = -52.29 °C

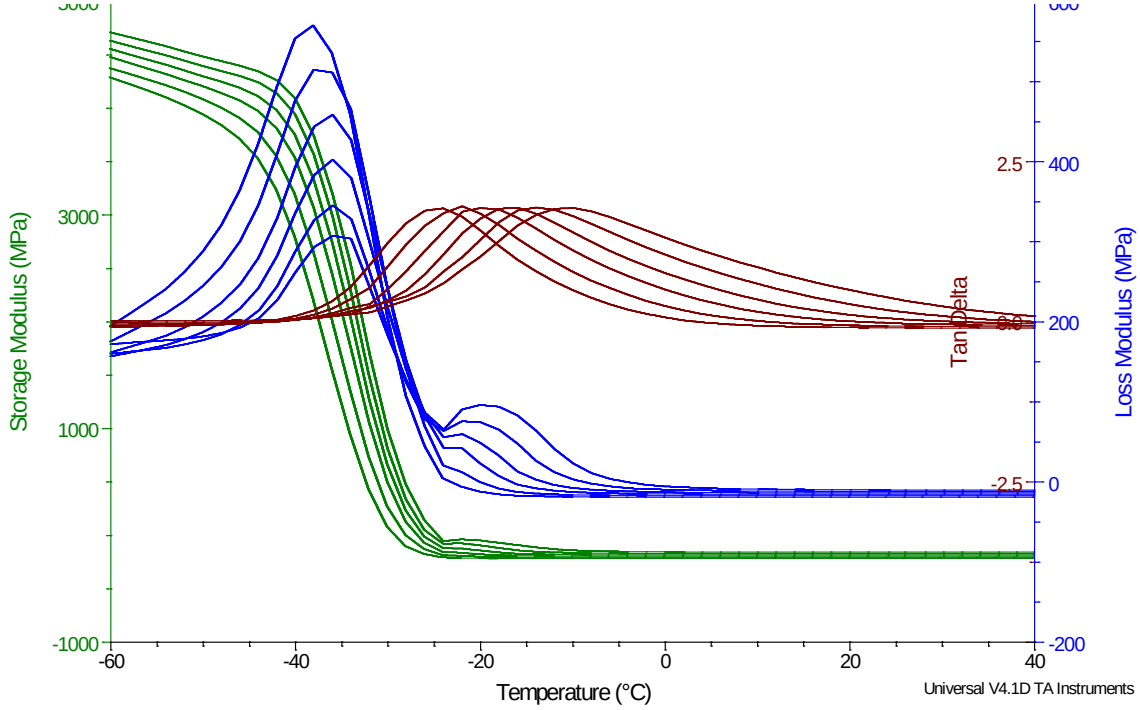

Figure 143. Multi-frequency DMA run of GAP/BPOB (T2-33). Time-derived temperature ranged between 0.20 – 0.30 °C/min. T_g = -36 °C. (100 Hz curve is removed, loss modulus curve is smoothened).

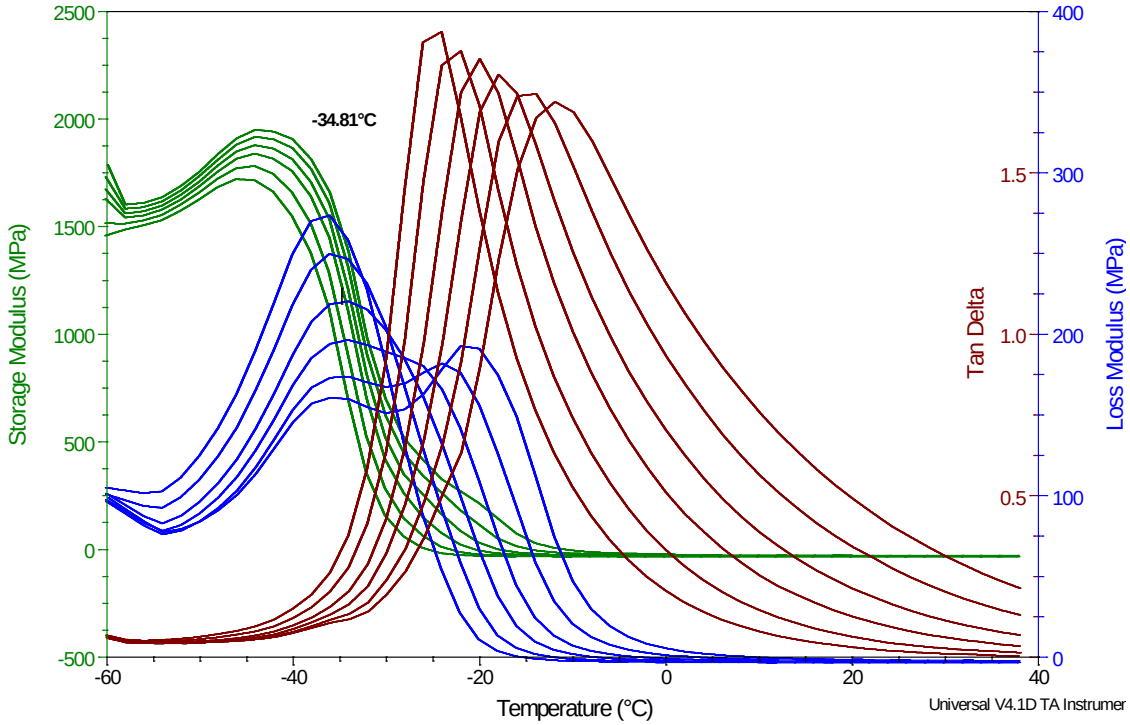

Figure 144. Multi-frequency DMA plot of T2-39. T_g is -35 °C, determined by the 1 Hz loss modulus curve. (100Hz curve excluded, loss modulus smoothened). Time-derived temperature ranged between 23.7 – 0.31 °C/min. T_g = -35 °C.

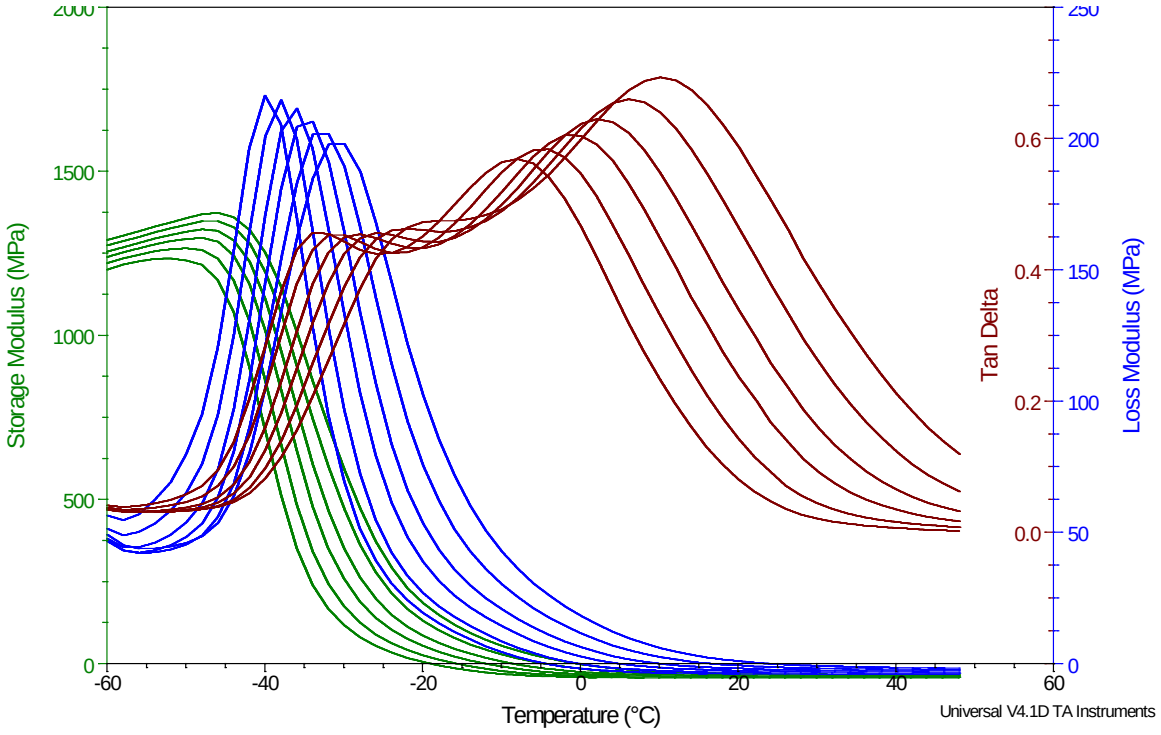

Figure 145. Multi-frequency DMA run of T2-41. Time-derived temperature ranged between 0.27 – 0.30 °C/min. T_g = -36 °C (100 Hz curve is excluded, loss modulus is smoothened).

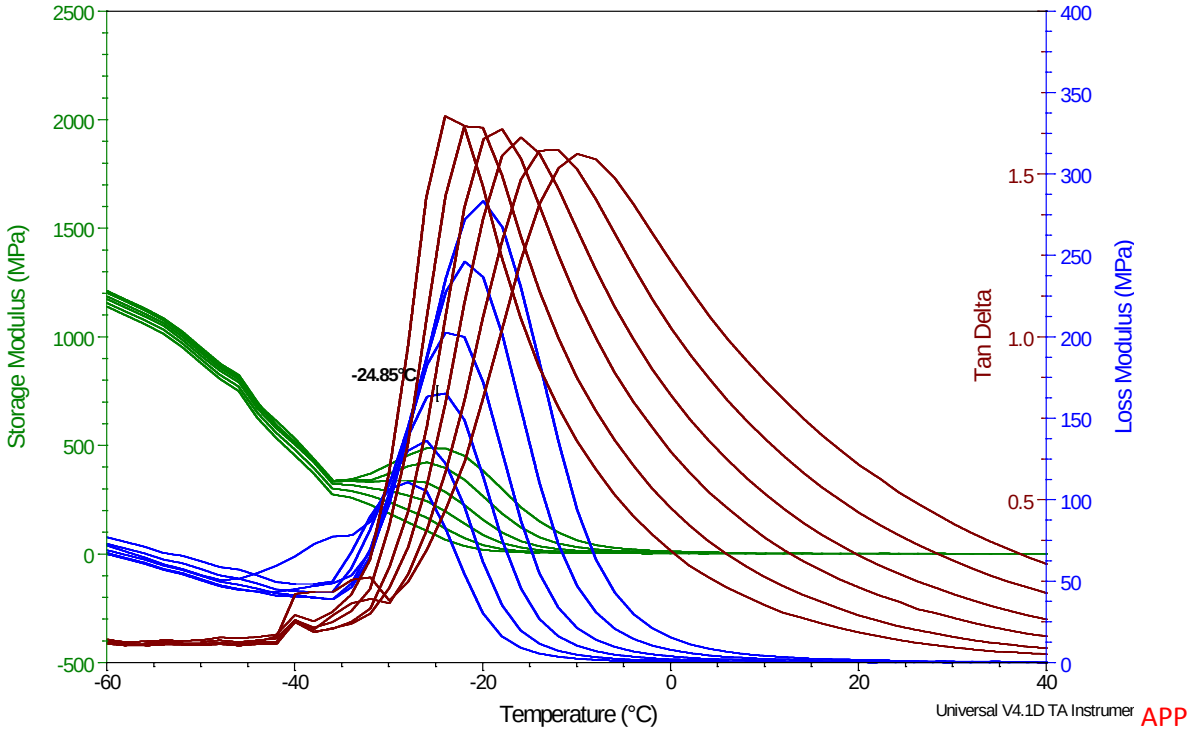

Figure 146. Multi-frequency DMA of T2-44. Time-derived temperature ranged between 0.24 – 0.31 °C/min. T_g was found to be -25 °C for the propargyl alcohol dual cure system (100 Hz curve is removed, loss modulus is smoothened).

5.9 Master curves

T2-39

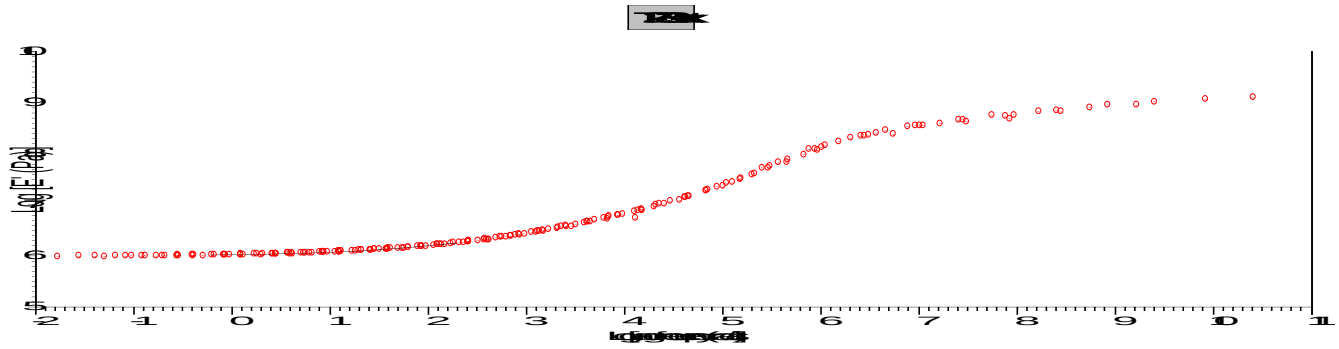

Figure 147. Shifted curves of T2-39, constructed from the storage modulus of a multi-frequency dynamic mechanical analysis. The material is considered to be well applicable with the time-temperature superposition principle.

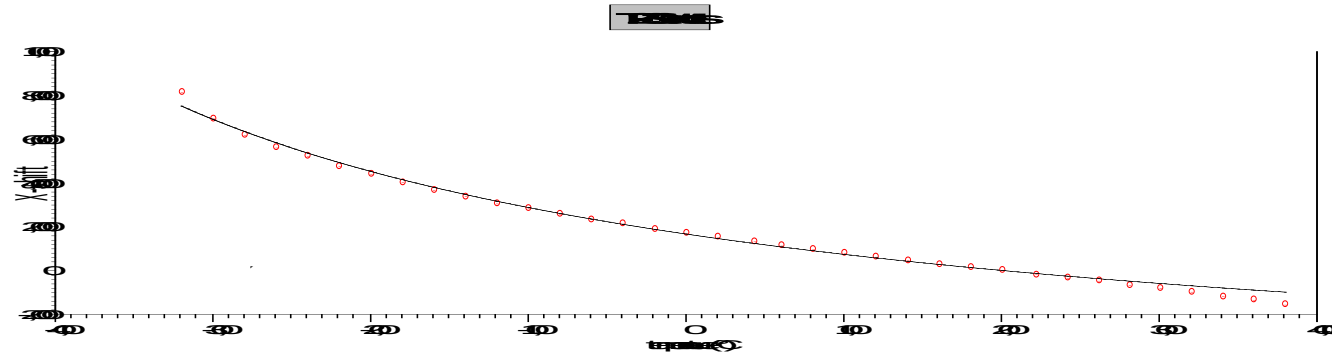

Figure 148. The WLF shift function of T2-39. C1=6.252, C2=95.35, Tref = 0 °C.

T2-41

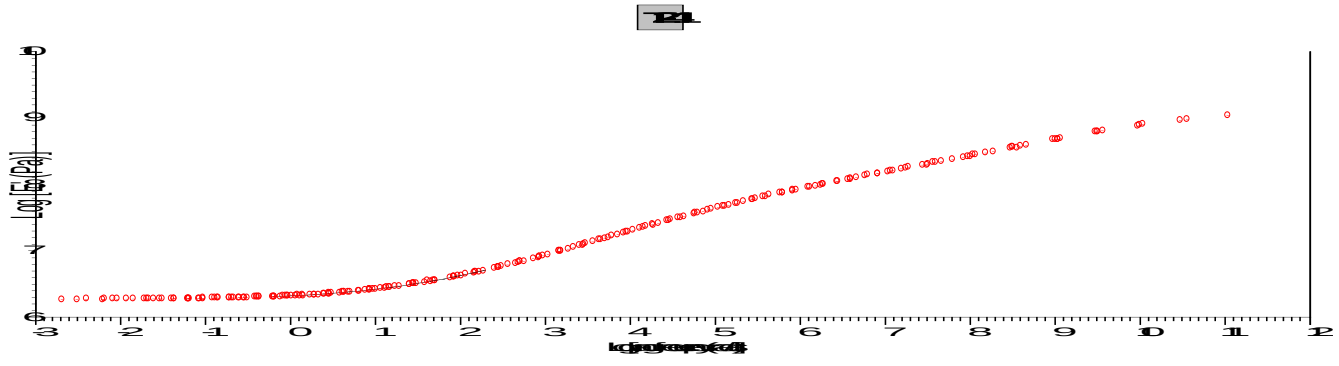

Figure 149. Shifted curves from a multi-frequency dynamic mechanical analysis of T2-41, obtained from the storage modulus (G') of different frequencies, in a temperature region from the samples' T_g, to about 40 °C.

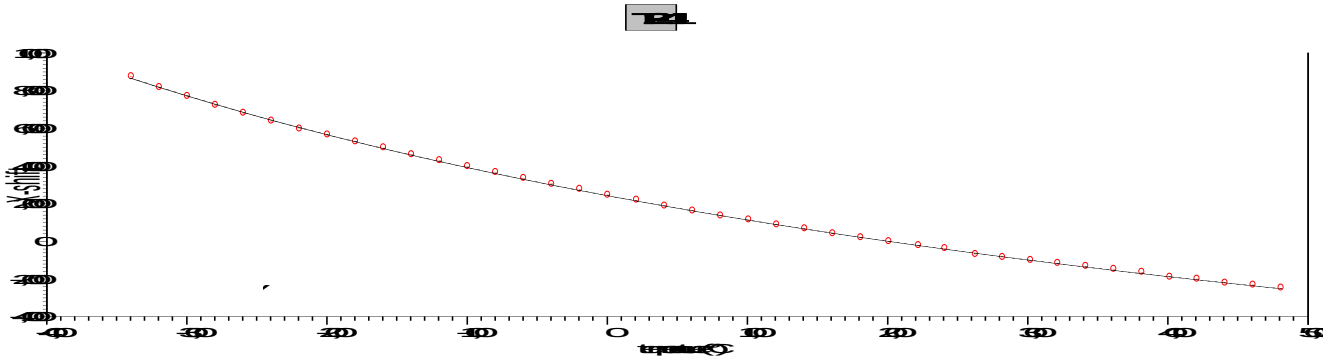

Figure 150. WLF shift function of T2-41. C1 is 16.77, C2 is 158.7. A standard error below 4 imply a good correlation between the shifted curves and the WLF shift function.

T2-44

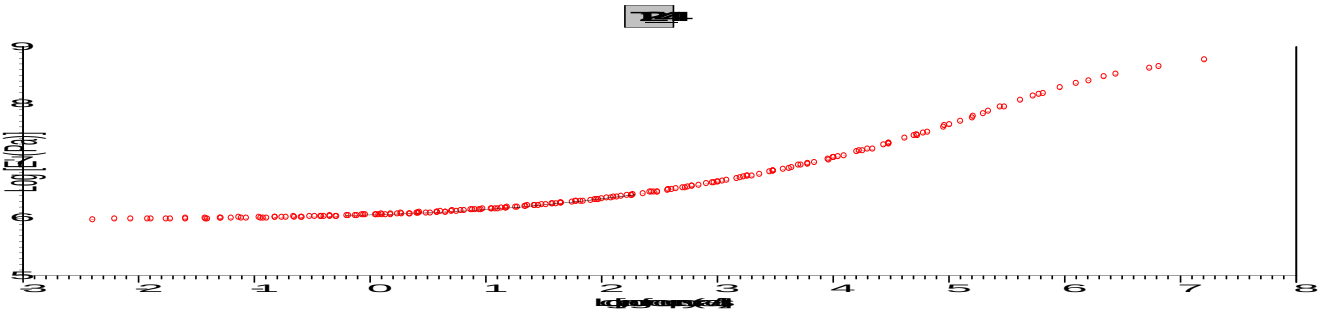

Figure 151. Shifted curves of T2-44, constructed from the storage modulus of a multi-frequency dynamic mechanical analysis.

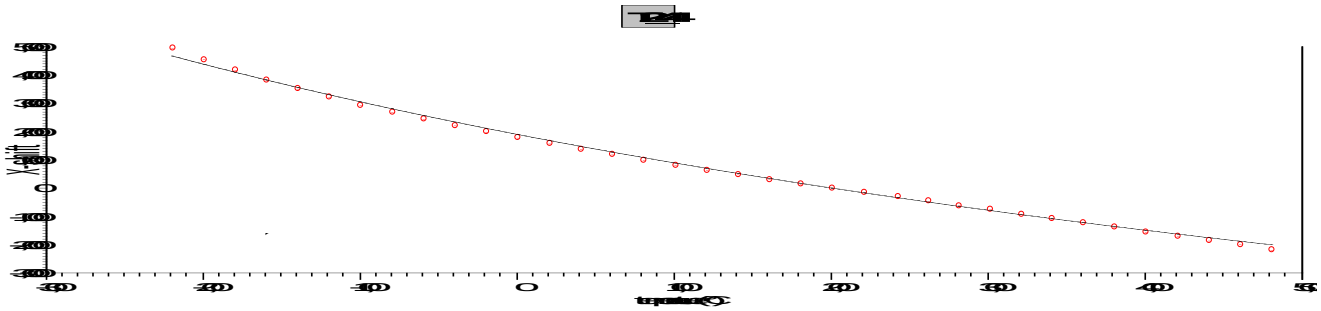

Figure 152. The WLF shift function of T2-44 and its graphic illustration, arguing for the applicability with an adequate correlation standard error of 14.60. C1=14.07, C2=168.6.

5.10 FTIR

T2-40

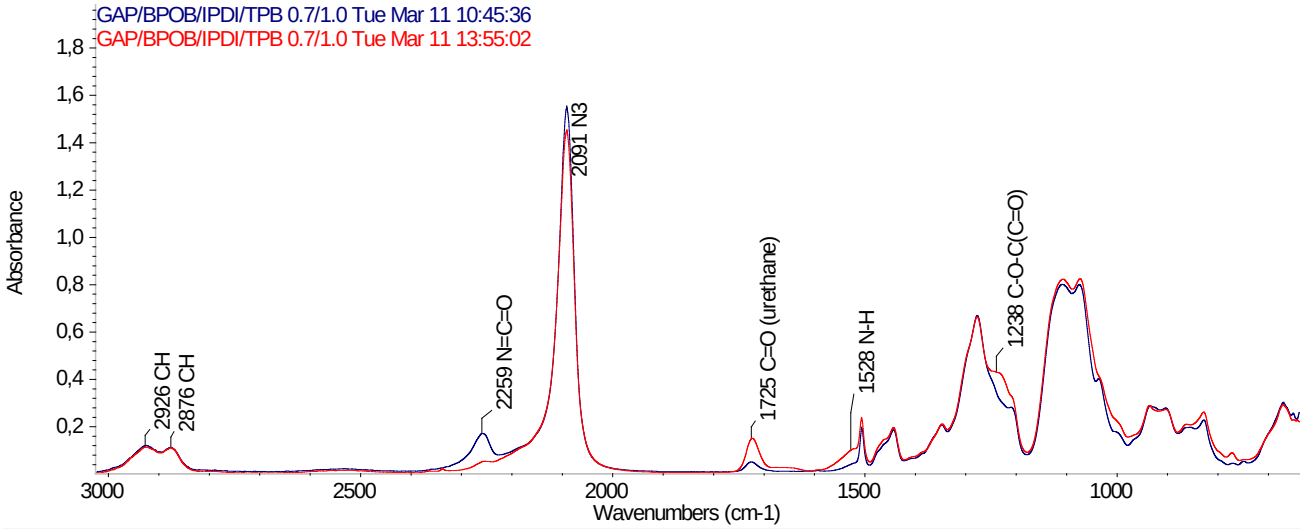

Figure 153. T2-40. An identical formulation of T2-40 was replicates in order to monitor the curing process.

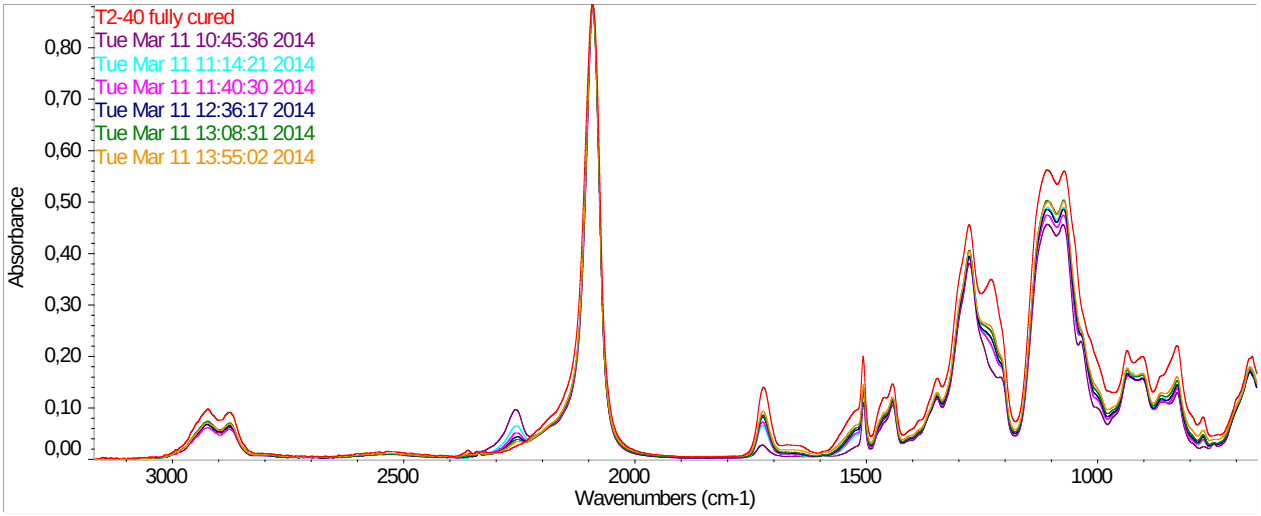

Figure 154. FTIR of sample T2-40, manual series while curing.

T2-33

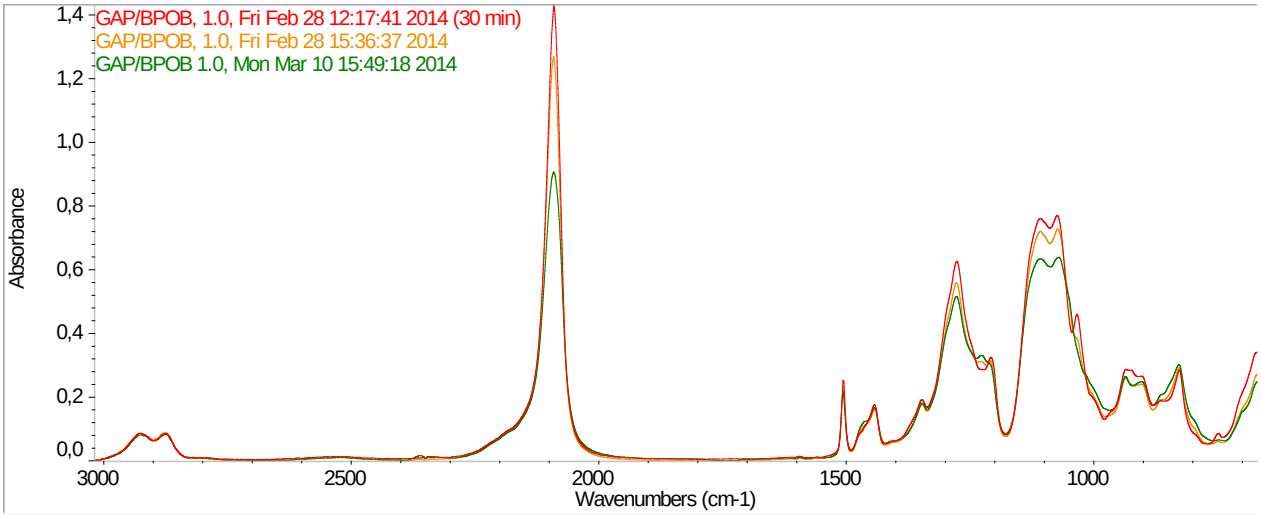

Figure 155. FTIR of sample T2-33, manual series while curing.

Aromatic isocyanates

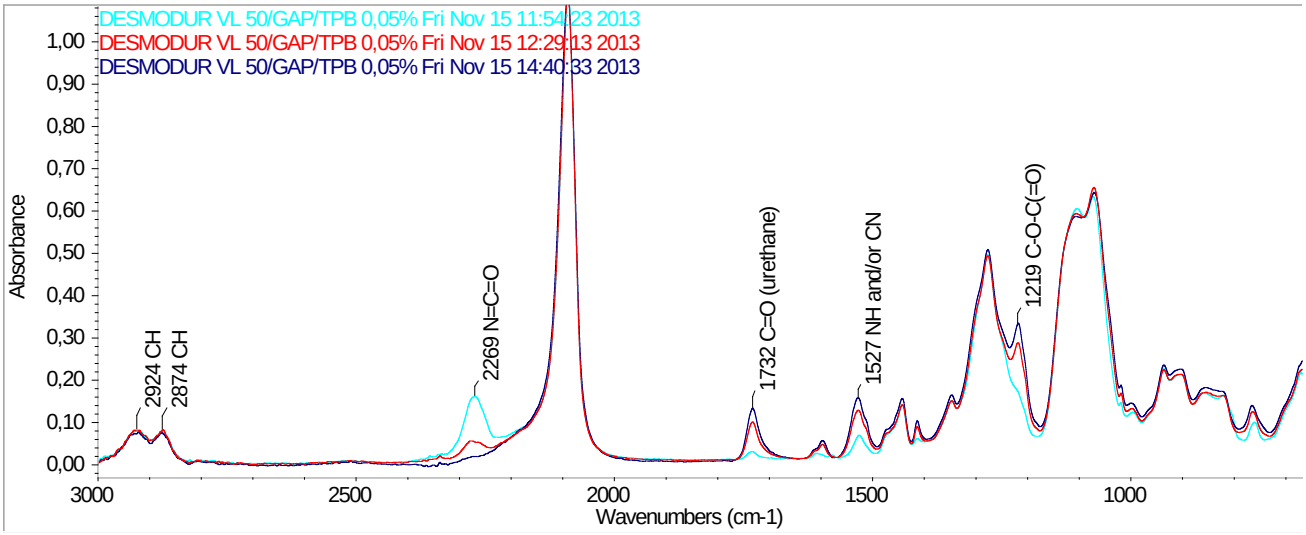

Figure 156. FTIR of GAP/VL50, manual series while curing.

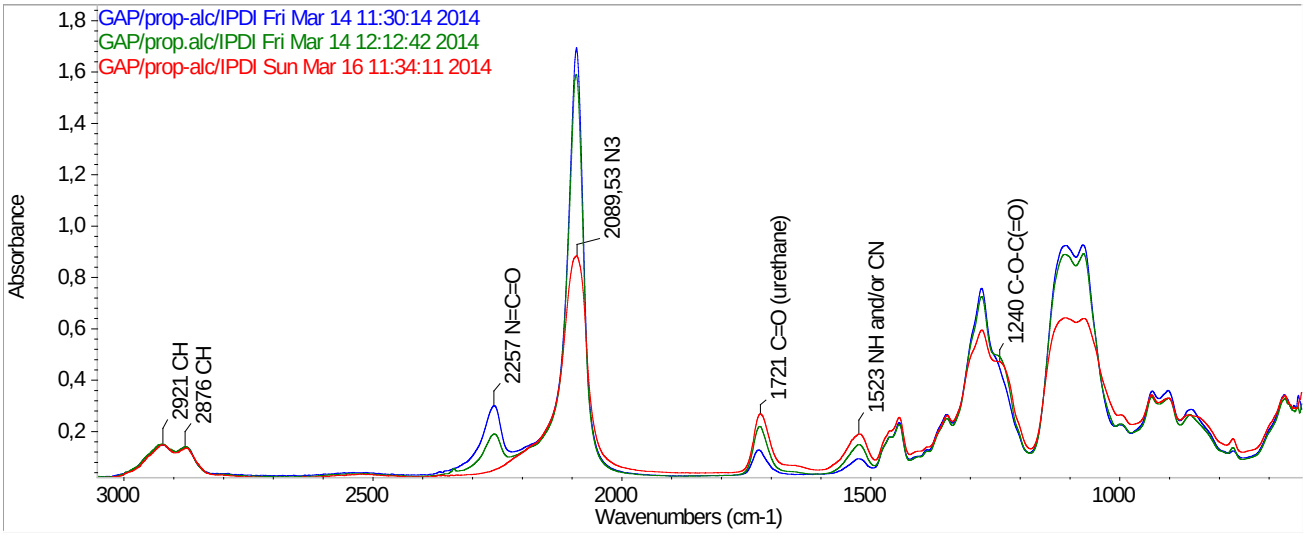

Figure 157. FTIR spectra of GAP/prop.alc/IPDI

The Huisgen cyclo-addition is taking place, which consumes azide. The loss of azide is suggested to be observed.

2921 + 2876: CH stretch
2257: isocyanate
2089: azide moiety
1721 urethane carbonyl
1523: N-H bend
1240: ether with carbonyl vicinity

5.11 Images

a) 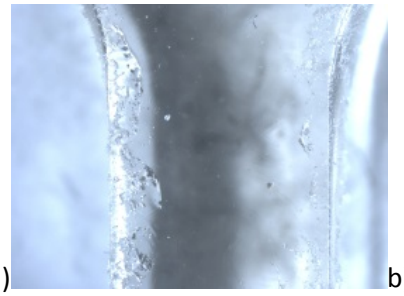 b) 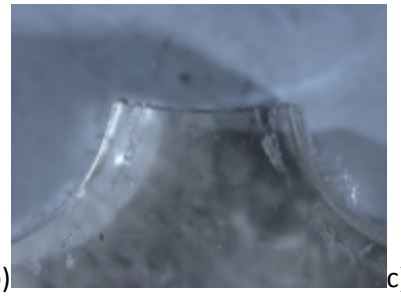 c) 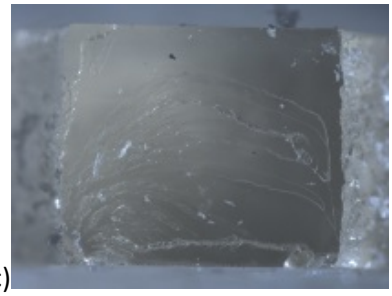

Figure 158. image through microscope. a) T2-18, parallel 5, b) T2-19, parallel 5, c) T2-19, Parallel 5.

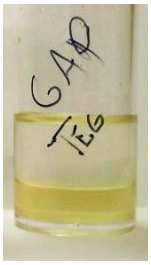

Figure 159. Two phases: TEG above, GAP below.

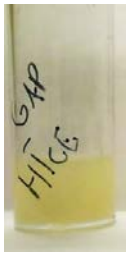

Figure 160. Simple miscibility test with HTCE and

Figure 161. simple miscibility test with GAP and

Figure 162. Simple miscibility test with GAP and PPG-PEG

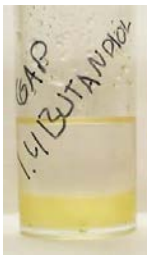

Figure 163. Simple miscibility test with GAP and 1,4-butanediol

Figure 164. Simple miscibilty test with the solid crystal flakes of BPOB

Figure 165. tensile tested specimens of sample T2-41. A rough surface, but surprisingly precise tensile results. Voids were apparent, but effectively avoided.

References

Ang, H. G. (2012). Energetic polymers : binders and plasticizers for enhancing performance, Wiley VCH.

Bayer, O. (1969). Polyurethane plastics, Google Patents.

Blank, W. J., et al. (1999). "Catalysis of the isocyanate-hydroxyl reaction by non-tin catalysts." Progress in Organic Coatings **35**(1–4): 19-29.

Bruttel, P. and R. Schlink (2003). "Water determination by Karl Fischer titration." Metrohm Monograph **8**(5003): 2003-2009.

Bui, V., et al. (1996). "Energetic polyurethanes from branched glycidyl azide polymer and copolymer." Journal of Applied Polymer Science **62**(1): 27-32.

Dewhurst, J. Catalysis of polyurethane systems: Selecting Catalysts To Achieve Desired Properties And Processing. Air Products and Chemicals, Inc. Allentown, Pennsylvania, U.S.A., Technomic Publishing AG.

Diaz, E., et al. (2003). "Heats of combustion and formation of new energetic thermoplastic elastomers based on GAP, PolyNIMMO and PolyGLYN." Propellants, Explosives, Pyrotechnics **28**(3): 101-106.

Fischer, K. (1935). "Neues Verfahren zur massanalytischen Bestimmung des Wassergehaltes von Flüssigkeiten und festen Körpern." Angewandte Chemie **48**(26): 394-396.

Haas, Y., et al. (1994). "Infrared laser-induced decomposition of GAP." Combustion and Flame **96**(3): 212-220.

Kasicki, H. P., F. Ozkar ,S. (2001). "curing characteristics of glycidyl azide polymer based binders." journal of applied polmyer science.

Knut Magne Hansen, E. U. (2003). Termogravimetrisk og dynamisk mekanisk analyse av polymermatriser. FFI Rapport, FFI**:** 102.

Landsem, E., et al. (2012). "Neutral Polymeric Bonding Agents (NPBA) and Their Use in Smokeless Composite Rocket Propellants Based on HMX-GAP-BuNENA." Propellants, Explosives, Pyrotechnics **37**(5): 581-591.

Luo, S.-G., et al. (1997). "Catalytic mechanisms of triphenyl bismuth, dibutyltin dilaurate, and their combination in polyurethane-forming reaction." Journal of Applied Polymer Science **65**(6): 1217-1225.

Mathew, S., et al. (2008). "Thermomechanical and Morphological Characteristics of Cross-Linked GAP and GAP–HTPB Networks with Different Diisocyanates." Propellants, Explosives, Pyrotechnics **33**(2): 146-152.

McCrum, N. G., et al. (1997). Principles of polymer engineering, Oxford University Press.

Mehta, P. S., et al. (1990). "Bhopal tragedy's health effects: a review of methyl isocyanate toxicity." Jama **264**(21): 2781-2787.

Min, B. S., et al. (2012). "A study on the triazole crosslinked polymeric binder based on glycidyl azide polymer and dipolarophile curing agents." Propellants, Explosives, Pyrotechnics **37**(1): 59-68.

NASA. "chinese rocketry." from http://history.msfc.nasa.gov/rocketry/03.html.

NASA.gov (7. January 2014). "Brief History of Rockets." from https://www.grc.nasa.gov/WWW/k-12/rocket/TRCRocket/history_of_rockets.html.

plastemart (2011). "global polyurethane market." from http://www.plastemart.com/Plastic-Technical-Article.asp?LiteratureID=1674&Paper=global-polyurethane-market-PU-foams-thermoplastic-elastomers.

Porter, G., et al. Water Determination in various plastics.

Provatas, A. (2000). Energetic polymers and plasticisers for explosive formulations-A review of recent advances, DTIC Document.

Provatas, A. (2001). Characterisation and polymerisation studies of energetic binders, DTIC Document.

Reed, R., Jr. and M. L. Chan (1983). Propellant binders cure catalyst, United States Dept. of the Navy, USA . 4 pp.

> Ph3Bi [603-33-8] and di-Bu tin dilaurate (I) [77-58-7] in approx. proportions of 2.5-14:1 are used as curing catalysts for glycidyl-azide polymer (GAP)-isocyanate binder systems for curing at ambient room temp. to ∼140°F for ∼24-72 h to obtain void-free propellant grains with burn characteristics suitable for missile propulsion. Thus, 56.25% HMX [2691-41-0] crystals ∼(10 μ) and 13.04% powd. Al (80-100 μ) were mixed with GAP 9.72, bis(4-isocyanatocyclohexyl)methane 0.61, hexamethylene diisocyanate biuret trimer 0.87, FEFO [17003-79-1] 19.43, I 0.035, and Ph3Bi 0.02%, poured into polyethylene tubes, and cured overnight at 120°F. The resulting cured propellant grains had acceptable phys. properties and substantially no voids. [on SciFinder(R)]

Rostovtsev, V. V., et al. (2002). "A Stepwise Huisgen Cycloaddition Process: Copper(I)-Catalyzed Regioselective "Ligation" of Azides and Terminal Alkynes." Angewandte Chemie International Edition **41**(14): 2596-2599.

Shusser, M. (2012). "Composite rocket propellants." Wiley Encyclopedia of Composites.

Sichina, W. J. (2000). Measurement of Tg by DSC. P. E. instruments.

Simmons, R. (1994). NENAs–New Energetic Plasticizers. ADPA International Symposium on Energetic Materials Technology, Orlando, FL.

STANAG Standardization NATO agreement 4540 Explosives, procedures for dynamic mechanical analysis (DMA) and determination of glass transition temperature.

Sun Min, B. (2008). "Characterization of the plasticized GAP/PEG and GAP/PCL block copolyurethane binder matrices and its propellants." Propellants, Explosives, Pyrotechnics **33**(2): 131-138.

Sun Min, B. (2008). "Characterization of the Plasticized GAP/PEG and GAP/PCL Block Copolyurethane Binder Matrices and its Propellants." Propellants, Explosives, Pyrotechnics **33**(2): 131-138.

Sutton, G. P. and O. Biblarz (2001). Rocket propulsion elements. New York, John Wiley & Sons.

Ulrich, H. (1996). Chemistry and technology of isocyanates, Wiley New York.

Wikipedia. "Goddard." from http://upload.wikimedia.org/wikipedia/commons/7/7c/Goddard_and_Rocket.jpg.

Wikipedia. "HMX." Retrieved 27.april, 2014, from http://en.wikipedia.org/wiki/HMX.

Wikipedia (2014). "John Whiteside Parsons." Retrieved 28. April, 2014, from http://en.wikipedia.org/wiki/John_Whiteside_Parsons.

Young, R. J. and P. A. Lovell (1991). Introduction to polymers, Chapman & Hall London.

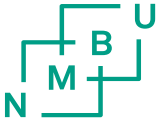

Norwegian University
of Life Sciences

Postboks 5003
NO-1432 Ås, Norway
+47 67 23 00 00
www.nmbu.no